Investigation of the Effect of Particle Size on Froth Stability

Tadiwanashe Chidzanira

B.Sc. (Honours) Chemical Engineering

Dissertation submitted to the Faculty of Engineering and the Built Environment, University of Cape Town

In fulfilment of the requirements for the degree of Master of Science in Engineering

Department of Chemical Engineering

University of Cape Town

May 2016

PLAGIARISM DECLARATION

I hereby certify that this thesis is the result of my own work and has not been submitted prior to this for any higher degree to any other university or institution. I know the meaning of plagiarism and declare that all the work in the document, save for that properly acknowledged, is my own.

Name: Tadiwanashe Chidzanira

Signature: Signed by candidate

Acknowledgements

I would like to express my sincere gratitude to my supervisors Mrs Jenny Wiese and Dr Belinda McFadzaean who not only served as my research supervisors but also assisted in providing the intuition, understanding and invaluable apparatuses on how to conduct a research. Special thanks are also given to the CMR team in particular the Flotation research group for the technical advice given during the course of the research, and the CMR laboratory staff for bearing with me during the experimental work and providing a conducive environment for my project. Sincere appreciation also goes to AMIRA P9 project for the financial and academic support.

Special mention goes to Gerald Mbele, Innocent Achaye, Tanaka Shumba, Tiisetso Moimane and Erick Gore for being good company and their assistance with various works related to this work. This project could not have been completed without your support.

Finally, most of all to my family more so to Mr and Mrs Chidzanira and my sibling Anesu Chidzanira: my deepest gratitude. Your support and encouragement during times when the journey got rough is much appreciated and duly noted.

SYNOPSIS

The flotation process has been used for more than a century to separate valuable minerals from bulk ores. The separation process is based on utilising the differences in the physico-chemical properties of liberated particles, mainly the particle hydrophobicity which allows the particles to be attached to air bubbles rising from the pulp phase into the froth phase and subsequently collected to the launder. The stability of the froth phase which is be defined as the ability of bubbles to resist coalescing and bursting (Triffet & Cilliers, 2004), has been shown to have a significant effect on the efficiency of the flotation process. An unstable froth will result in poor valuable mineral recovery as these desired hydrophobic particles are detached from air bubbles and drain with the water back into the pulp phase due to bubble coalescence. On the other hand, a very stable froth may result in poor concentrate grade as the unwanted gangue materials are unselectively entrained to the concentrate.

As a result, a substantial amount of research has been performed on improving control of froth stability by the manipulation of frother type and dosage. A recent study investigated the manipulation of flotation operating parameters such as air rate, froth height and depressant dosage which resulted in minimal changes in froth stability. The present study then investigated the effect of particle size and solids concentration on the stability of the froth phase using a UG2 ore and an Itabirite ore. Froth stability was determined using Bikerman tests on a laboratory scale non-continuous stability column. A novel continuously operated agitated hybrid cell was also used to assess froth stability, with water recovery and froth recovery used as proxies for froth stability. The agitated hybrid cell was then included in the experimental design as it allowed for continuous floatation system to be evaluated which resembles more industrial operations as compared to the stability column. The hybrid also incorporated the agitation zone benefits of a lab scale batch flotation cell which allows for better attachment of coarse particles and also allowing for the formation of deeper froths enabling improved froth stability measurements. The viability of using the top froth average bubble size and the side of froth axial bubble coalescence rate as froth stability proxies was also evaluated as the columns were clear glass.

An evaluation of the particle size distributions of the feed and the concentrate reporting to the launder showed that the concentrate was consistently finer than the feed. Feed particle sizes for the UG2 ore ranged from 157-78 μm with concentrate sizes ranging from 83-39 μm from the coarsest to the finest grind. Feed particle sizes for the iron ore ranged from 29-62% passing 38 μm with concentrate sizes ranging from 49-82% passing 38 μm from the coarsest to the finest grind. It is hypothesised that this was due to the increased weight of the coarse particles resulting in the particles draining back into the pulp zone at a faster rate. As a result, a smaller fraction of the coarser particles reports to the concentrate resulting in the finer particle size distribution. The effect was shown to be more pronounced for the UG2 ore as compared to the iron ore, as the UG2 ore forms a less stable froth which has a higher rate of bubble coalescence. Changing the feed particle size was also shown to alter the concentrate particle size thereby allowing for the investigation into the effect that the size of particles present in the actual froth has on froth stability.

Test results show that froth stability increased with decreasing particle size for both ores. It was hypothesised that a decrease in particle size would result in an increase in the maximum capillary pressure thereby reducing capillary drainage. It was also hypothesised that a decrease in the particle size of the entrained particles would increase the viscosity of the interfilm fluid, thereby reducing drainage rate and increasing stability. Froth stability was shown to follow a decreasing power law relationship with feed particle size. Froth stability was also shown to decrease sharply with increasing particle size over the fine feed size range of less than 100 μm, with the effect becoming less pronounced with increasing particle size over the coarser range. The steep decrease was shown to correspond to concentrate particle sizes approximately less than 50 μm, the range in which particles are expected to report to the froth through entrainment. Froth stability followed an increasing linear relationship with feed specific area for the size range tested (UG2 ore: 78-157 μm and iron ore: 48-118 μm). More importantly, froth stability was assessed as a function of total surface area imparted by the concentrate particles and stability was shown to increase with increased total surface area. Decreasing the feed particle size was shown to result in higher solids recovery and finer concentrate particle size thus higher specific area, therefore total surface area imparted was critical to the assessment of froth stability.

Increasing solids concentration was shown to result in an increase in froth stability and the effect was shown to be less pronounced for UG2 ore as it is a sparsely mineralised PGM-bearing ore. The rheology of the interfilm is suggested to play a more significant role in particle stabilisation of the froth as the stability increased steeply in the particle size range where entrainment is expected as shown by the entrainment factor increasing steeply in the same size range. Future work evaluating the rheology of the froth is recommended to further clarify this.

.

Table of Contents

List of Tables

List of Figures

ABBREVIATIONS AND NOMENCLATURE

BET	Brunauer–Emmett–Teller
cm/s	Centimetres per second
CCC	Critical coalescence concentration
CMC	Carboxy-methyl cellulose
CMR	Centre for Minerals Research
C1	First concentrate
C2	Second concentrate
C3	Third concentrate
C4	Fourth concentrate
D_{80}	Aperture diameter which 80% of the material can pass.
DOW 200	DOW Froth 200
Flotigam EDA	alkyl ether amine collector
Hmax	Maximum froth height
g/min	Grams per minute
g/t	Grams per tonne
GGS	Gates-Gaudin-Schulmann
Itabirite	Haematite ore
Jg	Superficial gas rate
PAR	Peak Air Recovery
PGE	Platinum group elements
PGM	Platinum group mineral
PSD	Particle Size Distribution
R_f	Froth Recovery

RRD	Rosin Rammler Distribution
SIBX	Sodium Isobutyl Xanthate
$t_{1/2}$	Froth half life
UG2	Upper Group 2
UCT	University of Cape Town
µm	Microns
nm	Nano metres
γ	Surface tension
Σ	Dynamic froth stability

Chapter 1. INTRODUCTION

1.1. Background

The flotation process has been used for more than a century to separate valuable minerals from bulk ore. The separation process is based on utilising the differences in the physio-chemical properties of liberated particles which include but are not limited to particle hydrophobicity and particle size. Hydrophobic particles attach to air bubbles forming a bubble-particle aggregate which rises through a slurry known as the pulp phase. The bubbles, along with the attached particles are then transferred to the froth phase which can be referred to as the separation phase. Most of the fluid is drained back into the pulp phase along with the particles entrained in the fluid between the bubbles. The draining of the entrained particles will result in an improved grade (Farrokhpay, 2011). The froth is then collected in the launder thus separating the hydrophobic particles from the unwanted hydrophilic gangue material. Figure 1 shows a schematic of the flotation process.

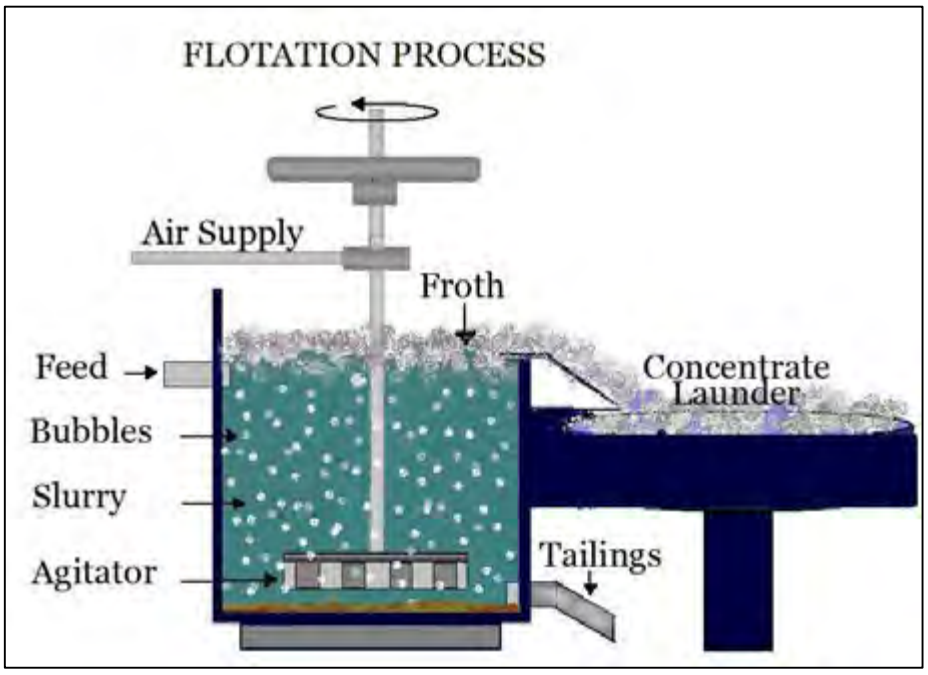

Figure 1: Schematic of a flotation process (Adapted from Mining Examiner).

The efficiency of the flotation process is critically dependent on the characteristics of the pulp phase and the froth phase. The effect of the froth phase on the flotation performance is dependent on the stability and mobility of the froth (Barbian et al.,

2005). Froth stability can be defined as the froth's ability to resist bubble rupture or coalescence (Triffet & Cilliers, 2004).

It has been shown that froth stability is a major factor in flotation efficiency as a whole (Barbian et al., 2003). An increase in froth stability has been shown to increase the recovery of valuable minerals. It has also been shown to have an inverse effect on the grade of the valuable minerals, with the grade reduced with increasing froth stability (Ventura-Medina & Cilliers, 2002; Banford et al., 1998). An unstable froth will result in the detachment of attached hydrophobic particles as the bubbles burst and coalesce resulting in poor recovery of the valuable minerals in the concentrate but (possibly) a higher grade (Ata, 2009). On the other hand, a very stable froth will reduce the grade of the valuable minerals in the concentrate as more of the entrained, unwanted gangue material is also transported to the launder thereby reducing selectivity. As a result, understanding froth stability is critical to improving flotation performance.

The instability of the froth is as a result of the liquid in the lamellae draining back into the pulp phase due to gravity and as a result the bubbles coalesce. The coalescence can be noted by the increase in bubble size as you move up the froth phase (Ata et al., 2003). A less stable froth is characterised by an increased burst rate at the top of the froth phase (Hunter et al., 2008). A decrease in froth stability as described will also result in less water being transported into the launder as more of the water drains back into the pulp phase. This can be noted by a decrease in the amount of water recovered in the concentrate (Tao et al., 2000).

Early research was focused on understanding froth stability in a two phase system with major emphasis put on gravity drainage and film thinning effects. The studies were also focused on discontinuous, non-overflowing systems (Dippenaar, 1982 a; Ata et al., 2003; Barbian et al., 2006, Ventura-Medina & Cilliers, 2002). Recent studies have shifted into considering the three phase system which also takes into consideration the effects of particles on the stability of the froth phase. In the studies that have been performed, the presence of particles has resulted in the limitations by which froth stability can be measured using the conventional system parameters such as gas holdup or bubble size accurately and thus new methods have been

proposed that can be applied to both laboratory and industrial scale operations (Ata et al., 2003).

Earlier research has showed that frothers are essential in the formation of fine bubbles and aiding in establishing froth stability but it has been shown that most frothers are marginally effective in the absence of particles (Farrokhpay, 2011). It has also been shown that particle size has a significant effect on froth stability (Dippenaar., 1982; Hunter et al., 2008). This has then presented the need for further investigation into the relationship between particle size and froth stability.

1.2. Problem Statement

Much research has focussed on the qualitative relationship between particle size and froth stability. However, in order to model the froth phase, it is necessary to establish quantitative relationships between particle size and froth stability. This project aims to develop a quantitative relationship between feed particle size and froth stability for two different ores. The project is also aimed at assessing the practicality of a number of froth stability devices and measurements in establishing the relationship with particle size.

1.3. Research Aims and Objectives

The aim of the project is principally to obtain a relationship between particle size and froth stability for two different ores. The project also aims at assessing the relative magnitude by which solids concentration affects the froth stability. The above aims can be summarised as follows:

1. Establish a relationship between particle size and froth stability so as to enable the future prediction of the relative impact that a change in particle size will have on the flotation performance.

2. Investigate relative influence of solids concentration on the effect of particle size on froth stability.

3. Assess the effect of particle surface wettability on the stability of the froth phase by using two ores of different mineralogy.

4. Establish a procedure on the agitated hybrid cell that enables the utilisation of solids-water recovery, top of froth bubble size, side of froth coalescence rate and froth recovery to evaluate froth stability. These are to be assessed in conjunction with the Bikerman test.

1.4. Key Questions

The key questions that where addressed in the thesis project are as follows:

1. What is the effect of changing pulp particle size on the froth phase particle size?

2. What is the effect of particle size on froth stability?

3. What is the effect of solids concentrations on froth stability?

4. What effect does the ore mineralogy have on the stability of the froth phase?

5. Can image analysis techniques be used to measure froth stability?

1.5. Thesis Proposed Scope

The project was aimed at understanding the effect of various factors on froth stability, which is critical to the efficiency of the flotation system. A summary of the factors affecting flotation efficiency is shown in the Figure 2, with the scope of the project highlighted in red.

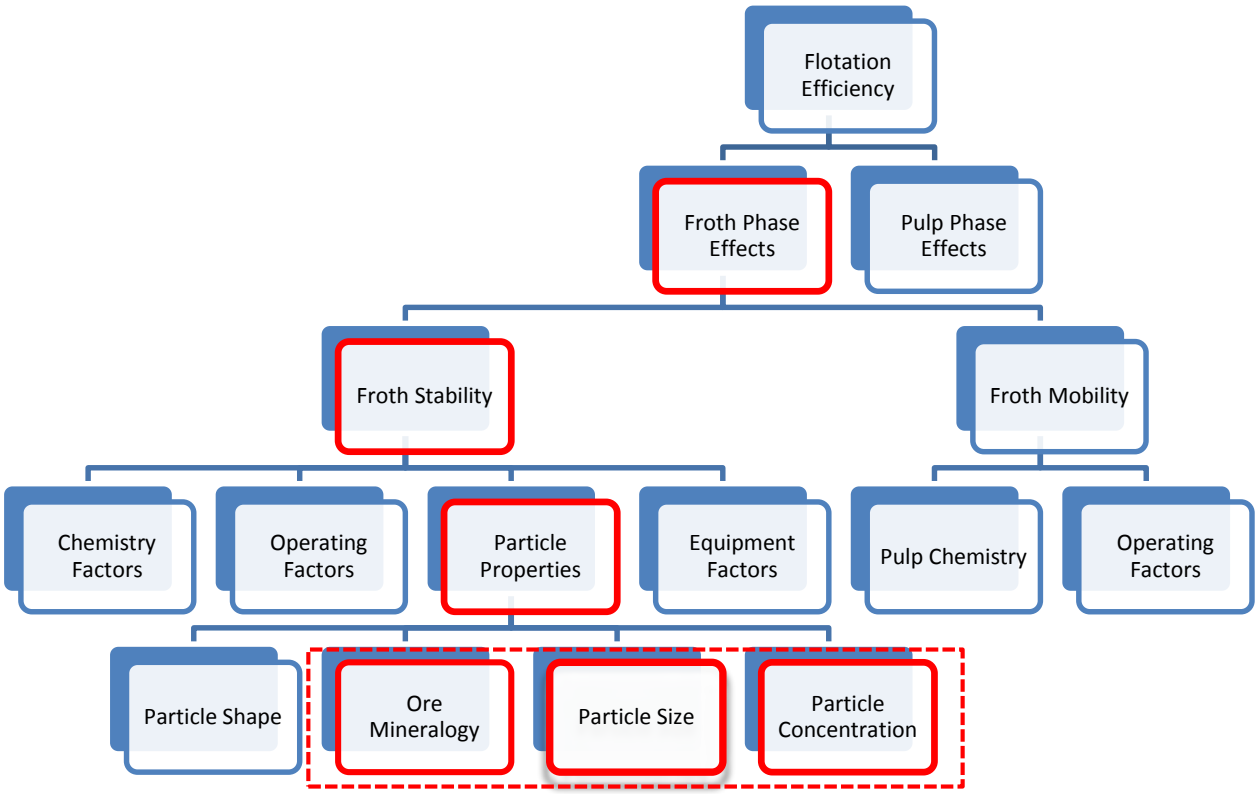

Figure 2: Schematic representation of the scope of the thesis.

The thesis was focused on understanding the effect of particle size on froth stability and thus, the effect of particle size on the flotation efficiency. The effect of particle size was assessed at various solids concentrations and two different mineral ores were used so as to establish a comprehensive understanding of this effect. The other operating conditions were kept constant throughout the investigations so as to isolate the particle size effect. The experimental tests were performed using a non-continuous stability column and also on a continuous agitated hybrid cell.

The thesis scope also focused on establishing and improving the methodology to quantitatively and qualitatively measure the froth stability. Top of froth bubble size and side of froth bubble coalescence rate were assessed in conjunction with the more conventional measurement tools, namely water recovery and froth recovery. The project also aimed at unifying continuous and non-continuous froth stability measurement techniques.

1.6. Thesis Layout

This thesis is structured into 6 chapters and appendices outlined as follows:

Chapter 1: Introduction

This chapter introduces froth flotation, with emphasis on the importance of froth phase. The chapter also introduces the importance of particles in flotation and the importance of understanding and controlling froth stability in optimising the performance of the flotation process. This is followed by the outline of the thesis objectives and key questions.

Chapter 2: Literature Review

The chapter provides review of the literature concerning the factors affecting froth stability. The chapter provides more detailed reviews on the effects various particle properties have on the stability of the froth with main emphasis on particle size and concentration. The chapter also provides a review on the various proxies used to quantify froth stabilities. At the end of the chapter the proposed hypotheses of this research work are outlined.

Chapter 3: Experimental Methodology

The chapter gives a detailed description of the experimental approach taken in testing the proposed hypothesis. This includes the set-up of test rigs, conditions under which the experiments were carried out and measurement techniques applied in the tests.

Chapter 4: Results

Results from the test work performed are presented in this section. Initially results obtained from test work performed on the stability column in assessing the effect of particle size and solids concentration on the stability of the froth are presented. These results are then followed by results from test work performed on the hybrid cell in assessing the effect of particle size on froth stability and also the feasibility of using image processing techniques to evaluate the stability of the froth phase.

Chapter 5: Discussion

This chapters aims to discuss the results presented in the preceding chapter.

Chapter 6: Conclusion and Recommendations

This chapter presents the key findings from this research followed by recommendations of future work.

Chapter 2. LITERATURE REVIEW

2.1. Fundamentals of Froth Stability

When air is passed through the pulp phase during flotation, the air emerges as bubbles which are surrounded by a thin liquid film. When at least three bubbles cluster together, they form a Plateau border which contains the liquid as shown in Figure 3.

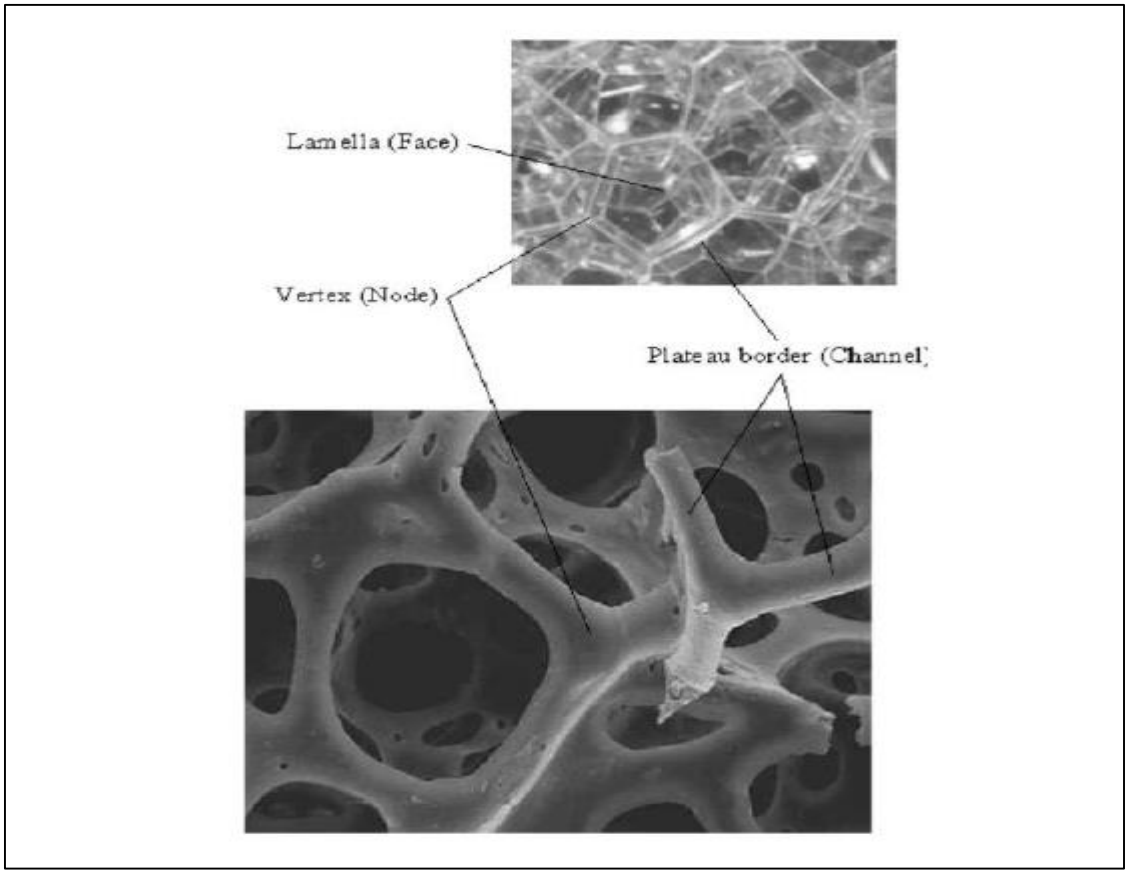

Figure 3: Image showing the structure of foam, lamellae, Plateau border and nodes (Ventura-Medina & Cilliers, 2002)

Continued clustering of the bubbles typically results in the formation of polyhedral gas bubbles with films in-between the bubbles. This is known as foam in the case of a two phase system. In the case of a three phase system also containing solid particles, the system is referred to as froth, which is characterised into either bulk froth or surface froth. Surface froth stability is therefore associated with the rate of bursting of the surface bubbles which results in the release of air into the

atmosphere. On the other hand, bulk froth stability is associated with the coalescence rate from the base of the froth to the surface (Morar et al., 2012).

Froth stability can then be generally defined as the ability of bubbles to resist coalescence or bursting (Triffett & Cilliers, 2004). The bursting or coalescing of the bubbles is due to drainage of the liquid in the Plateau borders and in between the bubbles back into the pulp. The more stable froths are referred to as metastable froth and the latter froths as unstable (Schedulko, 1966).

Froth stability can on the other hand be defined as the ratio between the volume flowrate of air in the concentrate stream and the volume flowrate of air in bubbles entering the froth phase which have a non-zero probability of entering the concentrate stream, which is based on air recovery as a froth stability parameter (Moys, 1984). Froth stability is then represented by the fraction of air entering the flotation cell that overflows into the weir in unburst bubbles which is referred to as air recovery (Qu et al. 2013). Hadler et al., 2012 showed that there is a maximum air recovered that is passed through at a constant air rate by changing the froth height. They also showed that the froth height at which PAR value was reached was a function of the air rate. This was postulated to be maybe as an attribute to the balance between froth mobility and solids loading on the bubbles (Smith et al., 2009). Lower air recoveries would be expected either when the froth is moving slowly with heavy loading of particles or when there is unstable froth moving fast with bubbles under-loaded with particles (Qu et al., 2013).

2.2. Factors affecting Froth Stability

The stability of the froth is affected by a number of factors, mainly particle characteristics, chemistry effects and operational conditions (Subrahmanyam & Forssberg, 1988). It is influenced to a greater extent by the particles properties (particle hydrophobicity, size and shape) in comparison to surface active agents (frothers, collectors and depressants) or operating conditions (aeration rate, gas dispersion and froth height). Additional factors such as the quality of the process water also affect the froth stability but less significantly (Sheludko, 1967).

2.2.1. Particle Property Factors

a. Particle Property Effect Overview

During the flotation process, particles attach to the air bubbles as they rise through the pulp phase due to properties such as hydrophobicity and particle size. The particles are transported to the froth phase were they affect froth stability due to their interactions with bubble surfaces as shown in Figure 4.

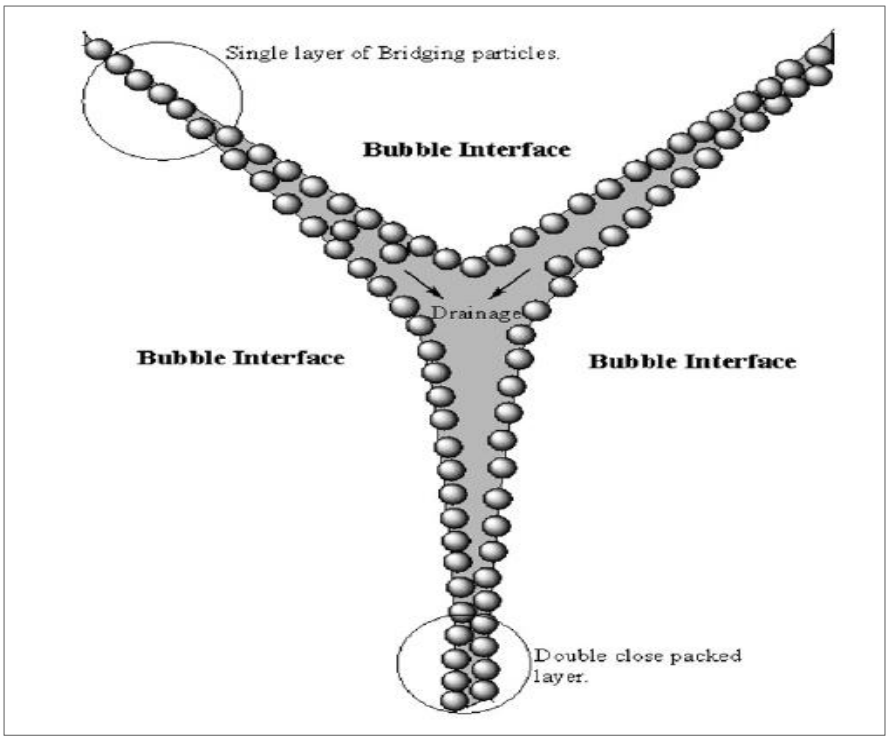

Figure 4: Schematic of the attachment of particles onto the bubbles (Hunter et al., 2008)

The particle properties that are of great importance in the bubble attachment such as particle hydrophobicity, size and shape, also have a significant effect on the stability of the froth thereby also having a substantial effect on the overall flotation performance that can outweigh the beneficial effects in the pulp phase (Aktas et al., 2008).

The presence of particles in the froth phase will result in the formation of steric barriers around the bubbles as shown in Figure 4 and this barrier results in an increase in the froth stability by preventing surfaces from touching (Johansson & Pugh, 1992). The effects of particle properties such as size, hydrophobicity and shape have been shown to have a more significant impact on the stability of the froth with increasing distance from the pulp/froth interface. The coalescing of bubbles

occurring at the pulp-froth interface can be mainly attributed to two phase properties such as film thinning or gravity drainage with the particle effects becoming more significant with increasing distance from the pulp/froth interface, where the bubble films are thinner allowing for bridging to occur (Ata et al., 2003). At the pulp-froth interface region, bubbles start to pack together as they arrange to the new environment. Bubbles move from being dispersed in the pulp (Kugelschaum) to a closed packed structure (limiting Kugelschaum) as a result of liquid drainage due to gravity and this is determined by the velocity profile of the water between adjacent rising bubble surfaces (Pugh., 1996). The rearrangement will result in most of the liquids and solids being squeezed out thereby causing bubble coalescence and thus a sharp rise in bubble size (Falutsu, 1994; Ata et al., 2003).

b. Particle-Bubble Film Interaction Stabilisation Mechanism

There are various mechanisms that have been proposed by which hydrophobic particles can be explained to affect the stability, namely particle detachment energy, maximum capillary pressure of coalescence (which is the widely accepted major contributor) and particle-particle interactions.

i. Particle detachment energy

The detachment energy is related to the free energy required to remove an adsorbed particle in equilibrium from an interface (either oil–water or air–water) (Hunter et al., 2008). As hydrophobic particles form a steric barrier to coalescence around the bubble interface, stronger particle detachment energy entails more force is required to disrupt the particle layers and allow coalescence thus a more stable froth (Levine et al., 1989). Detachment energies generally increase as the area of the great line tension (air / fluid interface area) is lost due to increased particle adsorption. The energy is mainly influenced by the particle area (i.e. its radius ‘R’) and immersion of the particle at the interface (i.e. θ) and the initial surface tension γ_{ow}/γ_{aw}. The energy required moving a particle from an equilibrium immersion depth and contact angle can then be calculated from fundamental principles as follows (if buoyancy/gravity effects are neglected);

$$\Delta G_{remove} = \pi R^2 \gamma_{ow/aw}(1 \pm cos\theta)^2 \qquad \textbf{Equation 2-1}$$

From **Error! Reference source not found.**-1, it is shown that the detachment energy depends on the square of the particle radius. This then suggests that smaller particles are detached more easily, allowing for coalescence to occur and thus acting as poor stabilisers (Hunter et al. 2008). Contrary to this, Seher Ata in 2009, showed that a decrease in particle size from 92 to 52 µm resulted in less particles detaching. This was attributed to the difference in the kinetic energies of the differently sized particles contrary to just the adhesion energy shown in Equation 2-1 which considers only the thermodynamics of the system and does not take into account the inertia force of particles (Ata., 2009).

ii. Maximum capillary pressure of coalescence

The opposing theory to that of the detachment energy is based on maximum capillary pressure of coalescence which can be referred to as the pressure gradient between a bubble and the interfilm fluid. The mechanism aims at explaining not only how a particle is attached to an interface, but rather how particles residing between two interfaces affect froth stability by altering the pressing force required to cause bubbles to coalesce, known as the capillary pressure (Hunter et al, 2008).

The higher the maximum capillary pressure, the more the bubbles can withstand the pressing force, thus the more stable the froth is. The maximum capillary pressure P_c^{max} for a single layer of particles stabilising the froth can be given as (Kaptay, 2006);

$$P_c^{max} = 2p\sigma(cos\theta)/R \qquad \textbf{Equation 2-2}$$

Where R = radius of the spherical solid particle; σ = interfacial energy between the liquid and gas; θ = contact angle of the liquid in gas phase on the solid particle; parameter *p* is a function of particle arrangement.

From **Error! Reference source not found.**, it can be shown that the maximum capillary pressure is inversely proportional to the particle size, *R*, and as a result, a decrease in particle size results in an increase in froth stability.

The two opposing effects of detachment energy and maximum capillary pressure were used to calculate an optimum contact angle for froth stabilisation to be 70° (Kaptay, 2006). Semi quantitative arguments have been used to estimate optimum particle sizes for highest froth stabilities (Kaptay, 2006). These show that particles should be neither too small nor too big to stabilise froths. The optimum lies in the region between about 10 nm to several micrometres. From a flotation perspective, it is unlikely that the smaller end of this range will be of interest and it can be concluded from a practical flotation perspective that smaller particles will stabilise froths.

iii. Particle-particle interactions

Complex interactions occur between hydrophobic particles that are adsorbed at the bubble interface forming the steric barrier. The interactions can be described by the steps required for coalescence, with one of the important final stages after film thinning being the formation of a critically sized hole in the film wall. An energy barrier must then be overcome to form a hole in the steric barrier of particles and thus particle-particle forces such as electric double layer repulsion and dipole–dipole repulsion, as well as van der Waals attraction and capillary forces are of utmost importance to overall stability of the froth. The finer the particles are, the more surface area to volume ratio is available for forces such as the van der Waals to prevent lateral movement along the interface and thus increasing stability (Hunter, 2008).

The finer particles were also shown to give a higher packing efficiency as compared to the coarser particles when forming the steric barrier around the bubble film and as a result produce a more homogenous layer. The increased packing efficiency can then be attributed to the inverse proportionality between the overall froth stability and the particle size. This trend was shown with fine silica particles enhancing the stability of foams, with the froth stability proportional to the particle concentration and inversely proportional to particle size (Tang et al., 1989).

c. Inter-film Fluid Rheology Stabilisation Mechanism

The presence of non-adsorbed, entrained hydrophobic and hydrophilic particles in the inter-film fluid has been shown to affect the rheology of the fluid. A decrease in

slurry particle size has also been shown to result in increased viscosity. From the flotation perspective, it was also shown that increasing the viscosity of the interfilm fluid will result in reduced drainage rates and thus increase the stability of the froth phase (Gergely & Clyne, 2004). Therefore reducing the particle size entrained into the interfilm fluid will result in increased fluid viscosity, thereby reducing fluid drainage rates. The presence of particles even of low adsorbance which will more likely report to the froth mainly through entrainment into the interfilm fluid has also been shown to increase stability by significantly reducing capillary flow and drainage (Wuebben & Odenbach, 2005). Ip et al (1999) also showed that increasing the system temperature resulted in reduced froth stability and this was attributed to a decrease in bulk fluid viscosity which was in-line with Gergely & Clyne (2004) proposal (Hunter et al., 2008). A reduction in the particle size can then be postulated to result in an increase in the viscosity of the inter-film, thereby reducing drainage as shown in Figure 5.

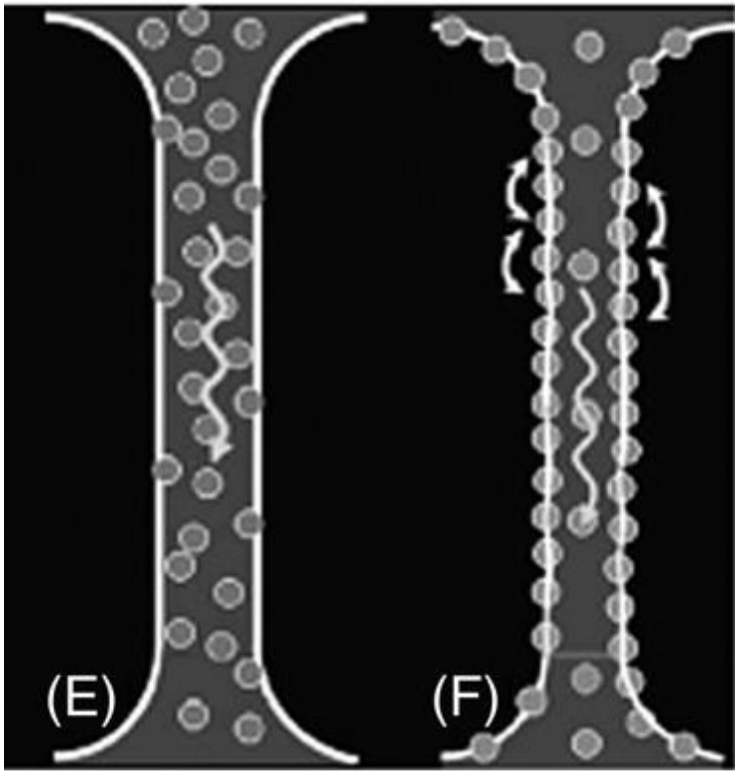

Figure 5: Mechanism of particle stabilisation for (E) non-adsorbing particles altering viscosity and (F) strongly adsorbing particles creating steric barrier, with added trapped particles inhibiting drainage and bulk rheology (Hunter et al., 2008).

d. Effects of Particle Hydrophobicity on Froth Stability

Particle hydrophobicity can be defined as the ability of particles to repel water. The particle property is the major mechanism utilised in the flotation process as the hydrophobic particles attach to the rising bubbles thereby being separated from the hydrophilic particles that remain in the pulp phase.

After a hydrophobic solid particle attaches to a gas bubble, the resulting angle between the bubble and particle is known as the contact angle. The interaction is based on the interfacial energies between the particle, gas bubble and the liquid and can be shown using the Young/Dupre equation shown below in Equation 2-3 (Fuerstenau and Han, 2003),

$$\boldsymbol{y_{lv}cos\theta = y_{sv} - y_{sl}} \qquad \textbf{Equation 2-3}$$

Where y_{lv} is the surface tension of the liquid/vapour interface, y_{sv} is the surface energy of the solid/vapour interface, y_{sl} is the surface energy of the solid/liquid interface and θ is the contact angle between the solid particle and the bubble as shown in Figure 6,

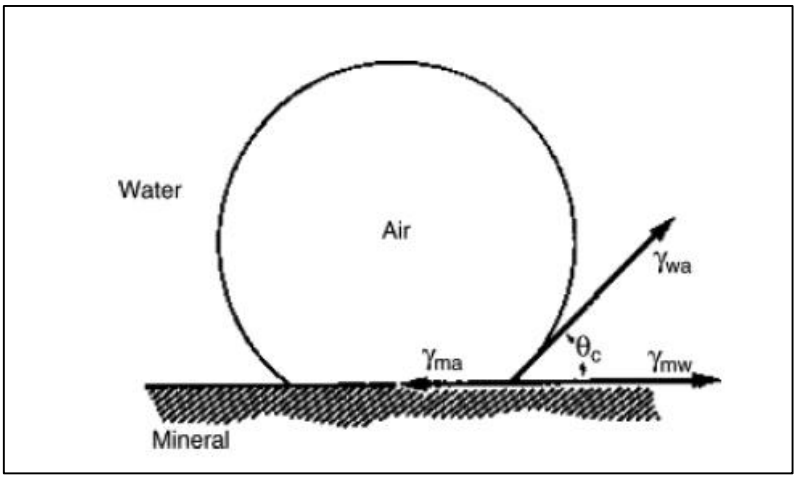

Figure 6: Contact angle in the Young/Dupre equation (Gence, 2005).

The interfacial energy values from the equation can be used to assess the effect of different contact angles on froth stability (Hunter et al., 2008). For gas bubbles to attach to the particles in the pulp, the contact angle has to be far greater than zero. As a result, the higher the contact angle, the greater the hydrophobicity of the particle and thus the easier it is for bubble-particle attachment.

In early research, it was believed that an increase in contact angle would result in an increase in froth stability. This would be as a result of an increased adhesion between solid particles and bubbles making them more resistant to external forces (Wills, 2006). Further research has shown that there is a critical hydrophobicity that will give the maximum froth stability with particles of high hydrophobicity (θ = 82º) resulting in a much greater interface penetration and film rupture, thus leading to unstable film bridging as shown in Figure 7 (Hunter et al., 2008). Research using spherical particles showed that particles with contact angles greater than 90 degrees resulted in the destabilisation of the froth (Dippenaar, 1982b). Further work from Johansson and Pugh (1992) also showed that contact angles greater than 80 degrees resulted in reduced froth stability with intermediate contact angles (65 degrees) resulting in the greatest froth stability.

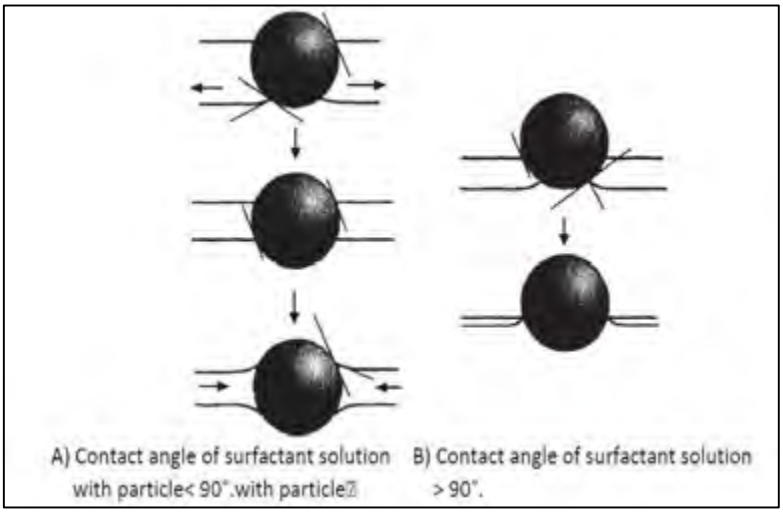

Figure 7: Particle film bridging behaviour in froth. A) Moderately hydrophobic, B) Highly hydrophobic particle (Ata, 2012).

In later research, it was shown that hydrophilic particles have minimal effect on the stability of the froth (Ata et al., 2003). Particles with high contact angles (highly hydrophobic) will penetrate the bubble films to an extent that will result in the rupturing of the film, with low contact angle particles streamlining back into the pulp through the lamellae (Ata et al., 2003). The particles of low hydrophobicity remain dispersed in the lamellae with little influence on the stability (Johansson & Pugh, 1992).

e. Effects of Particle Size on Froth Stability

In most manufacturing processes, foam stability has been achieved by adding particles of size ranging from 30 nm to 20 μm with a general rule stating that the smaller the stabilising particles, the lower the volume content required of such particles (Hunter et al., 2008). This in turn shows that finer particles provide higher stabilising effect for the same amount of particle as compared to coarser particles.

The ratio between thickness of the froth lamellae and the size of the particles has been shown to have a great effect on froth stability (Aktas et al., 2008). If the particle size is smaller than that of the film thickness, the particles can then be arranged at the liquid/gas interface resulting in the stabilisation of the film by the capillary mechanism (Chen, 2012) or by non-adsorbing particles changing the viscosity of the fluid (Ip et al., 1999; Gergely & Clyne, 2004). On the other hand, if the particle size is greater, the particles may then bridge the films resulting in the rupture of the films and thus an increased coalescence rate (Pugh, 2005).

Many qualitative studies have been done that relate the stabilising effects of fine particles and the destabilising effect of coarse particles on the froth phase. Johansson and Pugh (1992) showed that coarse quartz particles of between 74 -106 μm in sparsely mineralised froth of 2% by volume solids had a lower stability with reference to maximum froth height as compared to the finer 26 - 44 μm particle size range at the same frother concentration. It was shown by Aktas et al. (2008) that water recovery and dynamic froth stability increased with decreasing particle size for real ores. It has also been shown that the addition of fine particles to a coarse particle flotation system significantly improves the recovery of the coarse particles due to the increased froth stability.

However few research studies have gone into developing quantitative relationships between froth stability and particle size. Ip et al., (1999) developed a quantitative relationship giving an inverse linear relationship between particle size and froth stability as shown in Figure 8, which was also observed in emulsions and aqueous foams (Hunter et al, 2008).

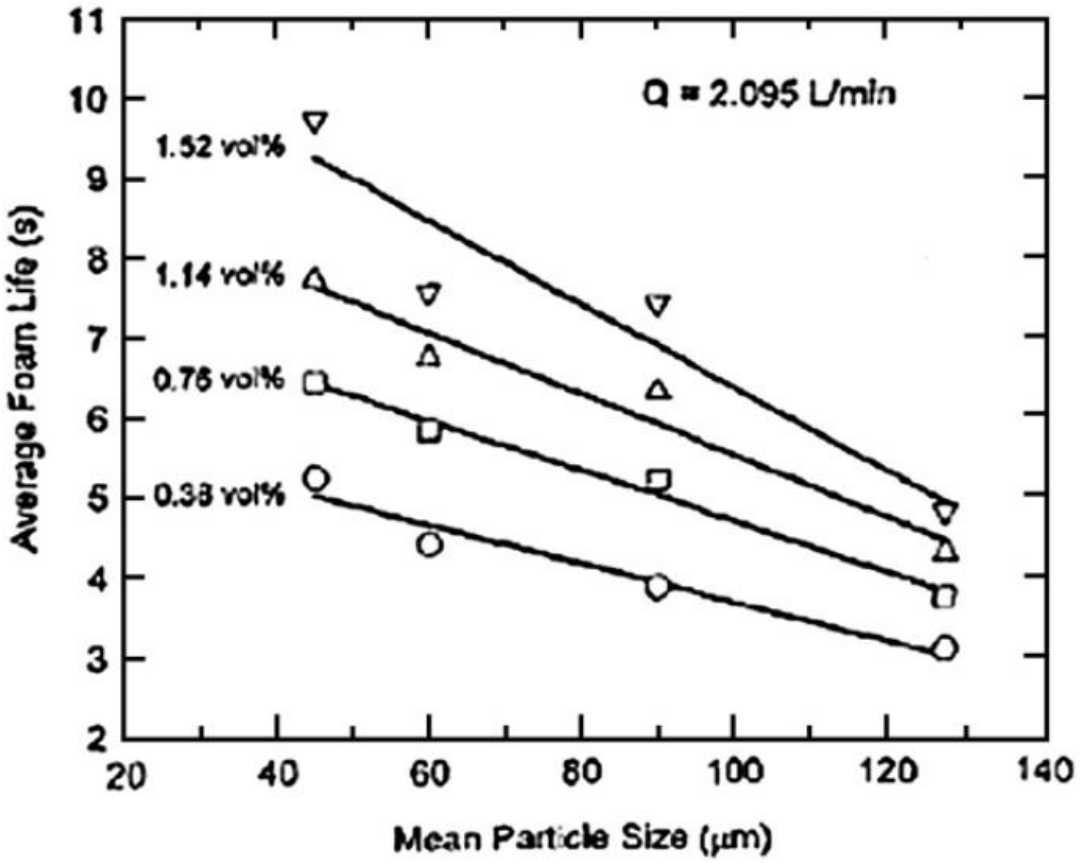

Figure 8: Inverse linear relationship between particle size and froth stability (Average foam life) (Ip et al., 1999)

f. Effects of Particle Solids Concentration

The effect of particle concentration has been shown to be critical to froth stability thus affecting the overall flotation performance. Since the concentration of particles in the pulp will affect the amount of particles that can attach to the bubbles, an increase in solids concentration will result in an increase in the bubble loading. The increased loading will result in reduced coalescence rate due to the greater surface coverage (Sun & Gao, 2002). The reduced froth mobility will also increase the residence time of the froth, resulting in increased time for the drainage of the liquid from the lamellae and resultant bubble coalescence (Farrokhpay, 2011).

The increased bubble loading due to increased solids concentration will result in reduced capillary pressure, thereby increasing the stability of the froth. It has been shown that the effect of particle concentration is interlinked with the particle size and the hydrophobicity of the particles.

An increase in solids concentration for non-adsorbing hydrophilic particles will also result in an increase in the stability of the froth phase by increasing the solids in the inter-film fluid thereby increasing the viscosity and reducing the drainage rate (Gergely & Clyne, 2004).

g. Effects of particle shape on froth stability

The shape of the particles is also critical to froth stability as the more irregularly shaped particles will pierce the film as compared to the more spherical particles (Livshits & Dudenkov, 1965). It has been shown that the thinning and rupture of a liquid film can be accomplished in roughly 0.1 s by rounded or spherical particles; however sharp-edged particles rupture the liquid film in about 0.02 s (Farrokhpay, 2011). It has been shown that flat particles increased the froth stability more than rounded particles of the same volume (Gaudin et al., 1957).

h. Overall effect of particle properties on froth stability

There is a great conflict in the evidence on whether the major contribution of particle properties on froth stability lies in the inter-film layer with the particles affecting rheology and drainage of the inter-film fluid or whether the particle-interface steric barrier foamed due to the presence of hydrophobic particles in the froth phase is the major component as shown in emulsions (Hunter et al., 2008). Gergely and Clyne (2004) showed that high particle concentration could increase the viscosity of the inter-film fluid and inhibit liquid drainage. Ip et al. (1999) also showed that particles that were attached to the interface resulted in the flattening of the bubble curvature around the plateau borders, thus reducing the capillary pressure and retarding drainage.

2.2.2. Chemistry Effects

During the flotation process, chemicals are added to the system to improve certain properties that allow for a more efficient separation. Some of the chemicals are added to control and modify the physico-chemical properties of the mineral surface to improve selectivity (Fuerstenau et al., 2007). Additional chemicals are also added to modify the pulp conditions and also control the gas bubble film properties. The three proposed chemicals that are to be used for the thesis are as follows: frother, collector and depressant.

i. Frothers

Frothers can be defined as hetero-polar surface active organic reagents which accumulate at the gas-liquid interface. The majority of the frothers contain a non-polar water-repellent group as well as a polar water-avid group (Harris & Jia, 2000). However there exists some polyglycol frothers like PPG 425 that have two polar (OH) groups (Farrokhpay, 2011). Frothers are added to the system to reduce the surface tension of the gas-liquid interface which results in increased froth stability and to also aid in gas dispersion in the pulp zone (Farrokhpay, 2011). The polar section reacts with the water and the non-polar non-reactive hydrocarbon tail is pushed into the gas phase as shown in Figure 9.

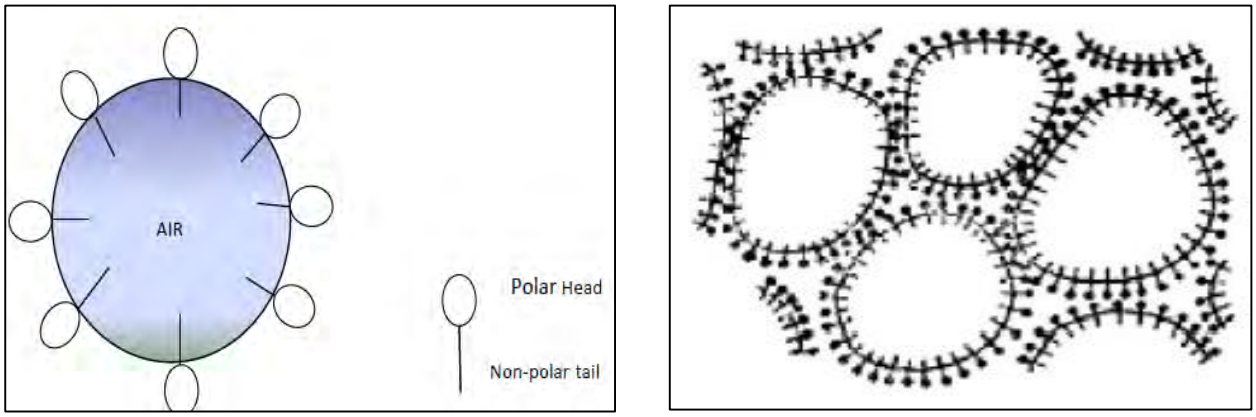

Figure 9: Schematic showing the effect of frothers on gas bubbles (Lu & Pugh, 2005)

The presence of frother in the flotation process will then allow for increased froth stability and thus generally may result in increased recovery to the concentrate. This will usually be at the expense of grade. Frothers have also been shown not only to affect froth stability in the froth phase, but also in the pulp phase, reducing the bubble coalescence (Laskowksi, 2004). An increase in the frother dosage will increase the froth stability resulting in a higher recovery of water and solids (Tang et al., 2010).

There exists a critical concentration of the frother in the pulp zone that stops the coalescence of bubbles and it is known as the critical coalescence concentration (CCC) (Grau et al., 2005). The variation of bubble coalescence with frother concentration is shown Figure 10.

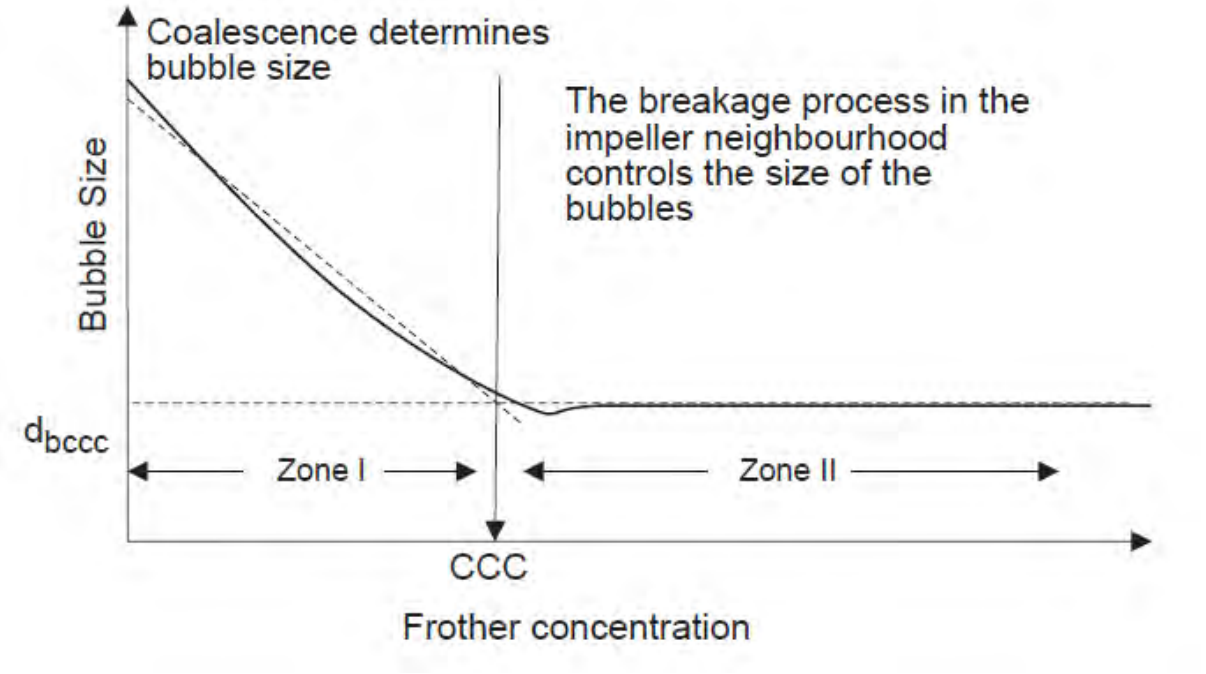

Figure 10: Effect of frother concentration on the bubble size (Grau et al., 2005).

Even if frothers have been shown to be essential in the formation of fine bubbles and therefore increasing the froth stability of the flotation process, they have been shown to be marginally effective in altering froth stability in the absence of solid particles (Farrokhpay, 2011). Cho and Laskowski (2002) deduced that frothers also control the stability of the bubbles in the pulp phase by decreasing the rate at which they coalesce.

ii. Collectors

Collectors can be defined as surface-active agents that are added to a flotation system to increase the hydrophobicity of the valuable mineral. Collectors can either be anionic or cationic depending on the charge of the valuable particles in the flotation process. The polar end of the molecule adsorbs onto the solid particle through chemisorption or physisorption suspending the non-polar end into the bulk solution. There are two types of collectors namely anionic and cationic with both used for the same purpose depending on the charge of the particle (Fuerstenau et al., 2007). The attachment of the collector on the particles will result in the formation of a mono-layer of non-polar hydrophobic hydrocarbons around the particle rendering the particle hydrophobic (Wills, 2006). An increase in the collector dosage will result in an increase in the hydrophobicity of the particles until a critical point

when further increase may result in a decrease in the hydrophobicity due to orientation of the collector molecules in the opposite direction (polar heads sticking out into the solution). As a result, the respective collector dosage can have a significant effect on the stability of the froth due to the different degree of hydrophobicity imparted onto the particles (Wills, 2006). Differences in particle hydrophobicity would affect the froth stability for the reasons stated in Section 2.2.

iii. Depressants

Depressants are added to a flotation system to render the minerals, (usually gangue minerals unless in reverse flotation processes), more hydrophilic thereby preventing them from floating and, thus, improving selectivity (Wills, 2006). They are two commonly used types of depressants, with inorganic and organic depressants. Inorganic depressants are used for sulphide minerals, with the organic depressants namely modified guar gum and carboxy-methyl cellulose (CMC) used in sulphide flotation for depressing silicious gangue (Wills, 2006). Typical guar gum is uncharged or has a low charge as compared to the CMC which has a negative charge and results in a dispersed pulp (Wiese, 2009). High dosages of depressants have been shown to reduce froth stability and this was attributed to the removal of the naturally floating gangue, such as talc, in the froth phase (Bradshaw et al., 2005). Depressants would affect the froth stability by changing the hydrophobicity and amount of particles reporting to the froth.

2.2.3. Operating Condition Effects

i. Air Flow Rate

Early research proposed that an increase in the air flow rate would increase the stability of the froth. The increase in the froth stability would be as a result of the reduced residence time of the bubbles in the froth phase (Tao et al., 2000).

On the other hand, subsequent research suggested that an increase in the air rate will destabilise the froth phase due to the increased turbulence (Barbian et al, 2003). In further research by Hadler and Cilliers (2009), it was shown that there is a critical air rate that gives the maximum stability which coincided with the peak in air recovery (PAR). Air rates below the PAR resulted in froth with low mobility and thus increased the chances for coalescence. Air rates above the PAR resulted in the

formation of bubbles with minimal particle loading thus forming an unstable froth. There existed a point (PAR) that allowed for sufficient mobility and sufficient particle loading that would result in the maximum froth stability as illustrated in Figure 11.

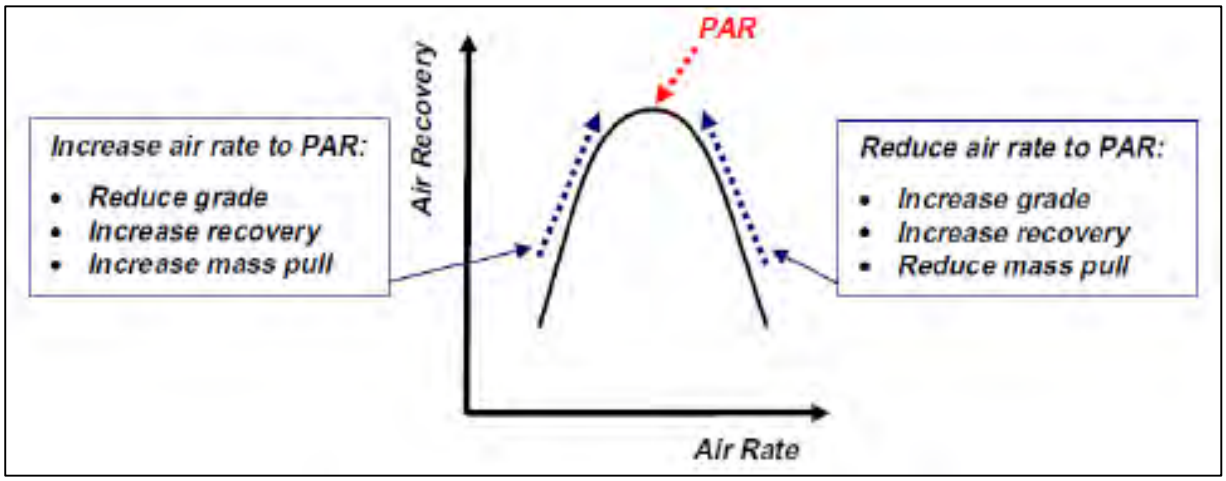

Figure 11: Variation in air recovery with air rate to illustrate the PAR (Hadler et al., 2010).

ii. Froth Height

Changes in the froth height have been shown to have an effect on froth stability as represented by the water recovery. Research has shown that there is a linear negative relationship between the froth height and the amount of water recovered to the concentrate (Tao et al., 2000). An increase in the froth height will result in an increase in the residence time of the bubbles in the froth phase thereby increasing the fluid drainage time from the lamellae. This will then result in the increased bubble coalescence and thus a less stable froth.

Research by Hadler et al. (2012) showed that at a constant air rate, the air recovered (measure of froth stability) passed through a maximum (PAR) when increasing the froth height. It was also observed that the froth height at which the PAR was attained was a function of the air rate. Low air rates reported the PAR value at lower froth heights as compared to higher air rates as shown in Figure 12.

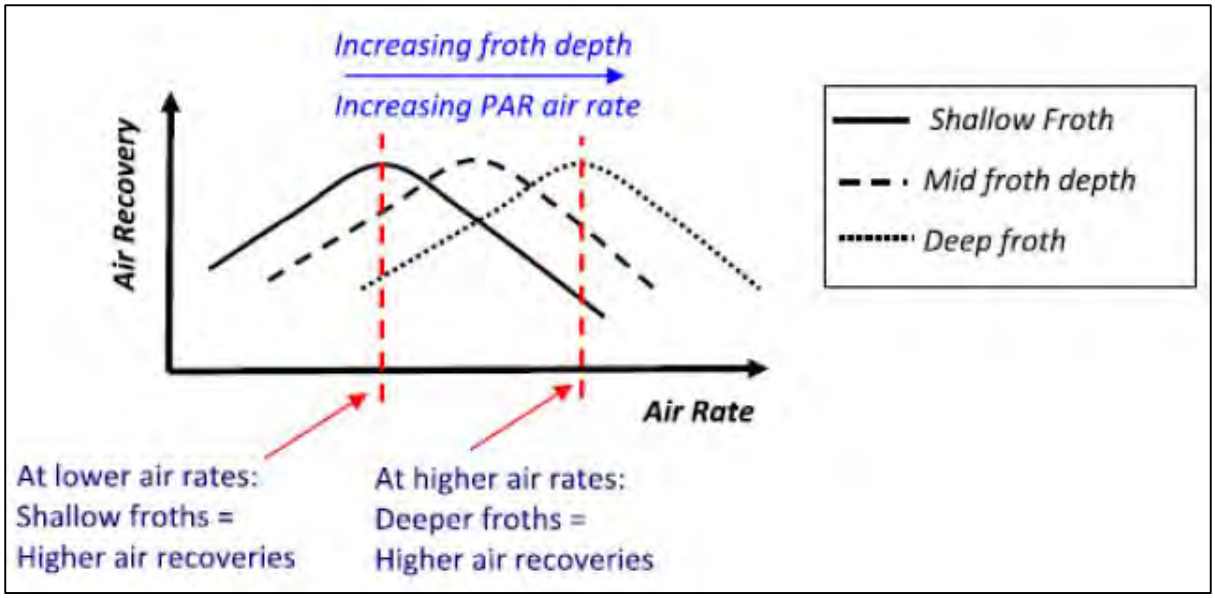

Figure 12: Relationship between froth height and air recovery as a function of air rate (Hadler et al., 2012).

2.3. Measurement of Froth Stability

Several parameters have been used to measure froth stability, but measuring froth stability quantitatively in a consistent manner still needs research (Barbian et al., 2003). Many methods have been proposed and used to measure the stability of the froth and these include rate of bubbles bursting at the top surface of the froth, velocity of the froth and the amount of solids loaded onto the bubble lamellae (Ventura-Medina & Cilliers, 2002).

The froth stability measurement techniques using a non-overflowing column can be categorised as dynamic and static tests. The dynamic tests involve the dispersion of air through the slurry until a dynamic equilibrium is reached between the growth and decay of the froth. Static tests on the other hand don't have any air dispersed through the slurry after dynamic equilibrium is reached or further agitation and thus the froth phase collapses (Barbian et al., 2003). Measurement techniques can also be categorised as continuous and non-continuous techniques. The continuous method entails that the flotation equipment used allows for an overflowing concentrate to be collected. The dynamic tests resemble the actual flotation process more than the static tests, with the continuous system allowing for an even more accurate representation of the flotation process (Barbian et al., 2003; Hunter et al., 2008; Aktas et al., 2008).

2.3.1. Non- Overflowing Systems

The non-overflowing method of assessing froth stability was based on tests performed in a frothing stability column as proposed by Bikerman (1953).

i. Bikerman's Test (Froth Stability Factor)

This test is based on the dynamic tests using a non-overflowing system. Bikerman (1953) determined the dynamic stability factor ($\sum$) as the ratio at equilibrium of the volume of froth from the gas supplied at a given flowrate.

The dynamic froth stability factor can then be determined from a ratio of the froth volume (V_f) to gas flow rate (Q). The factor can be determined by observing the height of the froth at equilibrium (H_{max}) and this is performed in a sparged froth column with cross-sectional area (A) (Aktas et al., 2008) as in Equation 2-4.

$$\sum = \frac{V_f}{Q} = \frac{H_{max} \times A}{Q} \qquad \textbf{Equation 2-1}$$

The physical meaning of the dynamic stability factor is the average time the gas remains entrained in the froth (Barbian et al., 2003). It was observed by Bikerman (1953) that the $\sum$ values were independent of the gas flowrate, shape and size of the column. The method has thus been implemented extensively for both the two phase foams and three phase froth systems (Barbian et al., 2003).

ii. Froth Rise Velocity

In addition to the standard Bikerman test which measures the maximum equilibrium froth height, the exponential growth of the froth height with time can also be recorded as a measure of froth stability (Barbian et al., 2003). The experimental data can then be fitted to an exponential equation as follows:

$$H = H_{max} * (1 - e^{-\frac{t}{\tau}}) \qquad \textbf{Equation 2-2}$$

Where H_{max} is the maximum equilibrium height and τ is the characteristic average bubble lifetime, also defined as the dynamic stability factor $\sum$ in the Bikerman test. The experimental data is then fitted to the model curve as in Figure 13,

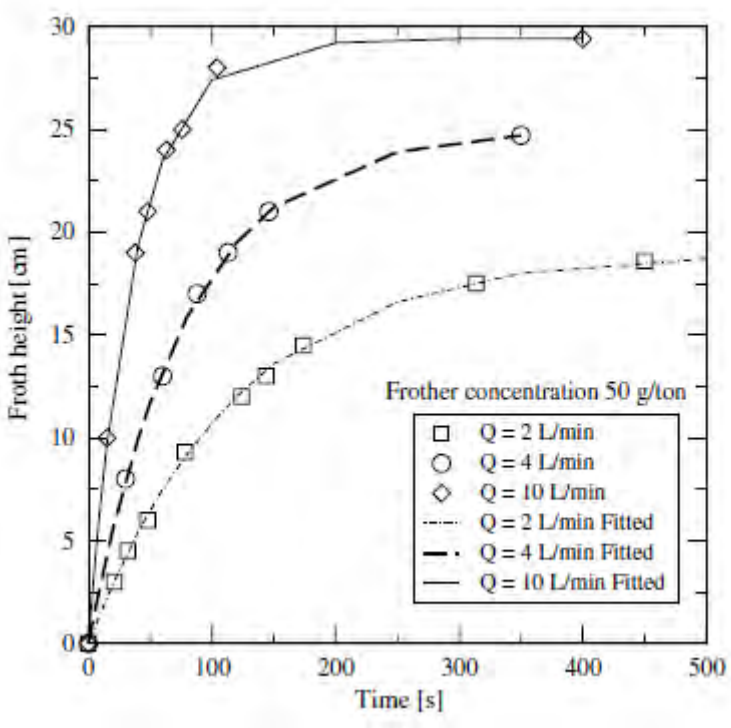

Figure 13: Equilibrium froth height as function of time for different air flowrate at 50 g/ton of frother concentration (Barbian et al., 2003).

iii. Static Tests (Froth Decay Rate)

In addition to the froth rise velocity, and dynamic stability factor, the stability of the froth can also be assessed by observing the decay of the froth with time. The froth decay is irrespective of the method applied in the froth generation and thus can also be performed in a frothing stability column (Iglesias et al., 1995). The frothing column is used to create a dynamically equilibrated froth, air supply is then cut off and agitation switched off before the froth height decay can be observed with time as in Figure 14.

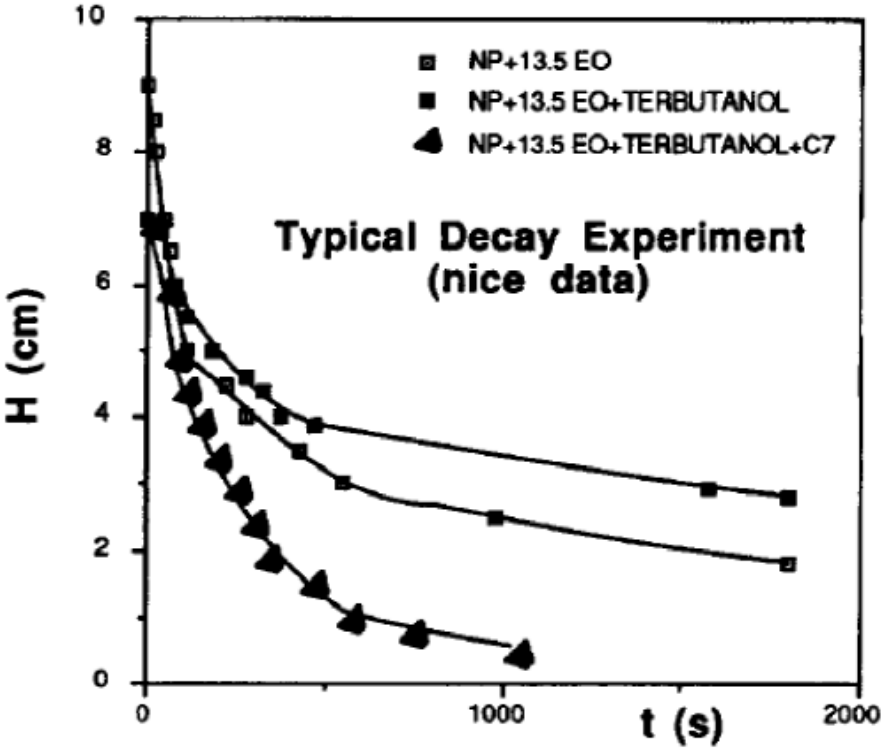

Figure 14: Variation in froth height with time during froth decay (Iglesias 1995).

The rate of change of the froth height during the froth decay can be given by,

$$\frac{\delta H}{\delta t} = -\frac{\alpha}{t} \qquad \textbf{Equation 2-3}$$

Where α is the empirical constant, and *t* is the time. If $\frac{\delta H}{\delta t} = -\frac{\alpha}{t}$

Equation 2-3 $\delta H \delta t = -\frac{\alpha}{t}$ Equation 2-3 is then integrated over the time period, the froth decay process can be described using the following:

$$\frac{H}{H_{max}} = \frac{1}{2} - \alpha \ln\left(\frac{t}{t_{1/2}}\right) \qquad \textbf{Equation 2-4}$$

Where $t_{1/2}$ is the time at which the froth is half the original height reached during the Bikerman's dynamic equilibrium method. A plot of the dimensionless H/H_{max} vs. ln $(t/t_{1/2})$ which gives straight lines, this is then used to assess froth stability (Iglesias et al., 1995).

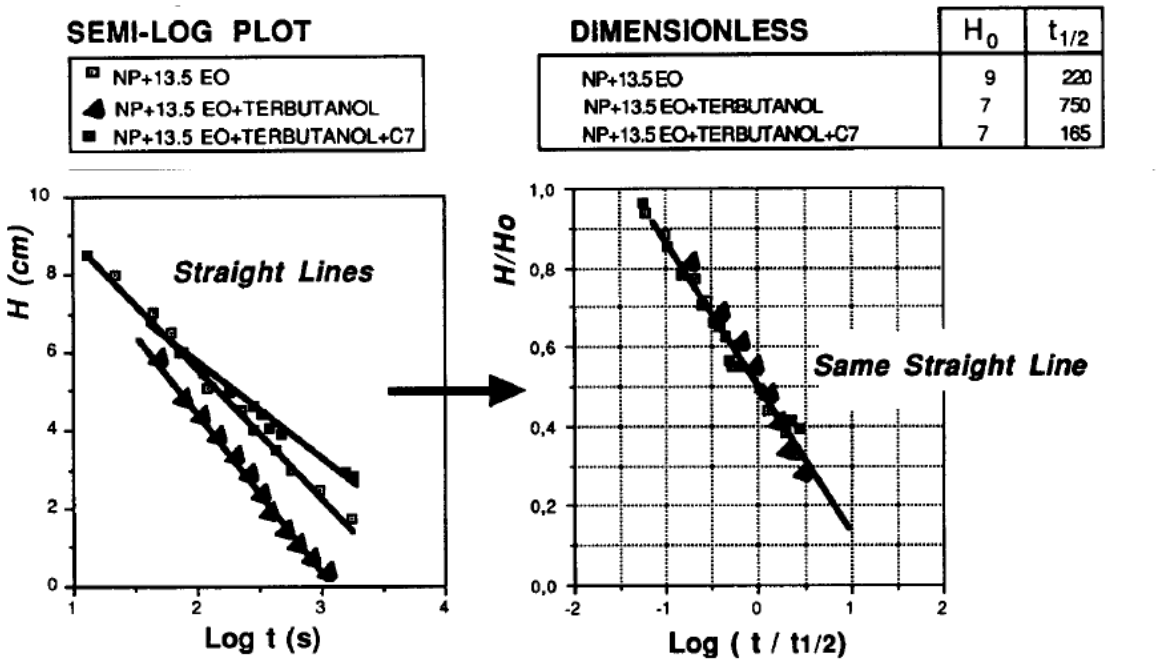

Figure 15: Data processing for the decay rate assessment (Iglesias et al., 1995).

2.3.2. Overflowing System

The overflowing system of measurement takes into consideration the continous systems. Most industrial operations are continous therefore the method is usually prefered compared to the non-overflowing system (Barbian et al., 2003).

i. Axial Sauter-mean bubble diameter profile

The rate of bubble coalescence as a measure of froth stability was proposed by (Ata et al., 2003) and measures the rate of bubble coalescence as a function of height from the pulp-froth interface to the froth surface. This froth stability proxy enables for the measurement of froth stability as defined as the ability of the froth phase to resist coalescing as it only considers coalescence in the froth zone. The average bubble size across the froth phase is then quantified using the Sauter mean diameter (d_{32}) and the (d_i)diameter of a bubble and (n_i) the number bubbles with respective bubble diameter.

$$d_{32} = \frac{\sum n_i d_i^3}{\sum n_i d_i^2}$$

The increase in bubble size with increasing distance from the pulp/froth interface shown as in Figure 16.

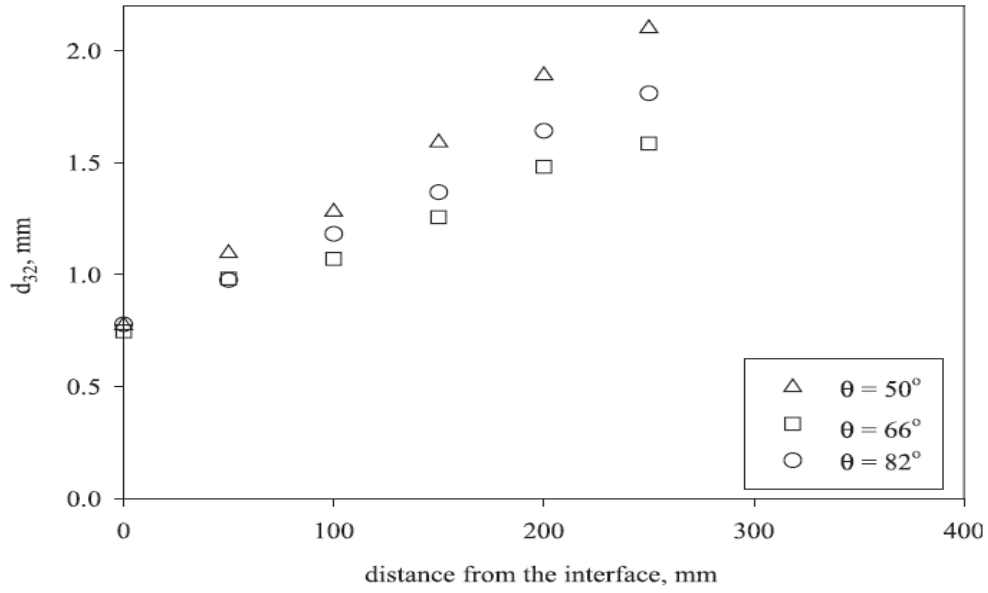

Figure 16: Variation of Sauter-mean diameter with froth height for the flotation of glass beads with different degrees of hydrophobicity (Ata et al. 2003).

From the graph, froth stability can be assessed from the gradient of the graphs, assuming the curves are straight lines. The conditions that generate the smallest gradient indicate the most stable froth, since this shows the least bubble coalescence.

ii. Top of Froth Average Bubble Diameter

With the limitations in visibility of the side of froth profile for most plant-scale operations, froth structure can be described by image analysis of the surface of the froth (Ventura-Medina et al., 2002). From the images of the top of the froth, image analysis can be used to determine the average bubble size, bubble size distribution and specific area using area-weighted averages by assuming bubbles are ellipsoids (Ventura-Medina & Cilliers, 2000). This froth stability proxy enables for the measurement of froth stability as defined as the ability of the froth phase to resist coalescing as it only considers coalescence in the froth zone. This technique was used to evaluate the effect air flowrate on froth stability as shown in Figure 17.

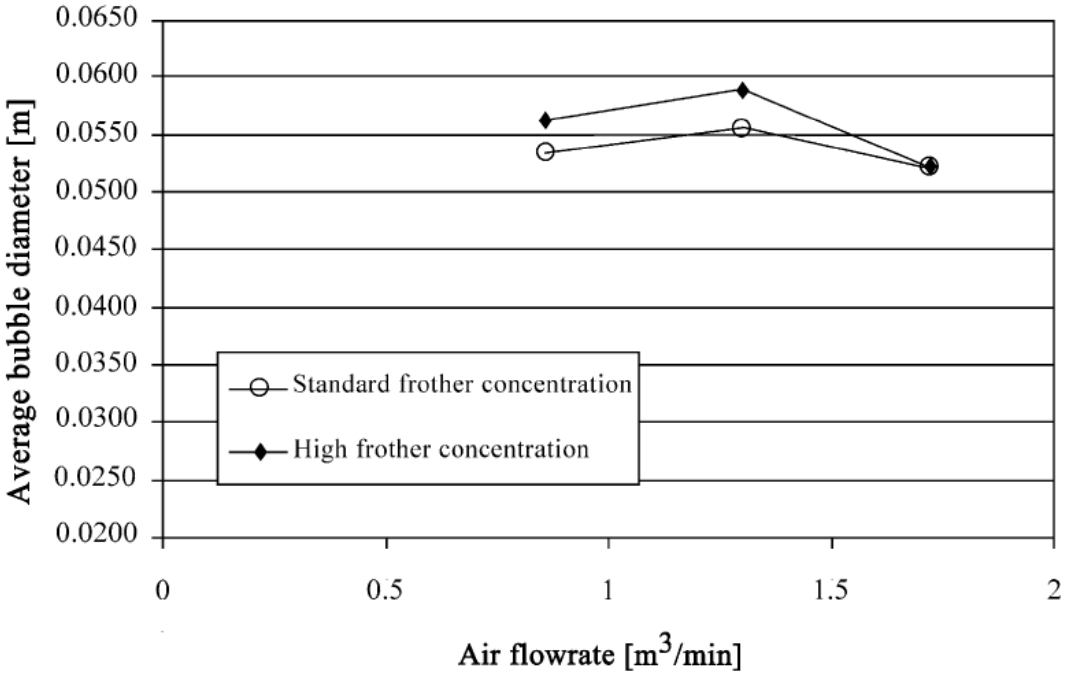

Figure 17: Graph illustrating the use of average bubble diameter to assess froth stability (Ventura-Medina et al., 2002).

There are limitations to the applicability of the use of image processing to estimate bubble size distribution as the edge-detection algorithm does not perform well for

either small or large bubbles (Ventura-Medina et al., 2002). A more sophisticated modified texture spectrum approach and a binary image based method can be used to give more accurate bubble size estimation that can even be used online (Lin et al., 2008).

iii. Top of Froth Bubble Burst Rate

The rate at which bubbles burst at the surface of the froth can be used as an indication of the stability of the froth, with a higher burst rate indicating an unstable froth. The rate of bubble bursting events can be assessed using imaging software as shown in Figure 18 which can allow for the number of bursts to be assessed after analysis of each frame of a video (Morar et a., 2012). The bubble burst rate froth stability proxy takes into consideration to a limited extent air recovery as it takes account of the number of bubbles on the froth surface bursting, on the assumption the latter are reporting to the launder thereby increasing air recovery.

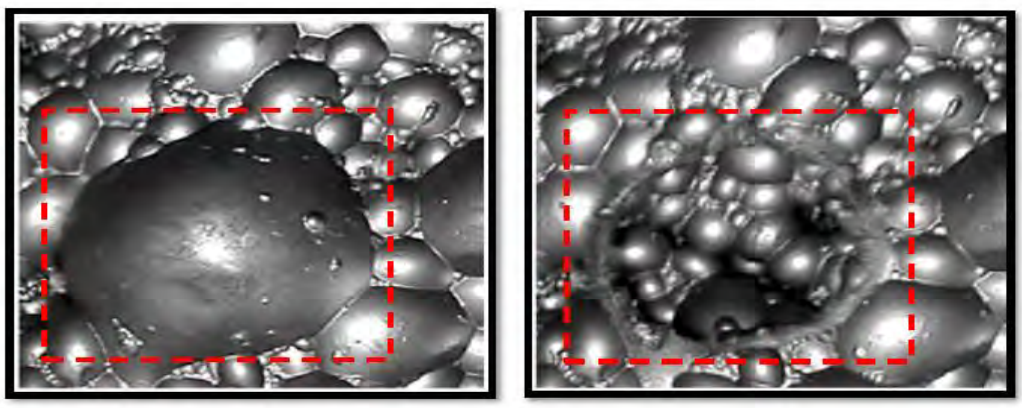

Figure 18: Illustrative pictures showing bursting in two consecutive frames (Morar et al., 2012).

Limitations have been noted on the method as it was shown that similar images can be obtained for different operating conditions (Moolman et al., 1995).

iv. Solids-Water Recovery

Water recovered to the concentrate can be used as a froth stability indicator in continuous processes. The amount of water and solids recovered during a flotation process can be used to assess the stability of the froth phase by using the solids-water recovery graphs. If the froth phase is unstable, water drains back into the pulp phase as the bubbles coalesce resulting in both lamellae and film thinning. This will

result in more bubbles bursting allowing more of the water drain back into the pulp. The decrease in the overall amount of water and solids being recovered in the concentrate can then be used as an indication of the froth stability (Corin & Wiese, 2014; Wiese et al., 2011; Tao et al., 2000). Water recovery is commonly used as froth stability proxy as it takes into account bubble coalescence in the froth phase as above stated and also the amount of bubbles reporting to the launder with water recovery measured from the launder. This therefore allows for a robust froth stability proxy.

v. Froth Recovery

The flotation process can be separated into two sections which are the pulp zone and froth zone as previously stated. Both zones of the flotation process have a significant effect on the performance of the flotation process with the major assessment tool being the overall recovery. The overall recovery can be described by the following relationship:

$$\boldsymbol{R}_{\mathrm{G}} = \frac{\boldsymbol{R}_{\mathrm{c}}\boldsymbol{R}_{\mathrm{f}}}{\mathbf{1}-\boldsymbol{R}_{\mathrm{c}}(\mathbf{1}-\boldsymbol{R}_{\mathrm{f}})} \qquad \textbf{Equation 2-5}$$

Where

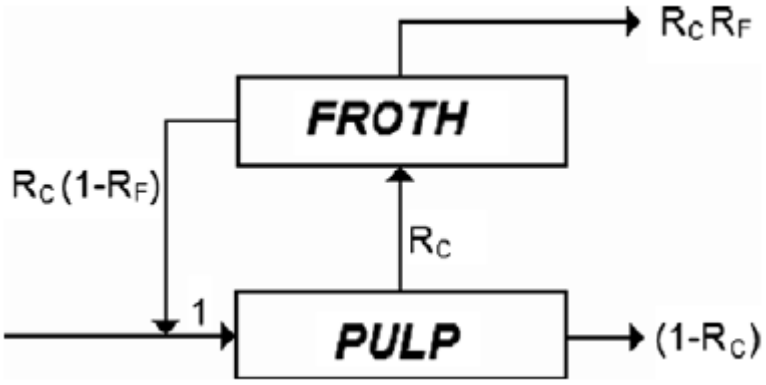

Figure

During

Froth recovery can be defined as the fraction of particles entering the froth phase attached to bubbles that are recovered to the concentrate launder as illustrated in

$Rf = \frac{mass\ flow\ to\ the\ concentrate}{mass\ flow\ into\ the\ froth}$ Equation 2-6 (Runge et al., 2010):

$$R_f = \frac{mass\ flow\ to\ the\ concentrate}{mass\ flow\ into\ the\ froth} \quad \textbf{Equation 2-6}$$

Low froth stability translates into low froth recovery as more of the attached particles are dropping back into the pulp phase reducing the overall recovery. There are three major techniques developed to measure froth recovery and these either include the actual measure of the pulp zone recovery or enable the pulp zone recovery to be determined from RG= $\frac{R_c R_f}{1-R_c(1-R_f)}$ Equation 2-5. These techniques can be grouped into the following categories (Runge et al., 2010):

- Changing Froth Depth Method
- Direct Measurement of Bubble Load
- Mass Balance Estimation of Bubble Load

a. Changing froth depth method

The method to assess froth recovery was initially proposed by Feteris et al (1987) for a continuously operated laboratory scale cell. A linear relationship was observed between the flotation rate and the froth depth. The extrapolation of the linear relationship was proposed to give the flotation rate at zero froth height and thus the collection zone flotation rate constant as no loss in recovery occurs due to the froth phase (Runge et al., 2010). The key assumptions for the methods are given as follows (Vera et al., 2002):

- Mass transfer of particles from the bulk pulp phase to the pulp-froth interface is dependent on processes occurring in the pulp phase.

- Mass transfer of particles from the froth phase to the concentrate is dependent on processes occurring in the froth phase.

Finch and Dobby (1990) developed a mathematical model with the froth recovery defined as a rate of mass transfer from the pulp to the concentrate (k) to the rate of mass transfer from the pulp to the froth phase (k_c) as in Equation 2-10:

$$R_f = \frac{k}{k_c} \qquad \textbf{Equation 2-7}$$

Since the overall first-order rate constant (k) is a function of residence time and the overall flotation recovery, the rate constant for a perfectly mixed environment can then be given by Equation 2-11 (Feteris et al., 1987; Mathe et al., 1998; Runge et al., 2010).

$$k = \frac{R_G}{\tau(1-R_G)} \qquad \textbf{Equation 2-8}$$

Where R_G is the overall recovery and τ is the mean residence time in the collection zone. As previously stated, the collection zone rate constant can then be determined by extrapolation of the linear relationship between the overall rate constant and the froth height as shown in Figure 20 (Feteris et al., 1987; Vera et al., 2002; Runge et al., 2010).

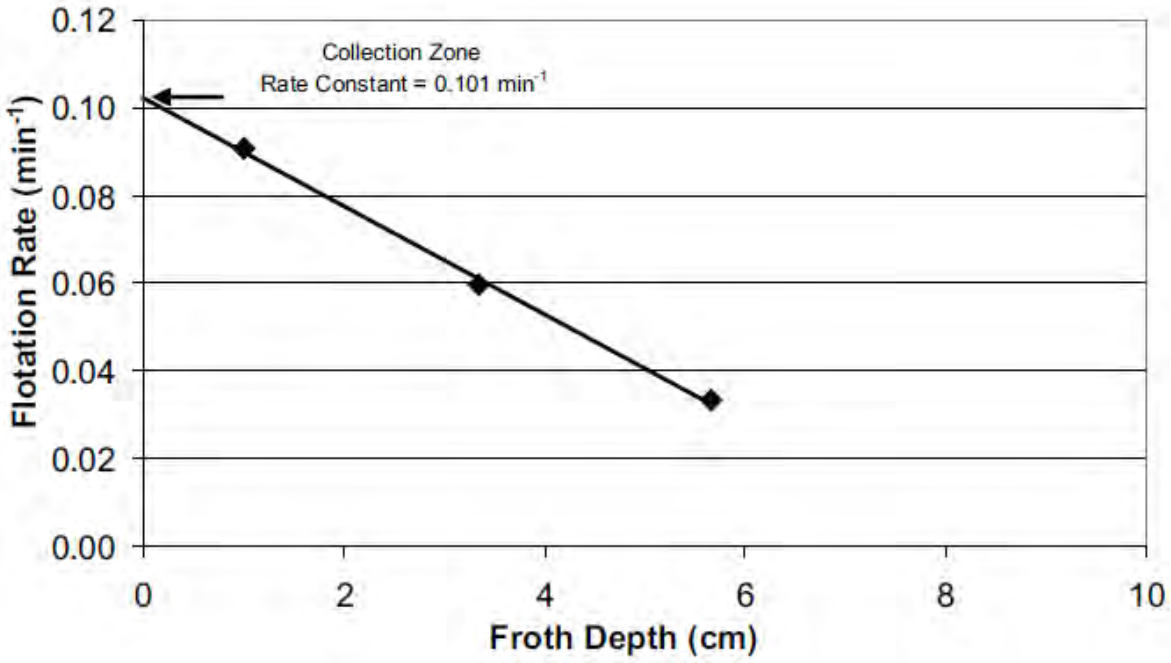

Figure 20: Using the flotation rate versus froth depth relationship to estimate the collection zone flotation rate constant (Runge, Seaman and Seaman, 2007).

The froth recovery can then be calculated as follows in Equation 2-12;

$$\boldsymbol{Rf} = \frac{\boldsymbol{k}}{\boldsymbol{k}_{\mathrm{C}}} \qquad \textbf{Equation 2-9}$$

Where R_f is the froth recovery, k is the overall rate constant and k_c is the collection zone rate constant calculated from Equation 2-11. The technique is not usually applied in full scale flotation cells successfully as the time required changing a froth height and also establishing steady state is too long (Runge et al., 2010).

Froth recovery as a froth stability proxy is based on the same principles as a recovery and hence is to measure froth stability defined as air recovery.

2.4. Entrainment in froth flotation

During the flotation process, transfer of hydrophilic gangue material into the concentrate is one of the critical factors in assessing the performance of the flotation cells as the gangue material dilutes the desired material thereby reducing the grade of the product. The transfer of the hydrophilic gangue material into the concentrate occurs through three major mechanisms namely, entrainment, entrapment and slime coating (Gaudin, 1957; Smith and Warren, 1989; Melo, 2001).

Slime coating occurs as a result of excessive grinding which results in reduced flotation rates and recovery of unwanted gangue as fine particles attached to larger particles.

The entrapment mechanism of transferring hydrophilic gangue material occurs due to gangue material being trapped between hydrophobic particles that are attached to the rising bubbles as shown in Figure 21. Entrapment of gangue minerals is common in flocculated and highly mineralised froths (Kirjavainen, 1996).

Entrainment is regarded as the major mechanism for the transfer of hydrophilic gangue material and this occurs via the unselective transport of material in the water rising from the pulp to the froth phase.

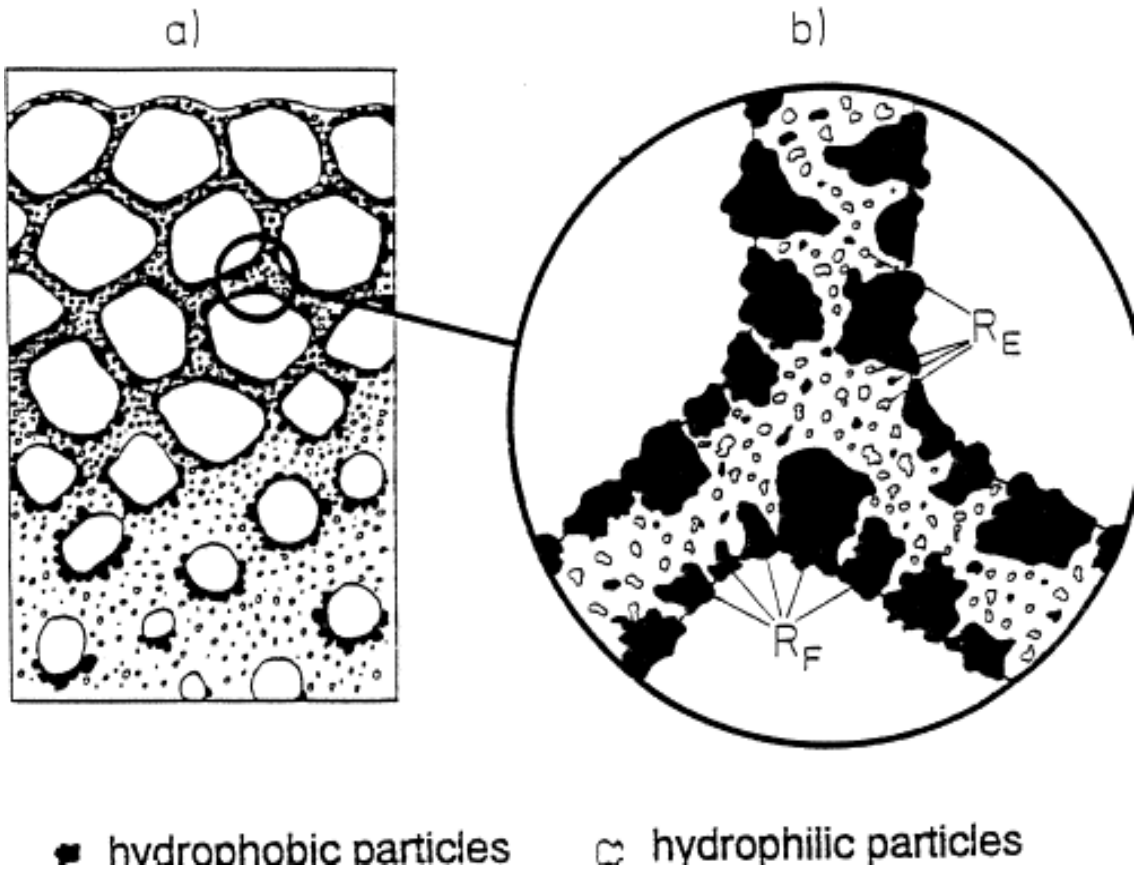

Figure 21: Flotation recovery by entrainment (Schubert., 2008). R_E is flotation recovery by entrainment and R_F is flotation recovery by true hetero-coagulation.

A number of entrainment mechanisms have been proposed and these include,

- The hydrophilic material is transported into the froth phase as a result of mechanical carryover in the water layers surrounding bubbles (Kirjavainen, 1996).
- Gangue material is transported in the wake of ascending bubbles (Savassi et al., 1997).
- Mechanical transportation of gangue material entrained in voids that exist between rising bubbles (Savassi et al., 1997; Moyo, 2005).

It has been shown that the amount of entrained gangue recovered is proportional to the amount of water recovered. The proportionality between the fractional gangue recovery and the fractional water is then often referred to as the entrainment factor or degree of entrainment (Neethling & Cilliers., 2009; Smith & Warren, 1989; Savassi et al., 1997). In the assessment of Upper Group 2 (UG2) ore, chromite is used to

assess entrainment as it is a naturally hydrophilic gangue mineral which is present in substantial amounts.

2.5. Summary of the Literature Review

From the literature review, the various particle properties that affect froth stability were analysed and mechanisms for stabilisation by particles of froths were reviewed. The various methods that were used to assess froth stability were also described. It was established that there exists a qualitative understanding of the effect of particle size and solids concentration on the froth stability, but quantitative relationships have not been established. As a result, more work on trying to assess the quantitative effect of particle size on the froth stability is required. It was also established that no one standard method of assessing froth stability was employed and thus a more comprehensive assessment of the various methods to quantify froth stability was to be performed. Froth stability for the non-overflowing system was then evaluated using the froth stability factor, average bubble lifetime and the froth decay rate. For the overflowing system tests, froth stability was evaluated using water recovery and froth recovery. The image analysis techniques to measure froth stability were also employed for the overflowing tests namely the axial sauter-mean bubble diameter profile and the top of froth average bubble diameter to evaluate froth stability defined as the ability of the froth to resist coalescing. From the literature review, the hypotheses in section 2.6 were formulated.

2.6. Hypotheses

i. Froth stability increases with a decrease in solids particle size per unit mass during a flotation process.

- As the particle size decreases, the maximum capillary pressure for the bubbles increases thereby increasing froth stability.
- A decrease in the size of the non-adsorbed particles in the interfilm fluid will result in increased viscosity and reduced drainage rates thereby increasing froth stability.
- As the particle size decreases, the surface area per unit mass of solid particles increases thereby increasing the interaction area between the particles and the bubbles.
- The decrease in particle size also increases the packing efficiency of the solid particles on bubble films thereby increasing froth stability.

ii. An increase in the solids concentration between 15 – 25% will result in an increase in froth stability.

- An increase in the solids concentration in the pulp will result in increased bubble loading. This will result in an increased steric boundary of particles available to stabilise the froth.

Chapter 3. RESEARCH APPROACH and EXPERIMENTAL DETAILS

3.1. Research Approach Overview

This project investigated the effect of particle size on the froth stability. Two mineral ores were used at different grinds (D_{80}) and pulp solids concentration.

3.2. Particle Size Reduction and Classification

3.2.1. Mineral Ore types

Two mineral ores were used for this investigation, namely Lonmin UG2 ore and Itabirite haematite ore (Vale, Brazil). The UG2 ore was chosen since it is a PGM bearing ore that is sparsely mineralised and is known to routinely result in froth recoveries less than 10% (Crosbie *et al*, 2009). On the other hand the iron ore was obtained as a deslimed sample of feed to float which consisted of 43% Fe and 36% SiO_2 which would be expected to result in higher solids loading.

a. Lonmin UG2 PGM-bearing Ore

The ore is mined from the Lonmin Platinum's Marikana Operation, which is located on the Rusternburg Layered Suite of the Western Limb of the Bushveld Igneous Complex about 70km northwest of Johannesburg, South Africa. The UG2 reef is a PGE bearing chromitite layer which is situated variably between 20 m to 400 m below the Merensky Reef. The major mineral constituents of the UG2 are chromite (~60wt.% to 90wt.%), orthopyroxene (~5wt.% to 30wt.%) and plagioclase (~1wt.% to 10wt.%) (Vermaak,1995). The minor mineral phases of the UG2 are phlogopite, biotite, clinopyroxene, ilmenite, rutile, magnetite and base metal sulphides. There are also secondary minerals present namely quartz, talc and serpentine (McLaren & De Villiers, 1982).

The major base metal sulphide assemblage is constituted by chalcopyrite, pyrrhotite, pyrite, pentlandite and, to a lesser extent, millerite. These occur interstitially within the silicates and, rarely, enclosed in chromite (McLaren & De Villiers, 1982). The PGEs are found in mineral assemblages ranging from sulphide to non-sulphide minerals, with the sulphide minerals including laurite (RuS2), cooprite (PtS),

malanite, braggite, and vysotskite in some cases. The non-sulphide minerals are constituted by Pt-Fe alloys, tellurides, bismuthinides, bismuthotellurides of Pt and Pd, PGE arsenides and sulphoarsenides. Table 1 shows the different particle sizes and solids concentrations used in the testing of the UG2 ore.

Table 1: Experimental conditions tested for the Lonmin UG2 Ore.

Conditions	Values
Particle size (D80 µm)	78, 88, 104, 127, 157 (µm)
Solids concentration	15, 20, 25 (%)

b. Itabirite (Iron) Ore

The term Itabirite originated from the high grade massive specular haematite ore from the Pico de Itabirito mine district in the state of Minas Gerais, Brazil. The ore contains 66-69% haematite in silica (Roberts, 1965). The haematite ore was formed through metasomatic replacement of quartz in the Itabirite resulting in the formation of canga, ocher, and laterite due to supergene processes. The Itabirite ore is usually mined with alternating laminae of quartz and haematite; with each composite sufficiently pure to give the rock a black and white banded appearance as shown in **Error! Reference source not found.**.

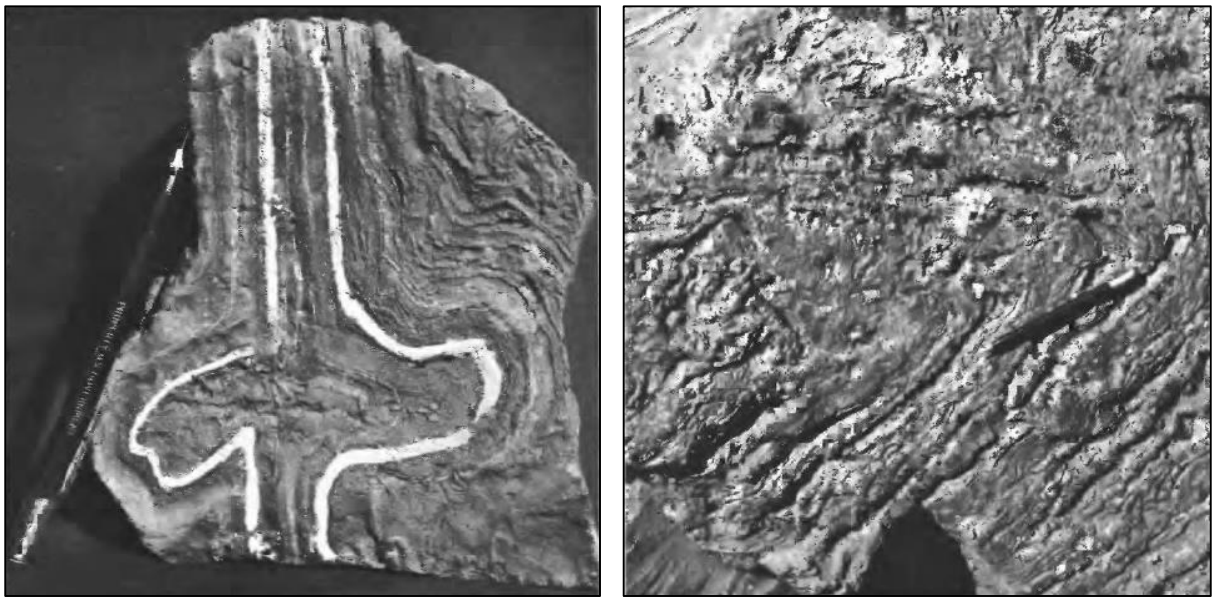

Figure 22: Image of itabirite completely replaced by haematite (left) and a compact haematite ore from Pico de Itabirato (Roberts, 1965).

The Pico de Itabirito district contains vast iron resources in the Itabira Group, mostly the Caue Itabirite. The ore is mainly haematite which occurs in deposits that can be classified as: (a) massive high-grade hard hematite, (b) high-grade soft or disaggregated masses of hematite, (c) intermediate-grade iron ore, (d) enriched itabirite, (e) rolado or eluvial deposits consisting of an aggregate of uncemented pebbles, cobbles, and boulders of hard haematite, and (f) canga, a type of hardpan consisting of fragments of hard haematite cemented by limonite.

The high-grade haematite ore is largely ferric oxide (66% or more) and small amounts of silica and alumina which is generally less than 2%. The silica is present as quartz and the alumina as clay, kaolin, talc and tourmaline. The maximum sulphur content was shown to be 0.04% (Roberts, 1965). Manganese appears only as traces in chemical analyses of the ore with phosphorus also appearing but in less than 0.05% of the high grade ore body (Roberts, 1965). Table 2 shows different particle sizes and solids concentrations used in the testing of the Itabirite (Iron) ore.

Table 2: Experimental conditions tested for the Itabirite (Iron) Ore.

Conditions	Values
Particle size (D80 µm)	48, 65, 87, 118 (µm)
Solids concentration	15, 20, 25 (%)

3.2.2. Milling Equipment

a. Milling Equipment Setup

In order to obtain the desired particle sizes shown in Table 1 and Table 2, a SALA stainless steel rod mill was used for the milling of the ore. The mill had an internal diameter of 30 cm and a length of 30 cm. The mill utilises 22 stainless steel rods that are each 28.5 cm long and 25 mm in diameter. The mill is operated at a rotational speed of 77.1 rpm. The setup of the mill is shown in Figure 23.

Figure 23: Setup of the 3 kg SALA stainless steel rod mill

The particle size distribution of the mill products was assessed using the Malvern sizer that utilizes laser diffraction to achieve particle size. Standard screens were also used for particle size assessment using wet screening. The standard screen sizes were used for the assessment at the following aperture sizes: 25 µm, 38 µm, 53 µm, 75 µm, 106 µm, 125 µm, 150 µm, 212 µm, 300 µm.

b. Milling Equipment Procedure

The mill was loaded with the rods and the respective ores added. The UG2 ore was added at 2.7 kg per load and the Iron ore added at 1.25 kg per load. Plant water was added to make up 66% solids density. No reagents where added into the milling stage. The ore was then milled at various milling times to give the desired particle sizes shown in **Error! Reference source not found.** Table 3 and Table 4**Error! Reference source not found.** that were fed into the flotation equipment.

Table 3: Milling times for the UG2 ore feed grinds

UG2 Ore Grinds	Flotation Feed D_{80}
30min-grind	78.4
25min-grind	87.8
20min-grind	103.9
15min-grind	127.3
10min-grind	157.2

Table 4: Milling times for the Iron ore feed grinds

Iron Ore Grinds	Flotation Feed D_{80}
0min-grind	118.0
2min-grind	87.0
5min-grind	65.0
10min-grind	48.0
15min-grind	35.0

3.2.3. Size Classification (Rosin Rammler Distribution)

With the desired particle size obtained for the two ores tested, a full assessment of the particle size distributions was done in order to confirm if the various size classifications were substantially different. In order to do so, Rosin Rammler distributions were used to assess the full PSDs.

The size distributions were initially expressed as a percentage by weight of each size fraction (a differential distribution, as the cumulative percentage of sizes below a

given value - (undersize) and as the cumulative percentage of size above a given value – (oversize) (Rosin-Rammler, 1933).

In order to get a mass fraction distribution F(ø) of in-between the given mesh sizes and the density function f(ø), the Rosin Rammler (RR) and the Gates-Gaudin-Schulmann (GGS) mathematical models were applied to the PSD data. The general expression for the RR model is given as:

$$\boldsymbol{F(ø) = 1 - \exp\left[-\left(\frac{ø}{l}\right)^{m}\right]} \qquad \textbf{Equation 2-10}$$

Where, F(ø) is the distribution function, and ø is the particle size (mm), l is the mean particle size (mm), and m is a measure of the spread of particle sizes. l and m are adjustable parameters characteristic of the distribution (Marcias-Garcia et al., 2004). The model can then be re-arranged as:

$$\boldsymbol{\ln\{-\ln[1 - F(ø)]\} = m \ln ø - m \ln l} \qquad \textbf{Equation 2-11}$$

A plot of the left term against the natural logarithm of ø should result in a straight line with slope m if the material fits the RR model (Marcias-Garcia et al., 2004). The assessment of the straight line is usually done via linear regression to determine if the RR distribution is applicable to the data points. If a straight line is established, m and l can then be determined from the slope and intercept of the line.

The RR density function model can then be used to predict the full particle size distribution as shown in Figure 24 (Marcias-Garcia et al., 2004).

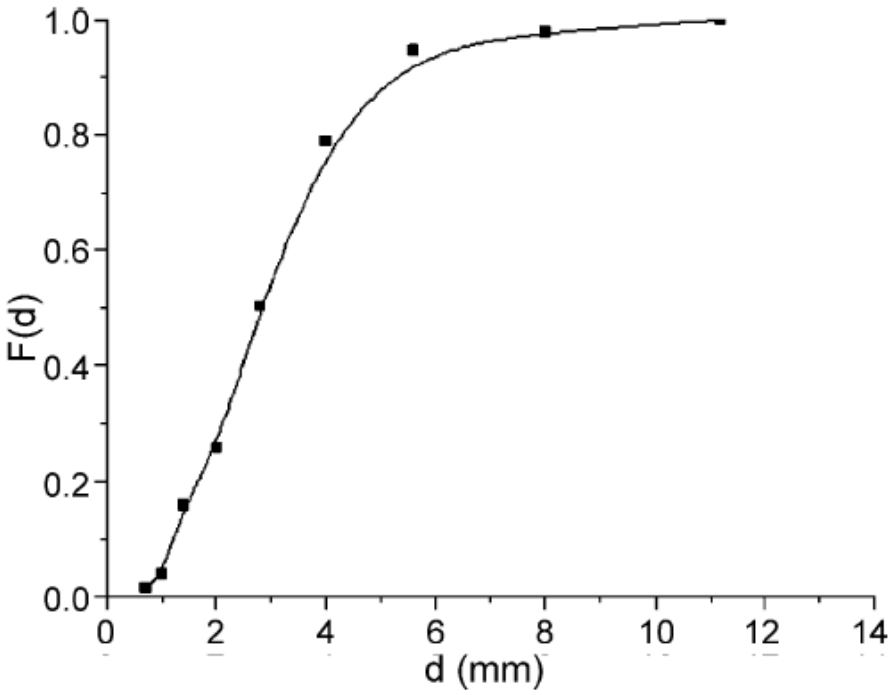

Figure 24: Plot of the distribution function vs particle size (Marcias-Garcia et al., 2004).

From the distribution function plots, the various grinds were then assessed if the full PSDs were substantially different. This method was applied to both the UG2 ore and Iron ore grinds.

3.2.4. Particle Specific Surface Area

A relationship between particle size and the specific surface area of particles has been shown based on the specific area determined by the BET technique (Brunauer, Emmett & Tell, 1938). An inverse relationship exists between specific surface area and particle size as follows,

$$\boldsymbol{d} = \frac{\propto}{\boldsymbol{A_{BET}\,\rho}} \qquad \textbf{Equation 2-12}$$

Where d = particle diameter; α = shape factor (6 ≤ α ≤ 18), α = 6 for spherical particles; A_{BET} = specific surface area as determined by the BET technique; and ρ = particle density (Jiqiao & Baiyun, 2001). This relationship was utilised in certain cases where surface areas of ores could not be obtained by Malvern Mastersizer 3000 laser particle size analyser. This will be discussed in more detail in the relevant sections.

3.3. Flotation Reagents

3.3.1. Lonmin UG2 Ore Reagents

Three reagents where used for the flotation tests performed using the UG2 ore, namely, frother, collector and depressant.

Frother

A polyglycol type frother by the name DOW 200 was used for the flotation tests. The polyglycol frother was supplied by Betachem in liquid form at purity close to 100%. The critical coalescence concentration of the frother is 17.3 ppm (Grau et al., 2005) and all flotation tests were done at a dosage above the CCC.

Collector

Sodium isobutyl xanthate (SIBX) was used as the collector for the UG2 ore flotation tests. The SIBX frother used is supplied by Senmin in powder form at purity close to 90%. The preparation of the collector entails dissolving the powder to make up a 1% solution using deionised water before being dosed into the slurry at the respective dosages.

Depressant

Sendep 348 was used as the depressant for the UG2 ore flotation tests and was supplied by Senmin. The depressant is a modified guar gum and is supplied in powdered form. It is supplied at 92% purity and 7.02% insoluble material. The depressant was dissolved and made up to 1% solution using deionised water.

3.3.2. Itabirite (Iron) Ore Reagents

Two reagents were used for the flotation tests performed using the iron ore namely the collector and the depressant. No frother was used for the tests as the collector used has frothing properties.

Collector

The

Depressant

A

i. Weigh approximately 2g of starch in a previously weighed 150 ml beaker containing a magnetic agitation bar.
ii. Add 20 ml of distilled water and put on a magnetic stirrer.
iii. Turn on the agitation (magnetic agitator) and add 1 ml of 50% NaOH.
iv. Keep agitating the solution until gelatinisation occurs (turns from opaque to clear) and then add 80 ml of distilled water.
v. Return the beaker to the weigh balance and add distilled water until 100g.

3.3.3. Water (Synthetic Plant Water)

The

Table

Ions	**Concentration (ppm)**
Ca^{2+}	80
Mg^{2+}	70
Na^{+}	153
Cl^{-}	287
SO_4^{2-}	240
NO_3^{-}	176
NO_2^{-}	-
CO_3^{2-}	17

Flotation tests on iron ore were performed using deionised water.

3.4. Equipment and Flotation Procedures

3.4.1. Non-Continuous Stability Column

a. Stability Column Setup

The

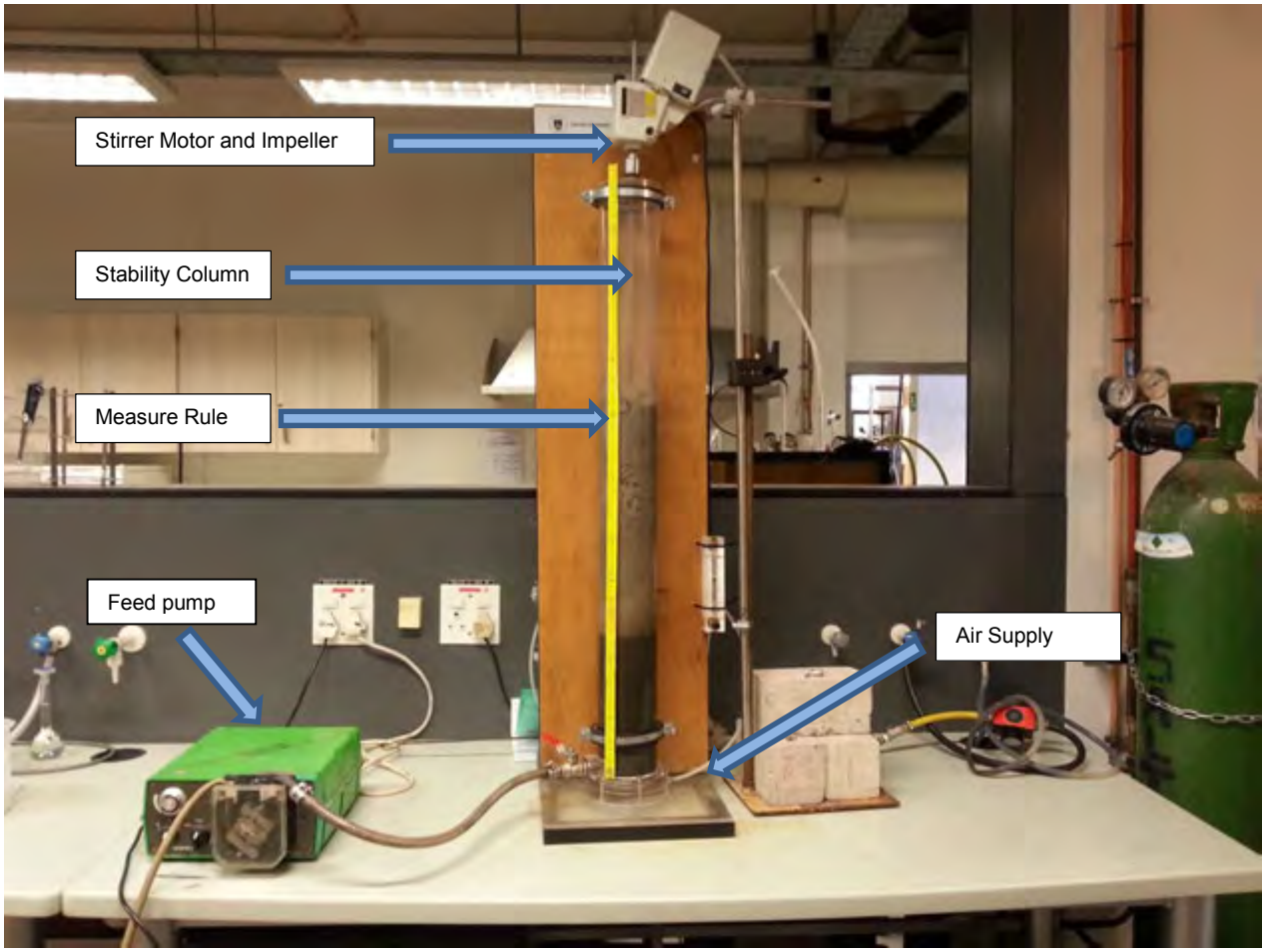

Figure

b. Stability column size classes tested

Size

c. Stability column reagent dosages

The

Table

Reagent	Name	Stability Column Dosages
Frother	DOW 200	60 (ppm)
Depressant	Sendep 348	100 (g/t)
Collector	SIBX	80 (g/t)

Table

Reagent	Name	Stability Column Dosages
Depressant	Starch Solution	500 (g/t)
Collector	Flotigam EDA	150 (g/t)

The frother dosage was based on the amount of water in the slurry made for each experiment. The dosages for the depressant and the collector were based on the amount of ore in the slurry.

d. Stability column scoping experiments

Initial

Scoping

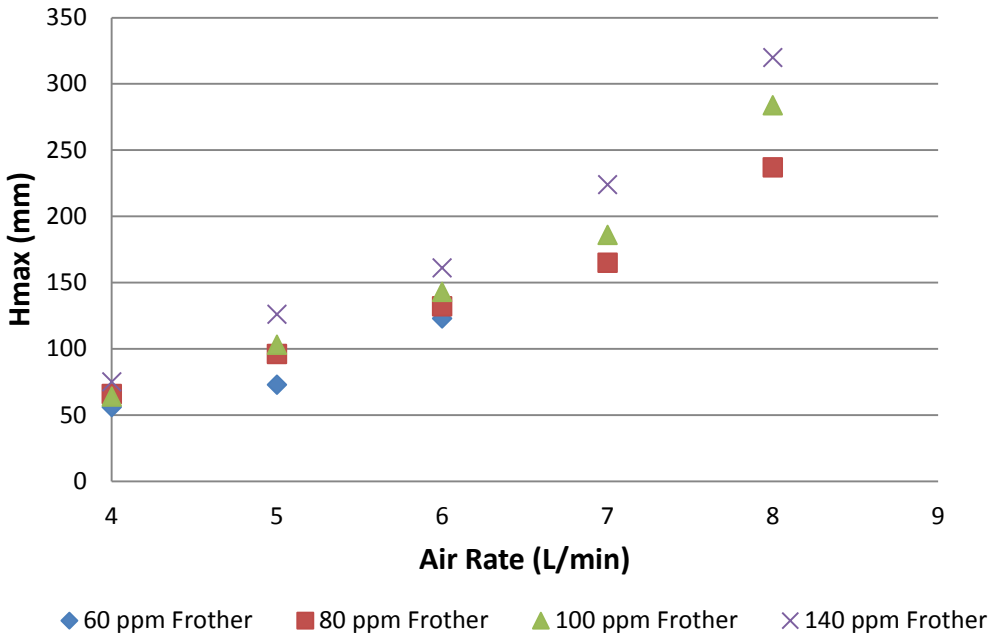

Figure

From

e. Stability column operating procedure

For the assessment of froth stability using the frothing column, three parameters were used for the analysis namely ∑ (froth stability factor), froth rise velocity and froth decay rate. The parameters gave a comprehensive overview of the froth stability variations.

The

Step

1. Using the respective milling times for the different ores (Lonmin UG2 Ore and Itabirite Ore), the ore slurries were milled to achieve the required particle size distribution.

2. The mill products were then diluted with synthetic plant water to give slurry of the desired pulp density (15%, 20% or 25%).

3. This slurry was then transferred into a continuously agitated slurry tank and left for 5 minutes to ensure a uniform pulp density.

4. The depressant, collector and then frother were added at 3 minute intervals in that order (no frother for iron ore). The slurry was then allowed to condition for a further 5 minutes.

5. The slurry was then pumped using a peristaltic pump into the frothing column, filling the column up to the 30 cm mark.

6. The air supply and timer where then switched on with a constant flow rate of air of 6 l/min. (This allows for a standard superficial gas velocity (Jg) established in scoping tests).

7. The height of the rising froth was then measured at 5 second intervals until the equilibrium maximum height was maintained for at least 30 seconds.

8. The air supply was then switched off and the decaying froth height measured at 2 second intervals for 30 seconds.

All

3.4.2. Agitated Hybrid Column Cell

a. Agitated Hybrid Cell Review

With

The

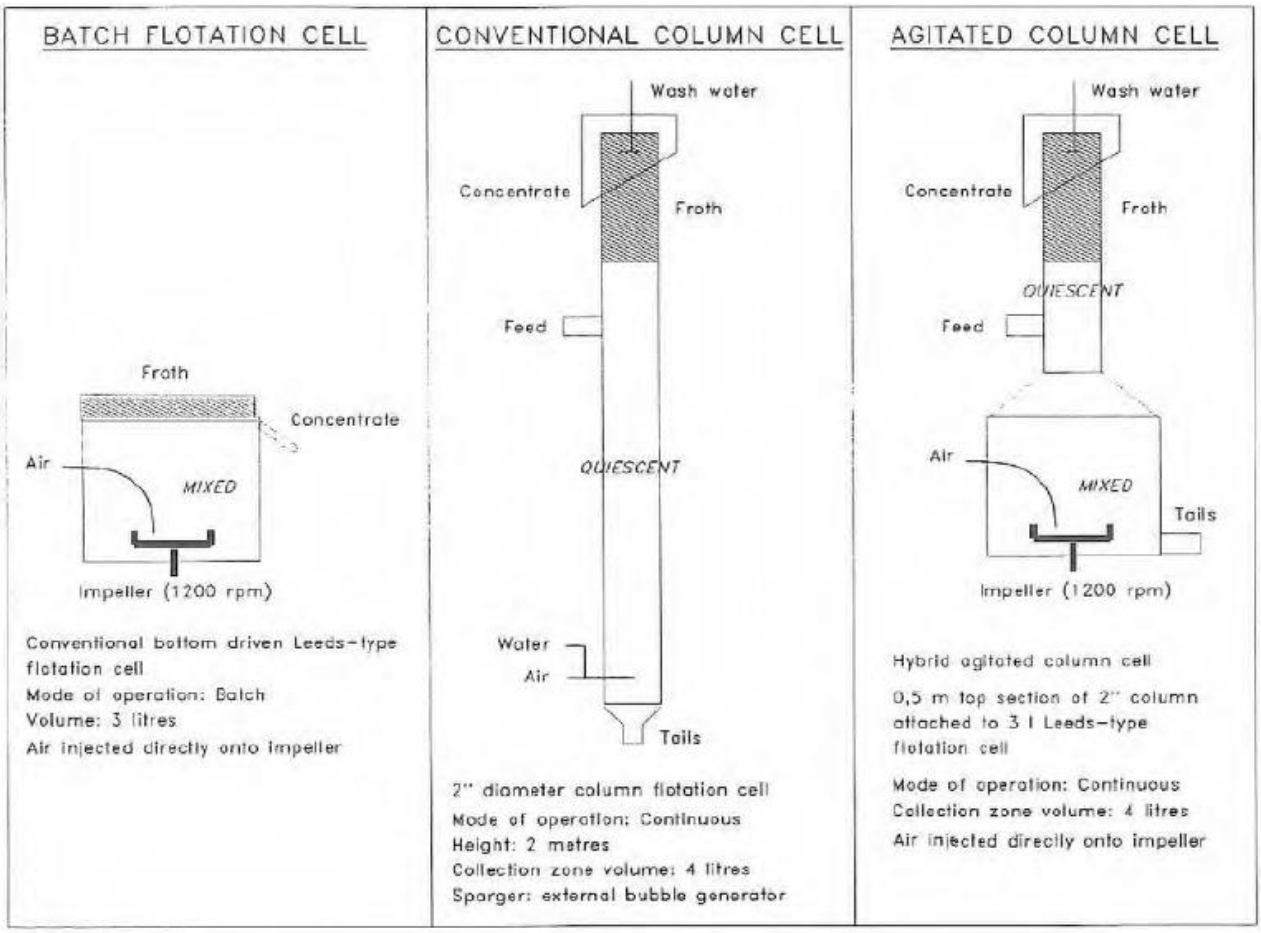

Figure

The

The

b. Agitated Hybrid Cell Setup

The

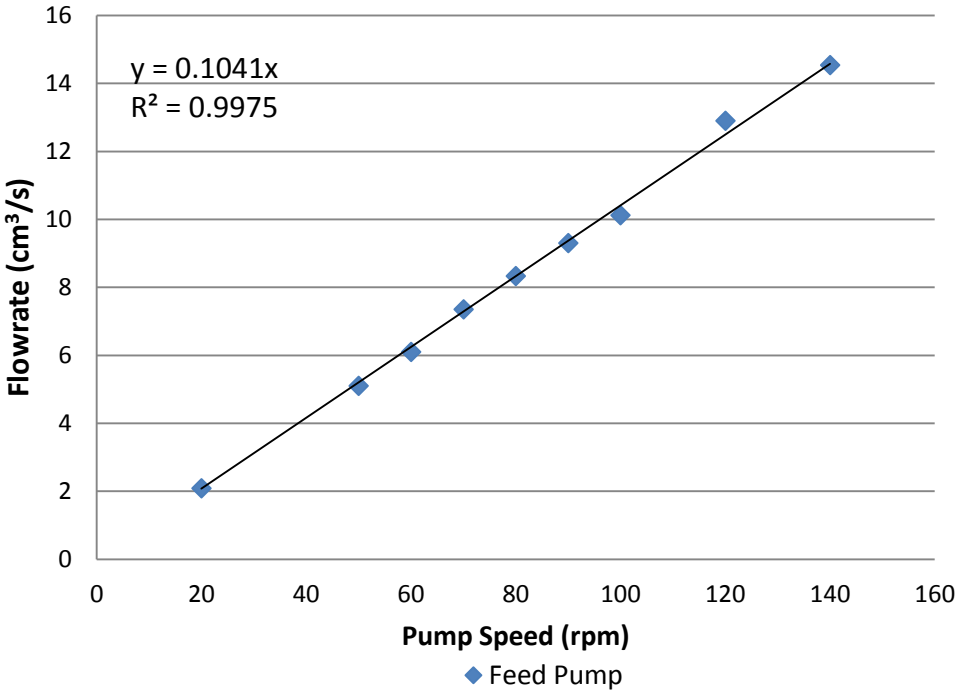

Figure

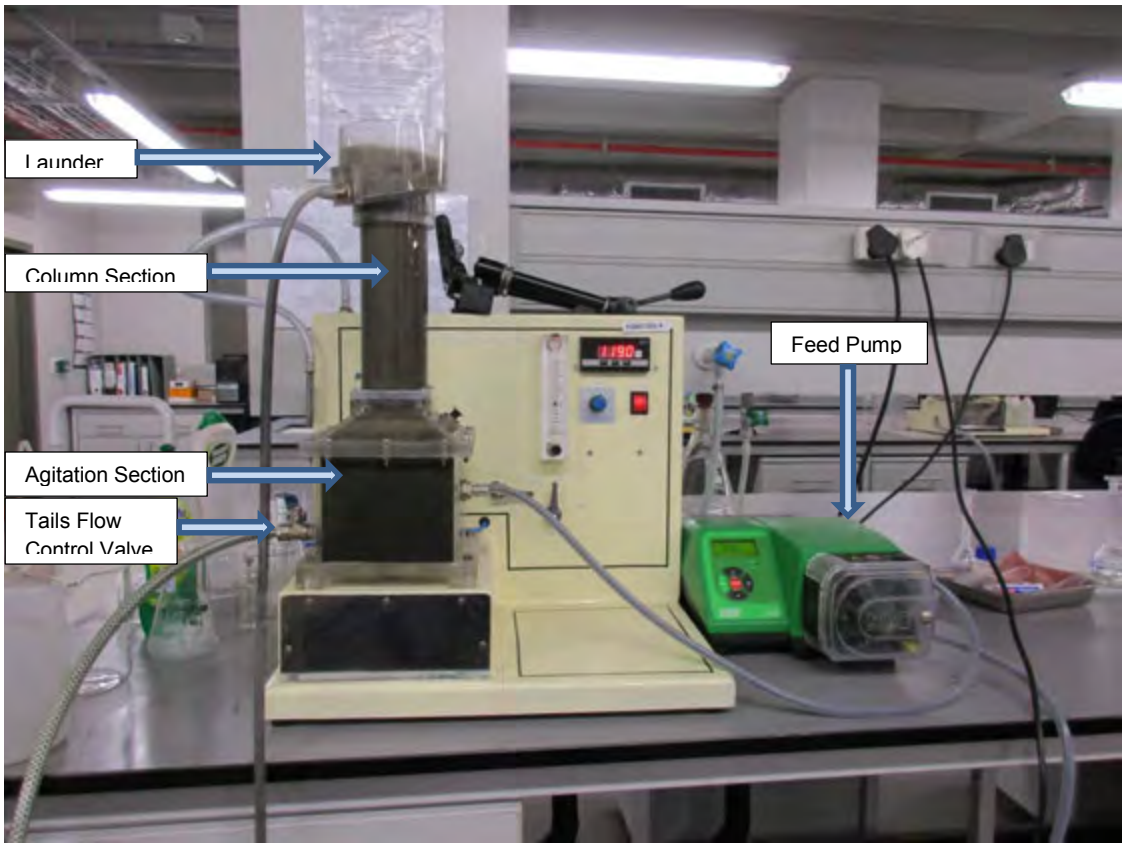

Figure

c. Agitated column cell size classes tested

Flotation

Table

Conditions	Values
Particle size (D80 µm)	78, 88, 104, 127, 157 (µm)
Froth depths	10, 15, 25 (cm)
Solids concentration	25 (%)

Table

Conditions	Values
Particle size (D80 µm)	48, 65, 87, 118 (µm)
Froth depths	10, 20, 25 (cm)
Solids concentration	25 (%)

d. Agitated hybrid cell reagent dosages

The

Table

Reagent	Name	Hybrid Cell Dosages
Frother	DOW 200	25 (ppm)
Depressant	Sendep 348	100 (g/t)
Collector	SIBX	80 (g/t)

Table

Reagent	Name	Hybrid Cell Dosages
Depressant	Starch Solution	750 (g/tonne)
Collector	Flotigam EDA	50 (g/tonne)

The

e. Agitated Hybrid cell flotation procedure

The

Step by Step Procedure

1. An 8.1 L batch of milled ore slurry at the desired solids concentration and particle size distribution was transferred into the feed tank and agitated for 3 minutes to ensure uniform mixing.

2. The depressant, collector and frother (no frother for iron ore) were added to the slurry in this order at 2 minute intervals and allowed to condition for a further 5 minutes.

3. The feed peristaltic pump was switched on at a flowrate of 0.5 l/min.

4. The impeller was switched on at a pre-set rotational speed of 1200rpm.

5. After the slurry level had reached the desired level at the base of the column section, the tails flowrate was adjusted using the tails valve so as to maintain the 3L slurry volume.

6. The air flow into the cell was then switched on at an air rate of 4 l/min with a Jg of 1.7 cm/s.

7. The system was then allowed to run in closed circuit for 30s, before the tails flowrate was adjusted again to maintain the 3L slurry volume.

8. After the slurry level had been maintained for at least 2 minutes, the system was then open-circuited and left for 8 minutes (2 residence times) to reach steady state.

9. A 40 ml feed sample was then collected using a 50ml disposable syringe.

10. Pictures of the side and top of the froth were then taken subsequently.

11. Samples (Concentrate and Tails) were then collected as per time intervals stated below;

0

1 min Collect C2 and T2 (1 min)

2 min Collect C3 and T3 (1 min)

3 min Collect C4 and T4 (1 min)

12. A second set of pictures of the side and top of the froth were then taken before shutting down the equipment.

13. The wet samples where weighed before being filtering and dried. The final dry samples were weighed before being sent for metallurgical analysis.

The experiments were performed in duplicate.

Metallurgical assays were done by fire assay and ICP-OES for the platinum group metals and chrome in the UG2 ore and by fused bead XRF for the Fe and Si in the Itabirite ore.

3.5. Image capturing equipment

The

3.6. Data Analysis Procedures

3.6.1. Froth Stability Factor Analysis

The froth stability factor was calculated by measuring the maximum equilibrium height. The stability factor was calculated by dividing the maximum froth height H_{max} = $\boldsymbol{H}_{\max}\boldsymbol{J}_{g}$ Equation 3-13 ;

$$\sum = \frac{\boldsymbol{H}_{\max}}{\boldsymbol{J}_{g}} \qquad \textbf{Equation 3-13}$$

3.6.2. Froth Rise Velocity

The froth rise velocity was determined by measuring the froth height at 5 second intervals until the equilibrium maximum froth height was reached. The froth height data over time data was fitted to $\boldsymbol{H}=\boldsymbol{H}\max * \left(\mathbf{1}-\boldsymbol{e}^{-\frac{\boldsymbol{t}}{\tau}}\right)$ Equation

3-14 using a regression tool (Excel Solver) that makes use of the principle of least squares. The maximum froth height, H_{max}, and froth stability (τ) were fitting parameters.

$$\boldsymbol{H = H_{\max *}\left(1 - e^{-\frac{t}{\tau}}\right)} \qquad \textbf{Equation 3-14}$$

3.6.3. Froth Decay Rate

The froth decay rate was determined by measuring the height of the froth after the air supply was shut off once the equilibrium maximum froth height was reached. The froth height was measured every 2 seconds until the whole froth had decayed. The froth height data over time was then fitted to $\boldsymbol{Hf}$$\boldsymbol{H}$fmax$= \boldsymbol{\frac{1}{2} - \alpha \ \ln\left(\frac{t}{t_{1/2}}\right)}$

Equation 3-15 using the regression tool (Excel Solver) that makes use of the principle of least squares. A proxy for froth stability (α) was then determined.

$$\boldsymbol{\frac{Hf}{H_{fmax}} = \frac{1}{2} - \alpha \ \ln\left(\frac{t}{t_{1/2}}\right)} \qquad \textbf{Equation 3-15}$$

3.6.4. Top of Froth Sauter-mean Bubble Size

The top of froth average bubble size was determined by using image processing software ImageJ. The launder diameter of 12 cm was used as a reference length to determine the number of pixels per unit length as shown in Figure 30. The diameter of individual bubbles was then measured by hand using the reference length as shown in Figure 31. A total minimum of 500 bubbles were measured in each of the two repeat experiments to give the average bubble size. Half of the bubble sizes were measured in the image taken at the beginning of the experiment and the other half, from the image taken at the end of the experiment.

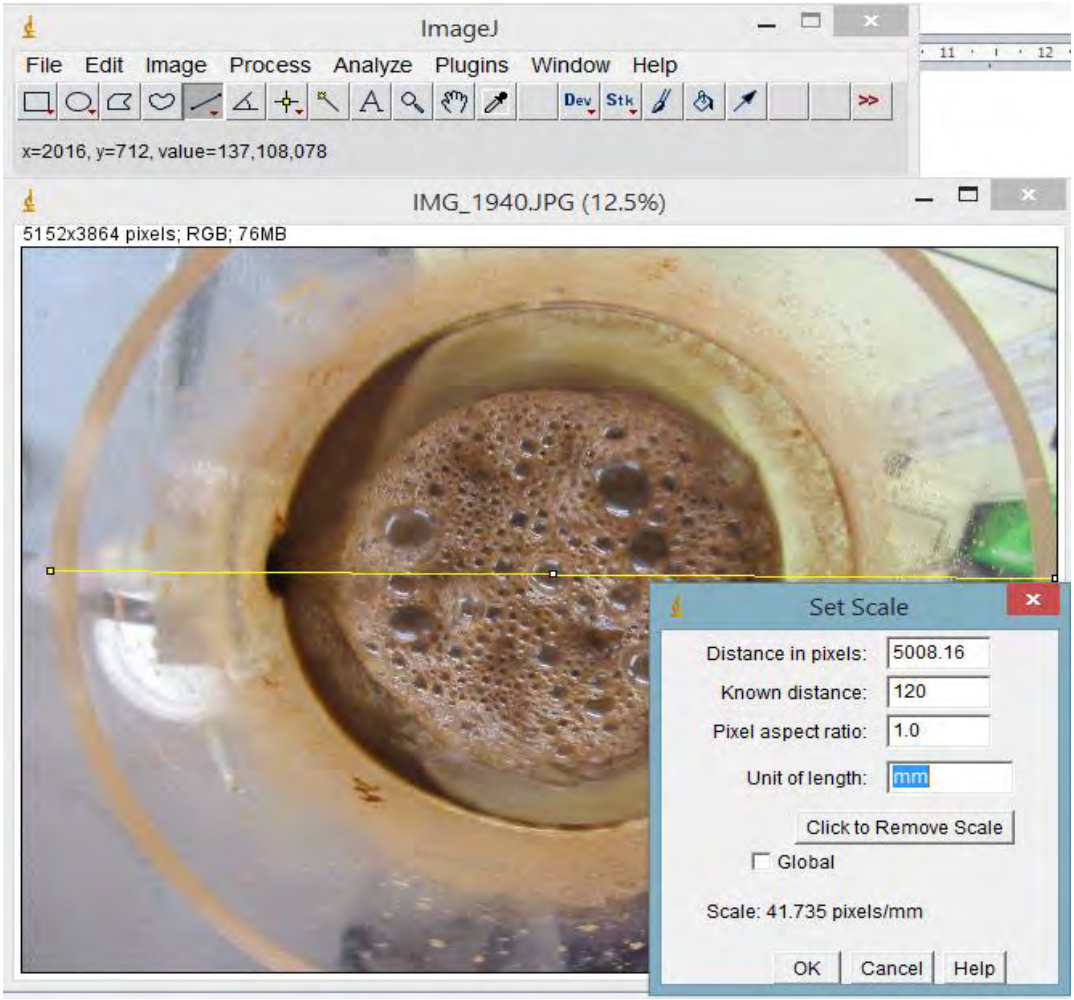

Figure 30: Establishing of the reference length (Scale).

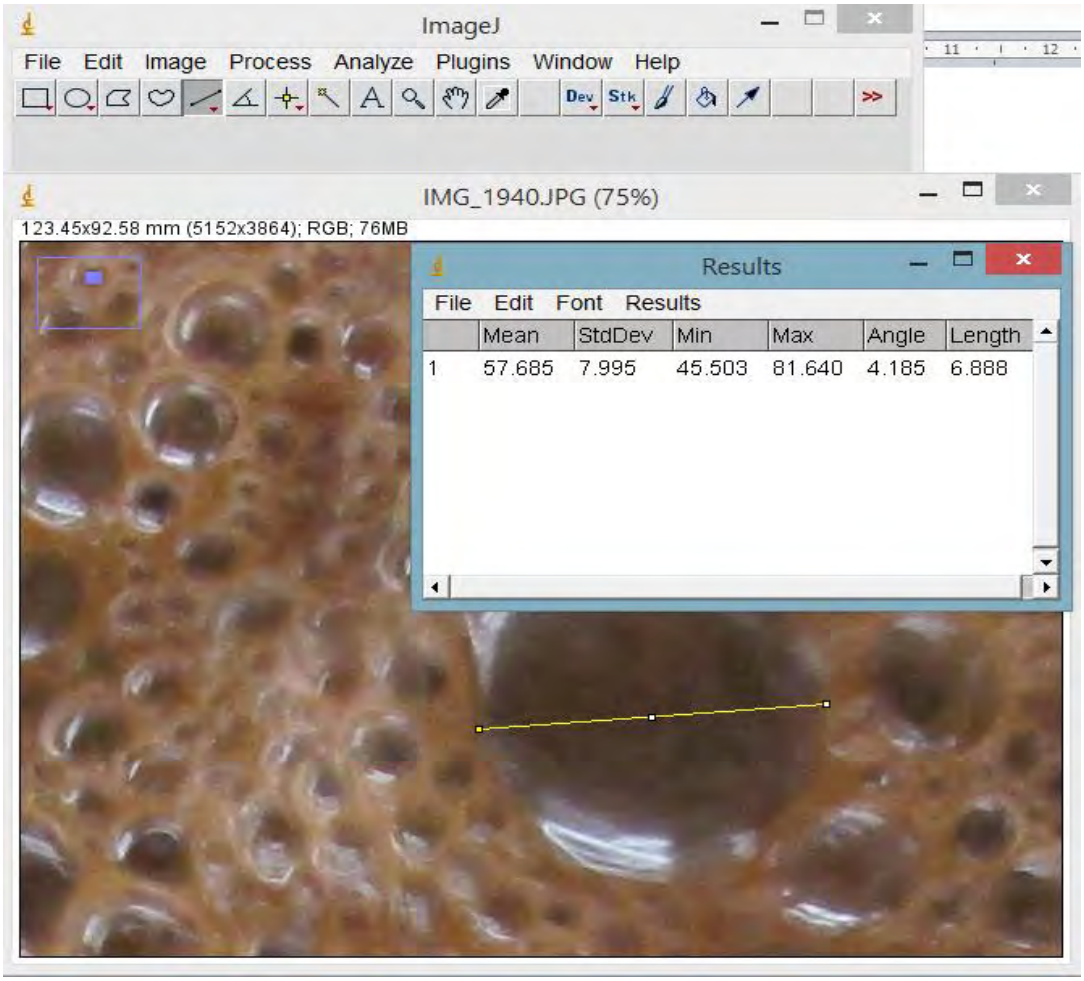

Figure 31: Measurement of a single bubble for the top of froth size.

3.6.5. Axial Sauter-mean bubble diameter profile

The side of froth bubble coalescence was determined by using image processing software ImageJ. The length of 2cm on the metre rule attached to the column was used as a reference length to determine the number of pixels per unit length as shown in Figure 32. The diameter of individual bubbles was then measured using the reference length with the average bubble size measured at 4 cm, 12 and 18 cm from the pulp-froth interface as shown in Figure 33. A minimum of 100 bubbles was measured at each height interval of the froth for both the duplicates. The bubbles where measured along the vertical plane of the column to avoid distortion due to the curvature of the column.

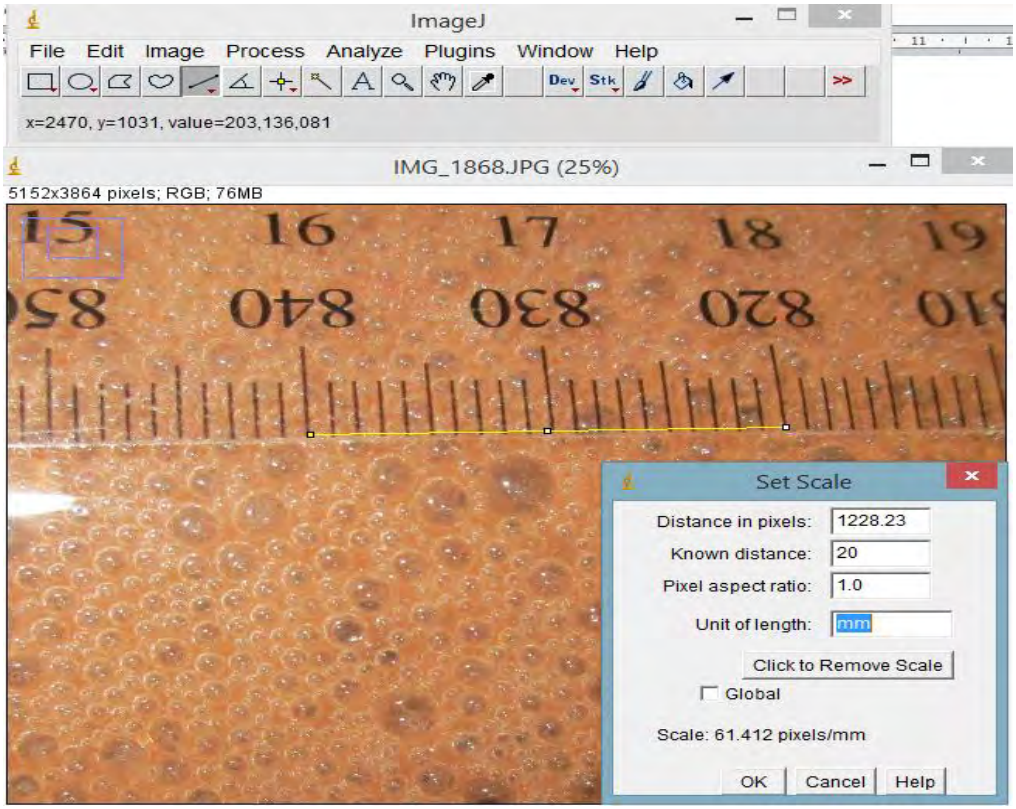

Figure 32: The establishing of the reference length (Scale).

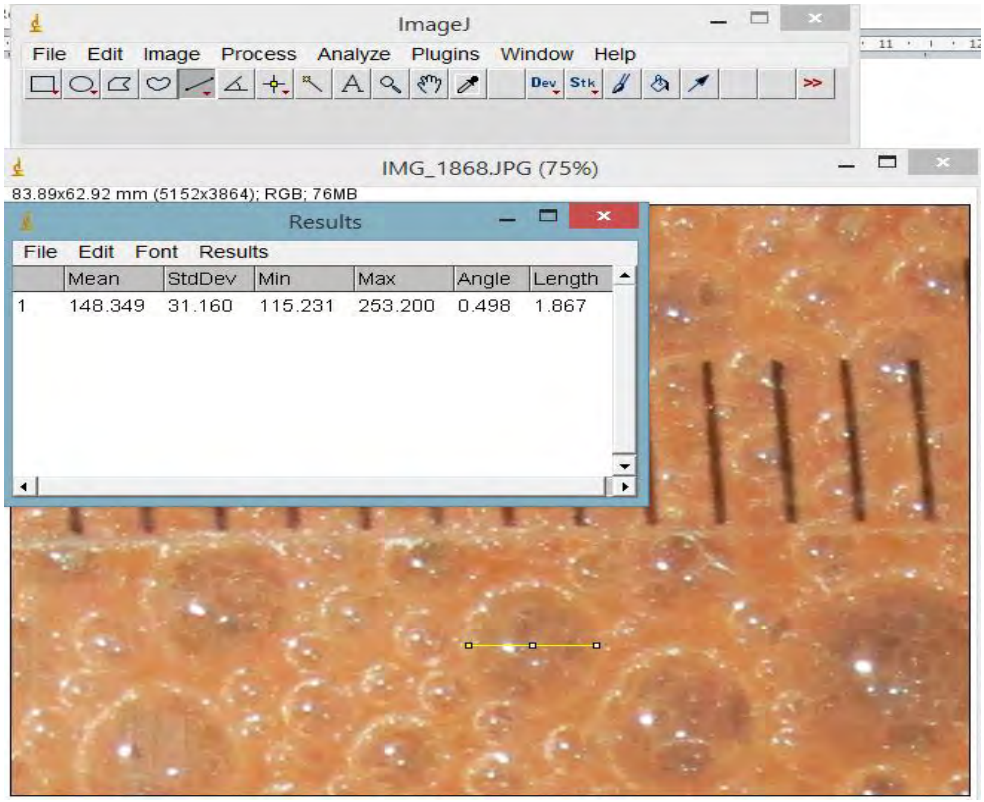

Figure 33: Measurement of a single bubble for the coalescence rate.

3.6.6. Froth Recovery

Froth recovery values where determined based on the standard froth recovery as shown from, $\boldsymbol{Ri}=\frac{\boldsymbol{F}_{\mathrm{C}}\boldsymbol{x}_{\mathrm{i,conc}}}{\boldsymbol{F}_{\mathrm{C}}\boldsymbol{x}_{\mathrm{i,conc}}+\boldsymbol{F}_{\mathrm{T}}\boldsymbol{x}_{\mathrm{i,tails}}}$ Equation 3-16 to $\boldsymbol{k}\mathrm{i}=\frac{\boldsymbol{R}_{\mathrm{i}}}{\boldsymbol{\tau}(\mathbf{1}-\boldsymbol{R}_{\mathrm{i}})}$ Equation 3-17 (Feteris et al., 1987).

$$\boldsymbol{Ri}=\frac{\boldsymbol{F}_{\mathrm{C}}\boldsymbol{x}_{\mathrm{i,conc}}}{\boldsymbol{F}_{\mathrm{C}}\boldsymbol{x}_{\mathrm{i,conc}}+\boldsymbol{F}_{\mathrm{T}}\boldsymbol{x}_{\mathrm{i,tails}}} \qquad \textbf{Equation 3-16}$$

$$\boldsymbol{k}_{\mathrm{i}}=\frac{\boldsymbol{R}_{\mathrm{i}}}{\boldsymbol{\tau}(\mathbf{1}-\boldsymbol{R}_{\mathrm{i}})} \qquad \textbf{Equation 3-17}$$

Where: R_i is Overall flotation recovery of constituent *i* (%), F_C is solids mass recovery in the concentrate (g/min), F_T is solids mass recovery in the tails (g/min), $x_{i,conc}$ is

mass composition of constituent *i* in the concentrate stream (-), $x_{i,tails}$ is mass composition of constituent *i* in the tails stream, k_i is overall flotation rate constant of constituent *i* (min^{-1}) and τ is froth residence time(min).

Extrapolation of the froth rate constant – froth depth relationship enables the evaluation of the pulp rate constant, k_c which is used to determine the froth recovery as shown in $\boldsymbol{R}f= \left[\frac{\boldsymbol{k}_i}{\boldsymbol{k}_c}\right] \times \mathbf{100}$ Equation 3-18 ;

$$\boldsymbol{R_f} = \left[\frac{\boldsymbol{k}_i}{\boldsymbol{k}_c}\right] \times \mathbf{100} \qquad \textbf{Equation 3-18}$$

Where R_f is froth recovery (%) and k_c is pulp rate constant (min^{-1}).

3.6.7. Entrainment Factor

The entrainment factor was also considered and it was determined as shown in $\boldsymbol{F}_{j,conc} = \boldsymbol{F}_c \boldsymbol{x}_{j,conc}$ Equation 3-19 and $\boldsymbol{Entrainment\ factor} = \frac{\boldsymbol{F}_{j,conc}}{\boldsymbol{F}_{H2O,\ conc}}$ Equation 3-20 (Yianatos & Contreras, 2010).

$$\boldsymbol{F}_{j,conc} = \boldsymbol{F}_c \boldsymbol{x}_{j,conc} \qquad \textbf{Equation 3-19}$$

$$\boldsymbol{Entrainment\ factor} = \frac{\boldsymbol{F}_{j,conc}}{\boldsymbol{F}_{H2O,\ conc}} \qquad \textbf{Equation 3-20}$$

Where: $Fj_{,conc}$ is mass recovery of chromite in the concentrate (g/min) and $F_{H2O,conc}$ is mass recovery of water in the concentrate (g/min).

The entrainment factor was defined as the mass of gangue material recovered per unit mass of water. The factor eliminates the effect of the different water recoveries

obtained under different experimental conditions which is necessary due to the effect of water recovery on entrainment.

Chapter 4. RESULTS

4.1. Introduction

This chapter of the thesis presents the results obtained from the test work conducted in the study, which was aimed at developing a relationship between the solids particle size and the stability of the froth phase. The chapter is divided into three major sections. Section 4.2 presents the particle size classification results for the two ores used in this project. This entails the various particle size distributions (PSDs) and Rosin Rammler distributions for the various particle sizes tested. Section 4.3 presents the results obtained from the various froth stability measurements obtained using the froth stability column based on the Bikerman test. The maximum froth height (H_{max}), froth growth rate and froth decay rate were used as stability proxies so as to quantify froth stability. Section 4.4 presents the froth stability measurement results obtained from the test work performed on the agitated hybrid flotation cell, with the following froth stability proxies used to quantify froth stability: water recovery, top of froth Sauter-mean bubble size, axial Sauter-mean bubble diameter profile, froth recovery and also entrainment factor.

4.2. Particle Size Classification

Since the major aim of the project was to develop a relationship between the particle size and froth stability, the classification of particle size was critical in enabling adequate analysis of the different particle sizes.

4.2.1. UG2 Ore Size Classification

The feed particles for the tests were initially characterised using the conventional method of displaying particle size distribution as shown in Figure 34. The UG2 ore was milled for the various milling times shown in Figure 34 viz. 10, 15, 20, 25 and 30 minutes and the percentage of ore by mass for each respective particle size class was determined using a Malvern particle size analyser.

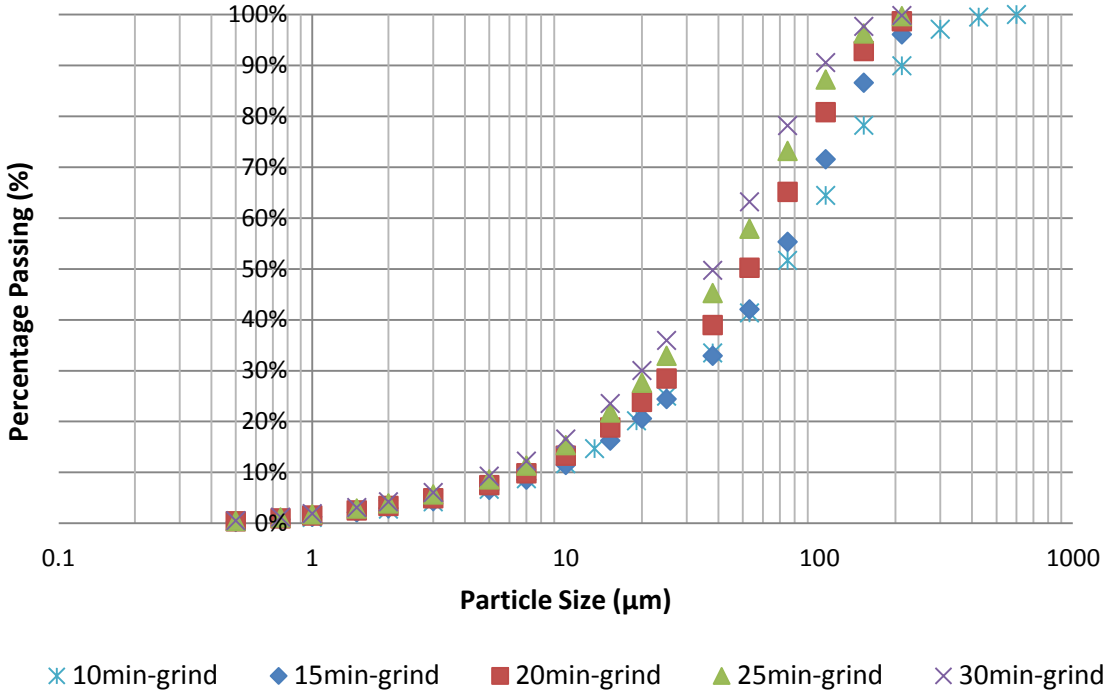

Figure 34: Feed particle size distributions for the different UG2 ore grinds.

To further assess whether the particle size distributions for the products of the different milling times were significantly different, a Rosin Rammler distribution was used. From the model, which is based on a linear correlation coefficient, the resultant particle size distribution curves exhibit significantly different slopes for the different milling times as shown in Figure 35. The longer the milling time, the steeper the slope of the curve and thus a finer particle size distribution. The shortest milling time viz. 10 minutes resulted in a curve with the shallowest slope indicating the coarsest particle size distribution.

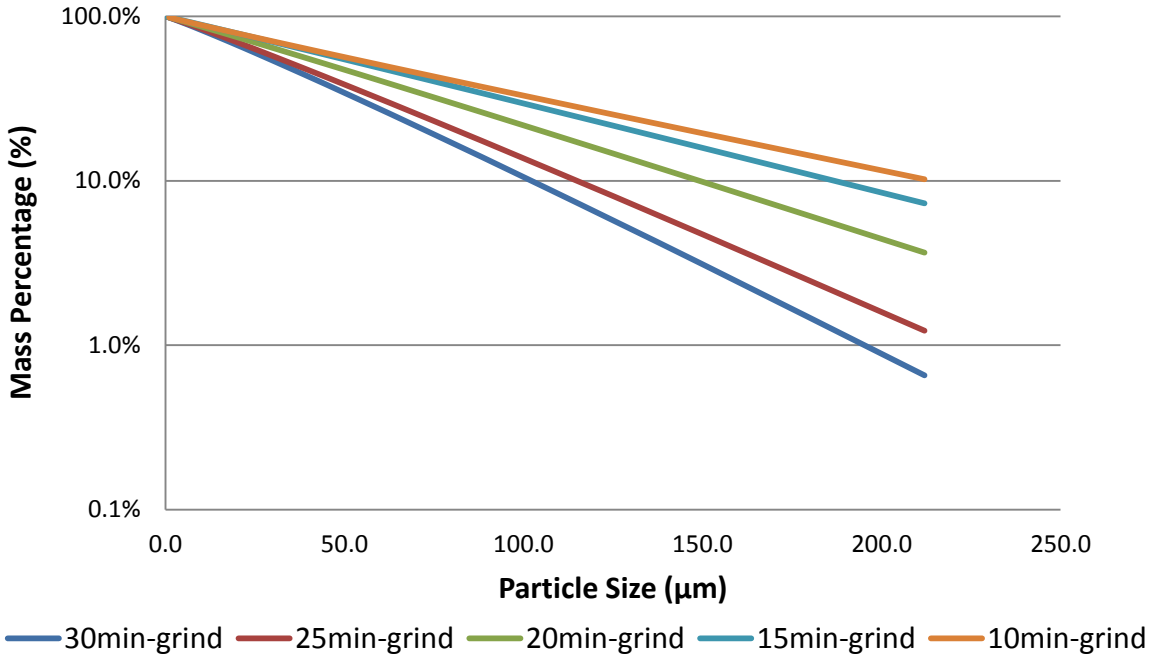

Figure 35: PSDs derived from Rosin Rammler density function model for the different feed UG2 ore grinds.

From the Rosin Rammler distributions, the particle size at which 80% of the material was less than (D_{80}) was determined and the results are shown in Figure 36. The D_{80} values obtained show that the particle sizes were different for the different grinds. The 10 minute grind had the highest D_{80} value of 157 µm while the finest grind had a D_{80} value of 78 µm.

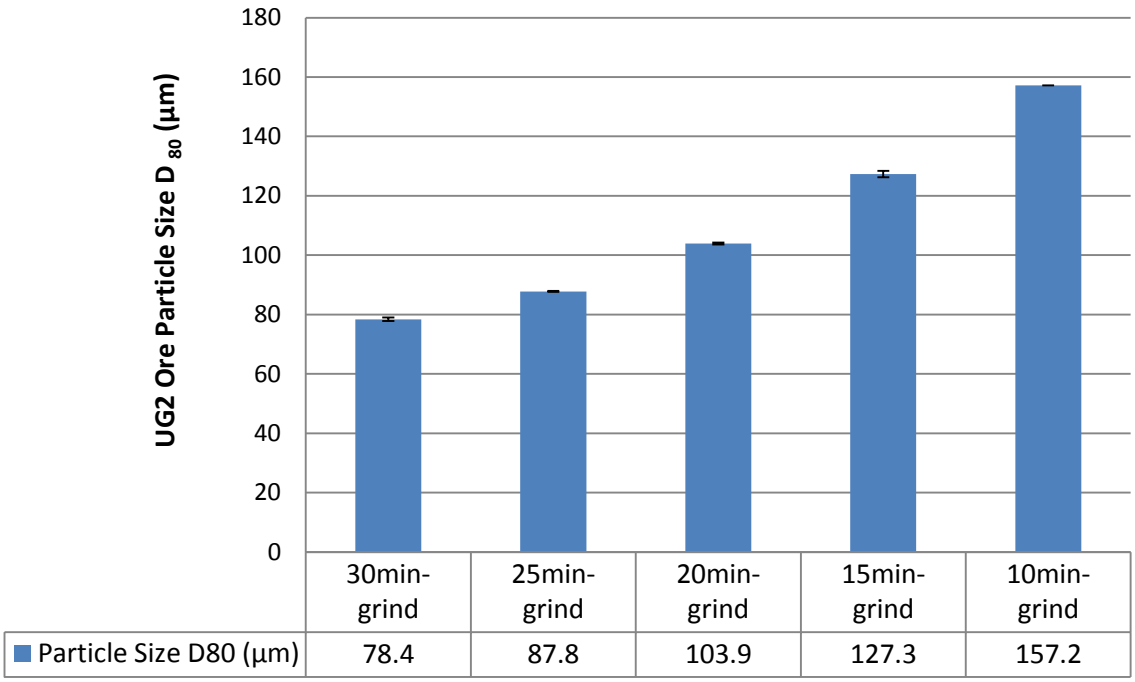

Figure 36: D_{80} values as determined using a Malvern particle size analyser for UG2 ore for the different grinding times.

Since the aim of the project was to investigate the effect of particle size on froth stability, it was important to assess the size of particles in the froth zone in comparison to the feed pulp particle size. Therefore particle size distributions of the concentrates collected from the continuous agitated hybrid cell flotation tests were measured using a Malvern particle size analyser. Figure 37 and Figure 38 show the size distributions of the concentrates as analysed using the Malvern and the Rosin Rammler distribution for the 25 cm column tests respectively.

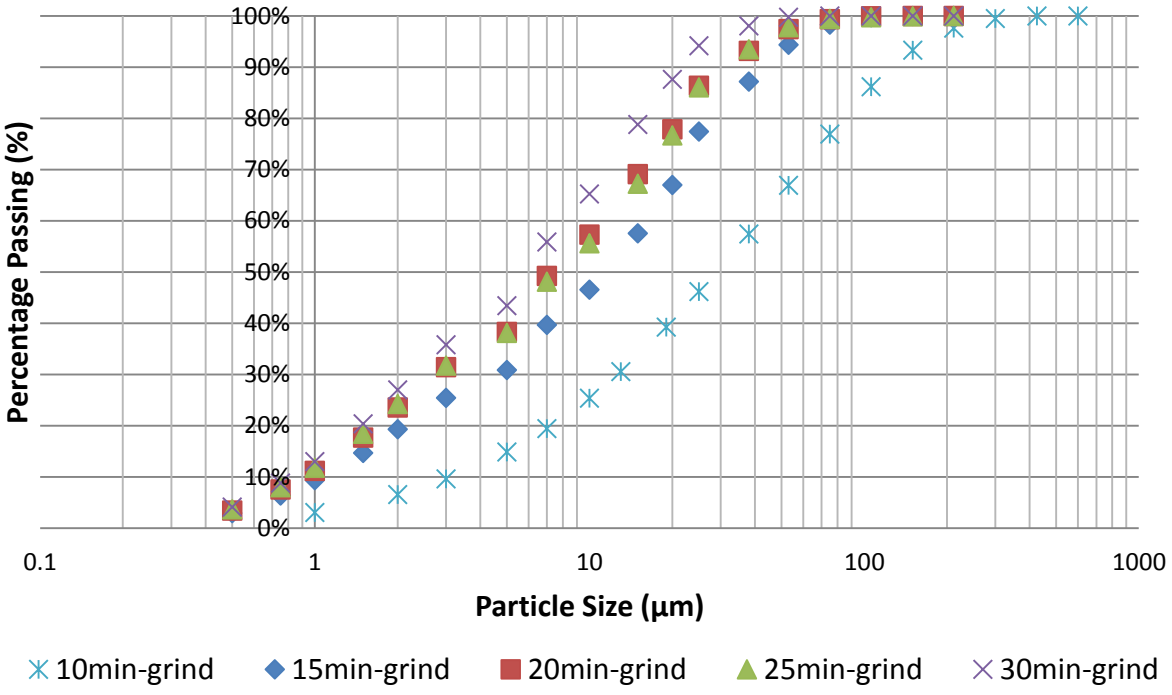

Figure 37: Concentrate particle size distributions for the UG2 ore from tests performed on the agitated hybrid cell at a column height of 25cm.

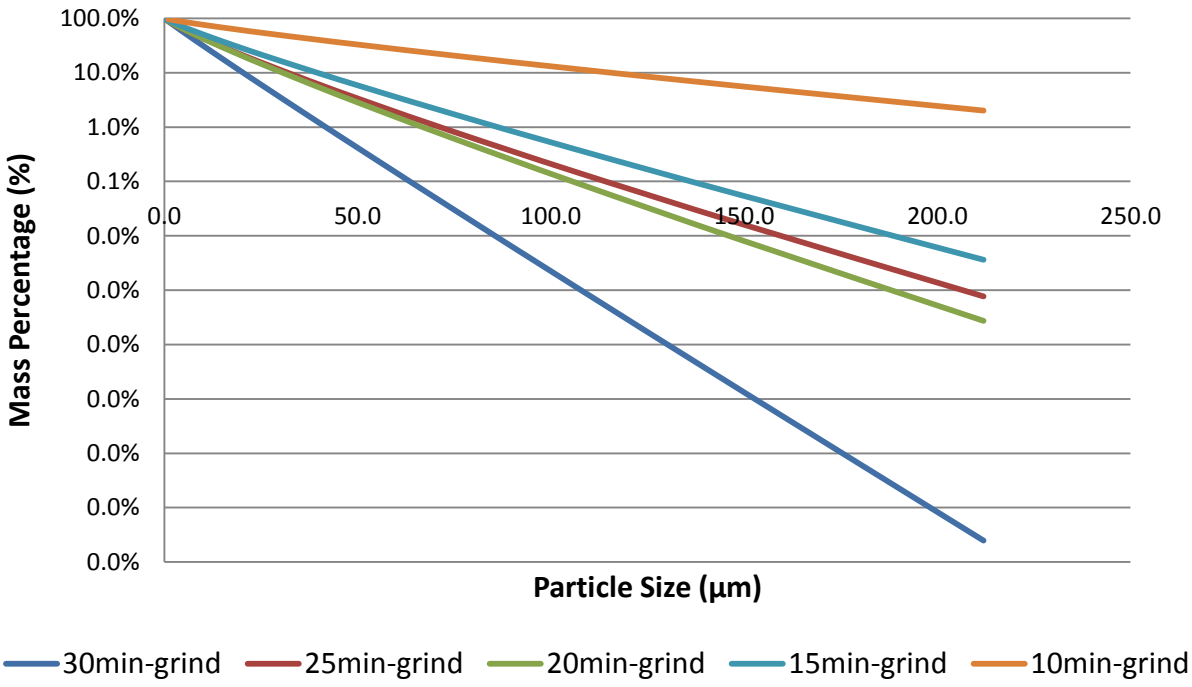

Figure 38: PSDs derived from Rosin Rammler density function model for the concentrate UG2 ore from tests performed on the agitated hybrid cell at a column height of 25cm.

From the results, it was shown that the particles reporting to the final concentrate were not of one size range but in fact differed with the different flotation feed sizes. The coarsest flotation feed particle resulted in the coarsest concentrate particle size as expected. The latter was also true with the finest feed size resulting in the finest concentrate particle size. The particle size distributions for the concentrates were also shown to be significantly finer than the feed size distributions.

In Figure 39 and Table 12, the D_{80} values for the feed particles were shown to be significantly higher than those for the concentrate particles as all the concentrate data points were below the equilibrium line. The D_{80} for the 30 minute grind dropped significantly from 78 µm to 40 µm for the test work performed on the 25 cm column. The same trend was observed for all the grinds and column heights tested, with the concentrate particle size significantly finer than the feed particle size.

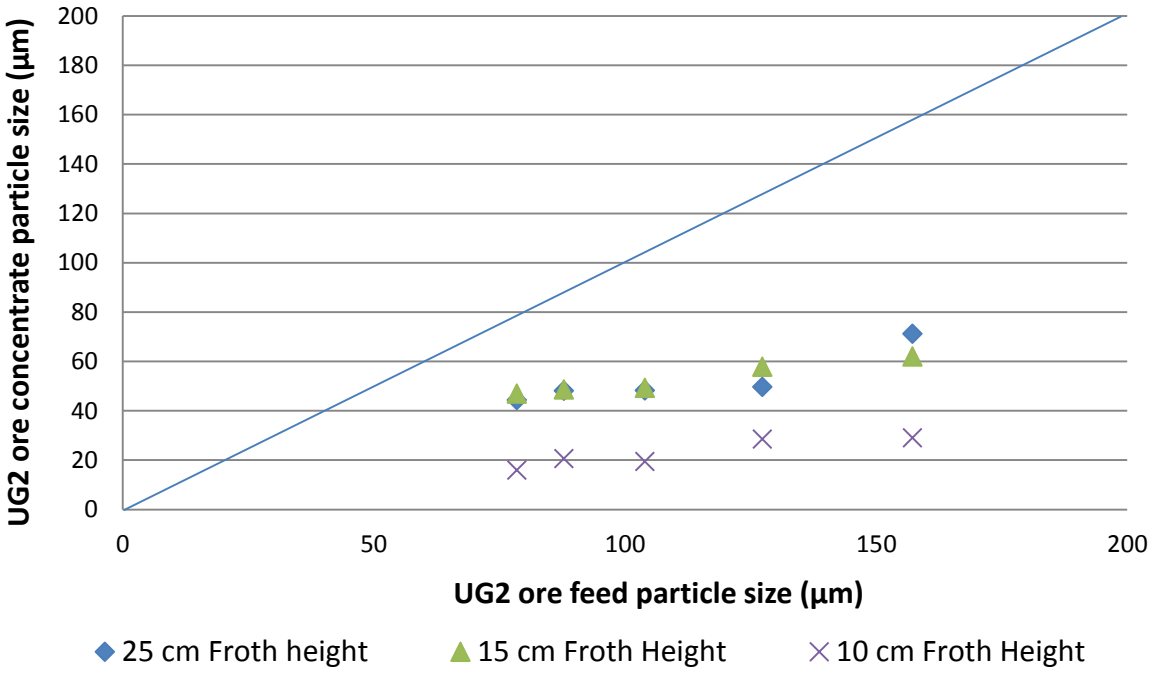

Figure 39: Feed and concentrate D_{80}s for test work conducted using the 25 cm, 15 cm and 10 cm columns.

Table 12: Feed and concentrate D_{80}s for test work conducted using the 25 cm, 15 cm and 10 cm columns.

Feed Milling Time	Feed Sample	Concentrate Particle Size D_{80} µm (With Column Height (cm))		
		10 cm Column	15 cm Column	25 cm Column
30min-grind	**78.42**	47.04	44.41	39.65
25min-grind	**87.79**	48.73	48.19	51.63
20min-grind	**103.92**	49.38	48.35	57.57
15min-grind	**127.34**	57.93	49.82	81.72
10min-grind	**157.21**	62.08	71.25	83.58

4.2.2. Iron Ore (Itabirite) Size Classification

The feed particle size distribution of the iron ore used (Itabirite ore) was assessed in the same way as the UG2 ore. The data used for the distributions was obtained using the standard sieving method at standard sieve mesh sizes as the Marlvern sizer was unable to measure the particle sizes due to clouding of the water in the machine by the ore resulting in highly in consistent measurements.

The particle size distributions for the iron ore feed samples were significantly different for the different milling times as shown in Figure 40 and Figure 41. Due to the limited number of data points provided by the available sieve sizes, the linear correlation is not a perfect fit. The Rosin Rammler distributions as shown in Figure 41 illustrate that the four grinds resulted in different size distributions.

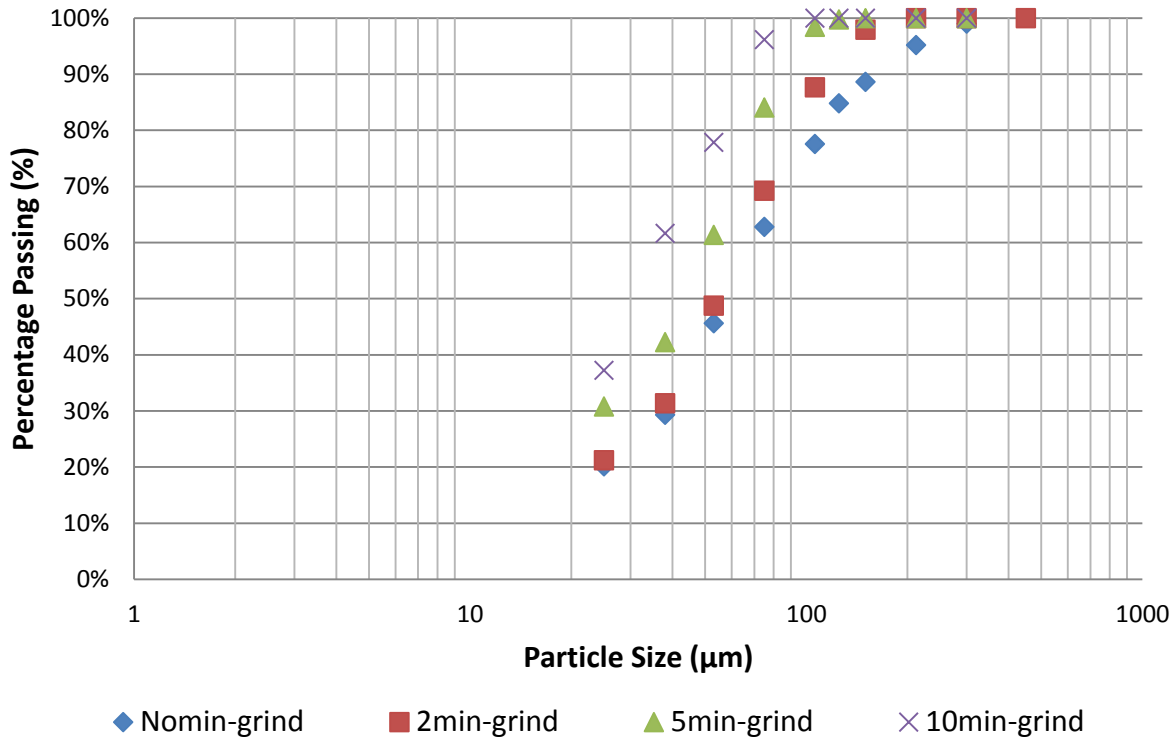

Figure 40: Feed particle size distributions for the different iron ore grinds.

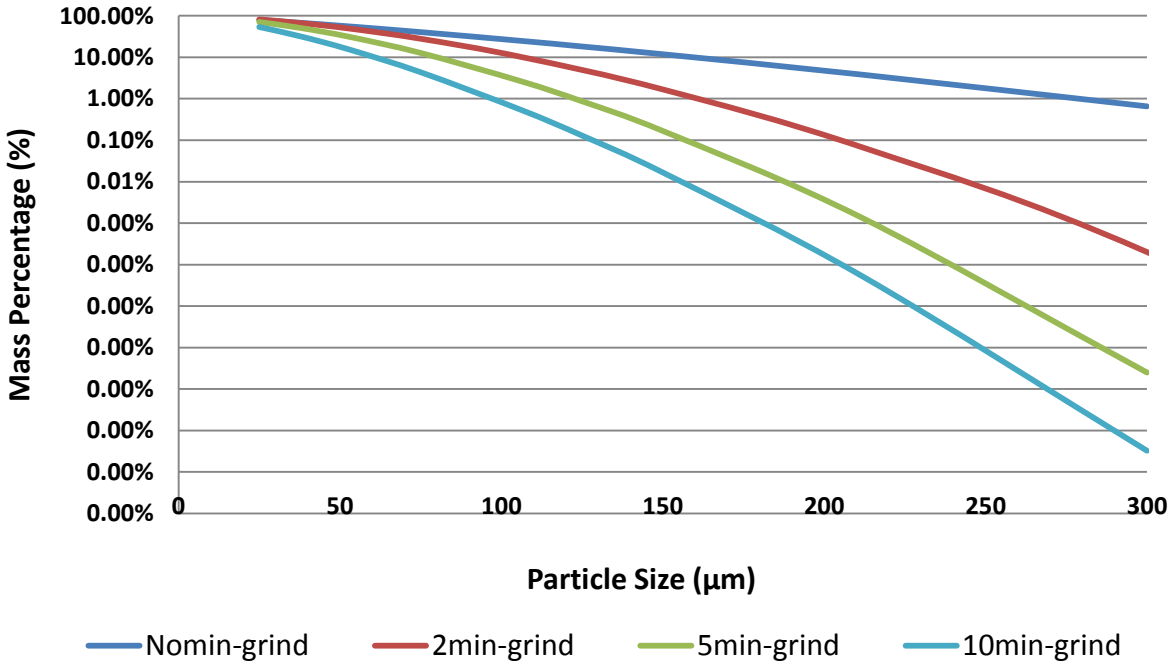

Figure 41: PSDs derived from Rosin Rammler density function model for the different feed iron ore grinds.

The respective feed D_{80} values were determined from the Rosin Rammler model density function for the iron feed samples and are shown in Figure 42. The initial feed sample which was a de-slimed cleaner feed sample had a significantly different particle size distribution to the other three mill products. The D_{80} values for the four ore samples varied from 118 µm (for the un-ground sample) to 48 µm (for the finest grind).

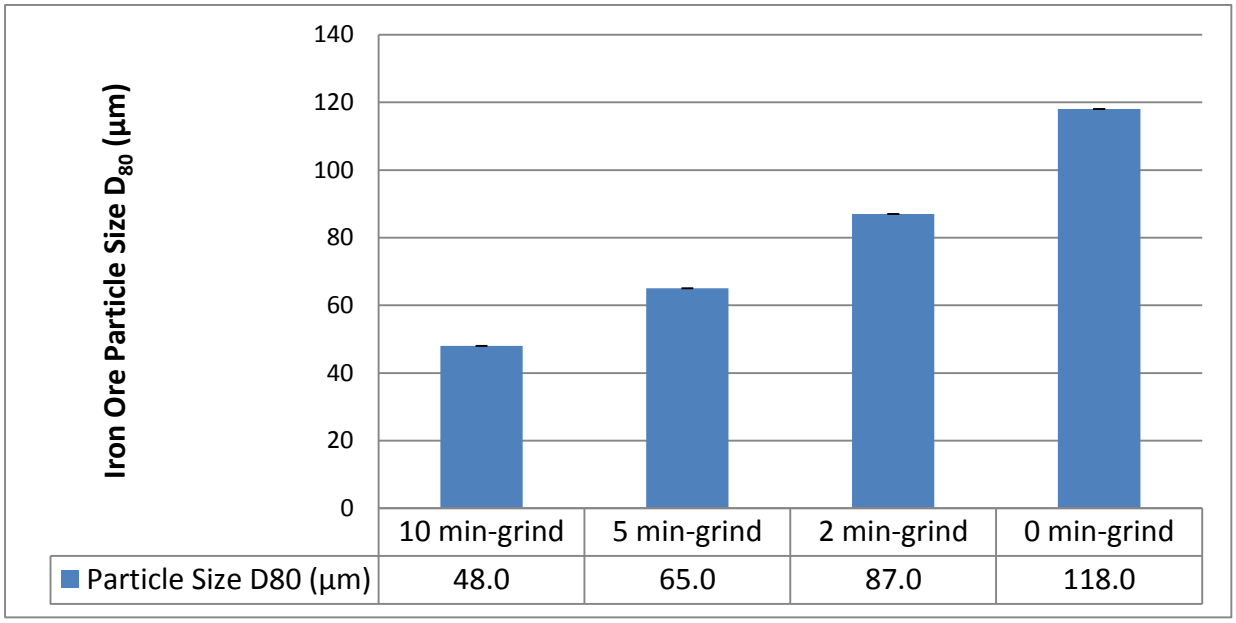

Figure 42: D_{80} values as determined using standard sieves and Rosin Rammler distributions for the iron ore at the different grinding times.

As previously illustrated for the UG2 ore, the concentrate particle size for the iron ore was assessed to provide a more comprehensive assessment of the size of the particles in the froth phase. Due to the limited amount of concentrate particles collected during flotation test which were above the minimum available sieve size of 25 µm and also clouding in the Marlvern Sizer, a full size distribution using different sieve sizes was not able to be performed. The concentrate particle sizes were assessed as a function of the percentage of particles passing 38 µm as shown in Figure 43 and Table 13.

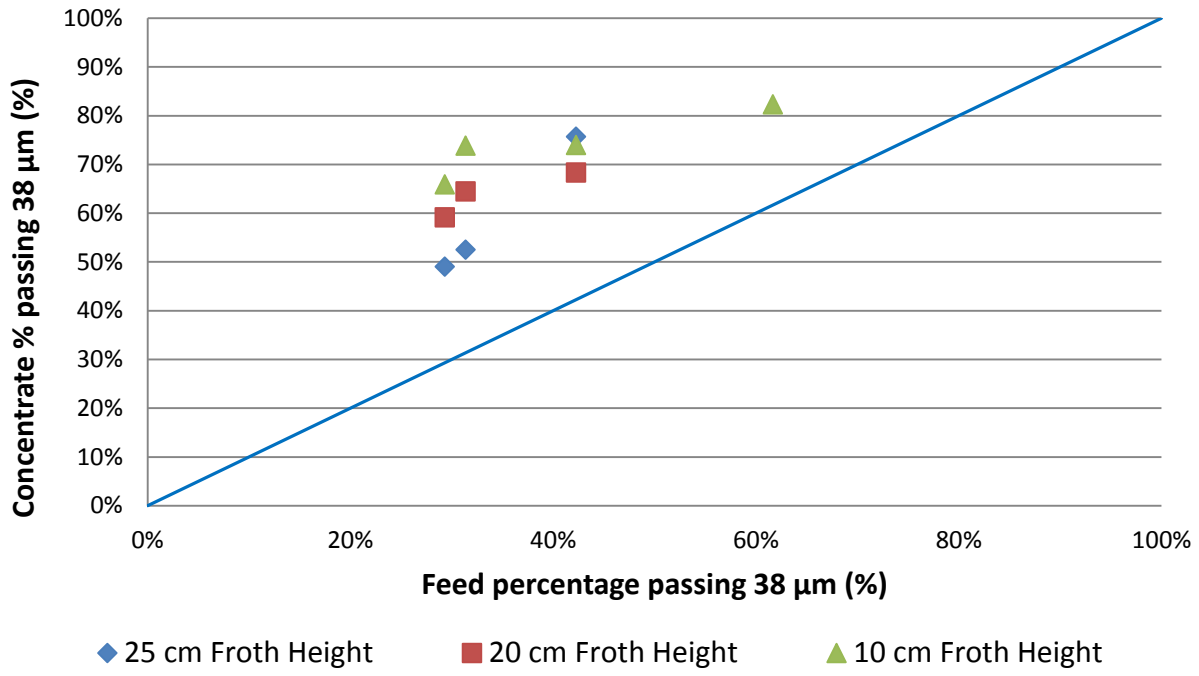

Figure 43: Percentage of feed and concentrate particles passing 38 µm for test work using the 25 cm, 15 cm and 10 cm columns for the Iron ore.

The concentrate particle sizes for the iron ore were shown to be significantly finer than that of the feed samples, following the same trend as the UG2 ore. This is illustrated in Figure 43 which shows that the concentrate particles had a higher percentage passing 38 µm by mass than that of the feed as all the points lie above the equilibrium line. The concentrates thus exhibit finer particle sizes than the feed.

Table 13: Fraction of feed and concentrate percentage of particles passing 38 µm for test work conducted using the 25 cm, 15 cm and 10 cm columns for the iron ore.

	Fraction by mass of particles passing 38 µm (Fraction)			
Feed Milling Time	**Feed Sample**	**10 cm Column**	**15 cm Column**	**25 cm Column**
0 min-grind	**0.29**	0.66	0.59	0.49
2 min-grind	**0.31**	0.74	0.65	0.53
5 min-grind	**0.42**	0.74	0.68	0.76
10 min-grind	**0.62**	0.82	n/a	n/a

The average concentrate particle sizes were significantly finer than the feed for the various grinds tested as illustrated in Figure 43. The concentrate particle size distribution also shown to be different for the differently sized flotation feed samples as illustrated in besides Table 13, besides the two intermediate grinds in the test work performed on the 10 cm column which might have been error associated with the size distribution measurements of the concentrates. Results for the test work at the finest grind of 10 minutes for the 15 cm and 25 cm column experiments were unable to be performed due to limitations of the equipment with the foam not collapsing as indicated in Table 13: Fraction of feed and concentrate percentage of particles passing 38 µm for test work conducted using the 25 cm, 15 cm and 10 cm columns for the iron ore..

4.3. Froth Stability Column Tests

The froth stability column was used to assess the effect of particle size on froth stability for the UG2 ore and the iron ore. As previously stated, froth stability was assessed using the following proxies where applicable; froth stability factor, froth growth rate and froth decay rate.

4.3.1. UG2 Ore Froth Stability Results

a. Froth Stability Factor

The stability of the froth phase was assessed by using a froth stability factor which is based on the equilibrium maximum froth height. Finer particles resulted in a more stable froth phase as shown in Figure 44. The maximum froth stability values achieved were at the finest grind which had a feed D_{80} of 78 µm, with the minimum value obtained at a feed D_{80} of 157 µm. The data set for the froth stability factor was then fitted with trend lines and a negative power law model was shown to best fit the data according to the R-squared values. The trend exhibited that the presence of fine particles affected the froth stability to a greater extent, with the froth stability increasing significantly as particles became finer. The same trend was observed for all the solids concentrations tested for the UG2 ore viz. 15%, 20%, and 25%.

Upon examination of Figure 44, it is evident that the solids concentration had a slight effect on the froth stability for the UG2 ore, and this was for the solids concentration range tested. The highest solids concentration tested viz. 25% showed the highest froth stability values. A general trend can be noted assessing the change in concentration, in that an increase in solids concentration from 15% to 25% resulted in an increase in froth stability signified by an upwards shift in the curve.

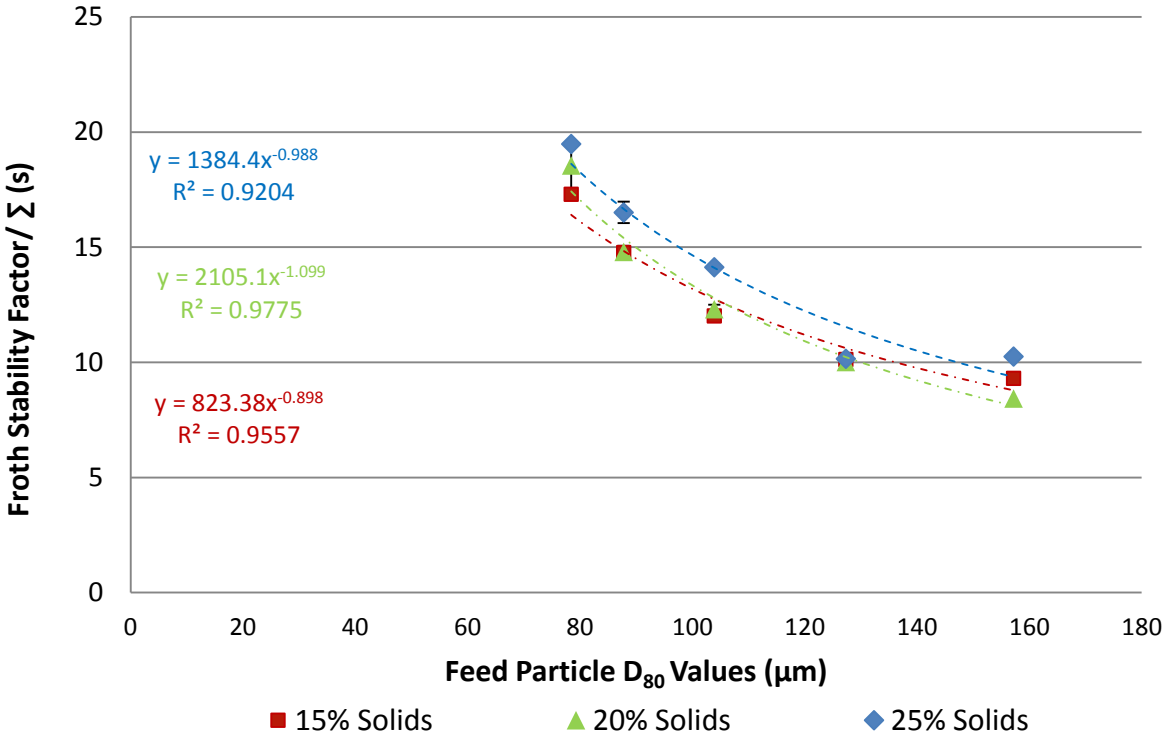

Figure 44: Dynamic froth stability as a function of feed particle size for UG2 ore.

The froth stability factor for the UG2 ore was also assessed as a function of the specific weighted surface area of the feed particles (m^2/g). An increase in the weighted specific surface area was shown to have a positive effect on the froth stability as shown in Figure 45. A general linear increase in the froth stability factor with an increase in the weighted surface area of the feed particles was shown for the particle size range tested. The linear trend model was fitted to the data points also according to the R-squared values. It was shown that the finer the particles, which in-turn means a higher surface area per unit mass, had the greater linear increase in the froth stability for the range tested.

The same trend with regards to the effect of solids concentration on the stability of the froth was shown, with a slight effect observed for the test work performed on the UG2 ore at the respective concentrations viz. 15%-25%.

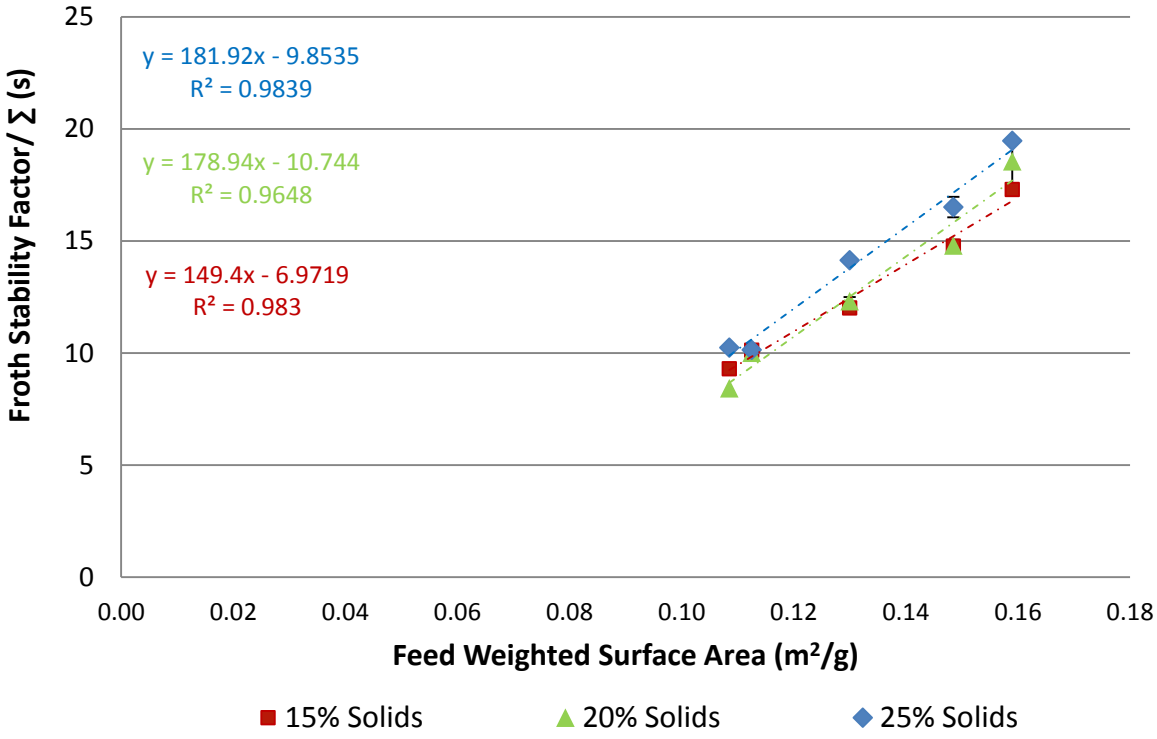

Figure 45: Dynamic froth stability as a function of feed weighted particle surface area for UG2 ore.

b. Froth Growth Rate

Froth stability was also assessed by noting the growth rate of the froth and this was assessed using the average bubble life as a proxy. From the exponential model for growth rate, an increase in the τ values which is the average bubble life-time indicates that the froth is more stable and bubble will have a longer lifespan.

Figure 46 shows that a decrease in the particle size resulted in an increase in the τ value which means that the froth bubbles had a longer lifespan and thus the froth was more stable. The finest grind of 78 µm resulted in the highest τ value of all the grinds and thus the finest grind had the highest froth stability as assessed by the froth growth rate for the UG2 ore. The trend showed that the average bubble lifetime values also follow the decreasing power law trend with increasing feed particle size as shown in Figure 46. Solids concentration was shown to have a slight effect on the froth stability as assessed by froth growth rate proxy values as shown in Figure 46 with an increase in the solids concentration resulting in an increase in froth growth

rate. The 25% solids concentration resulted in the highest average bubble life values and thus greater froth stability with the 15% solids having the lowest.

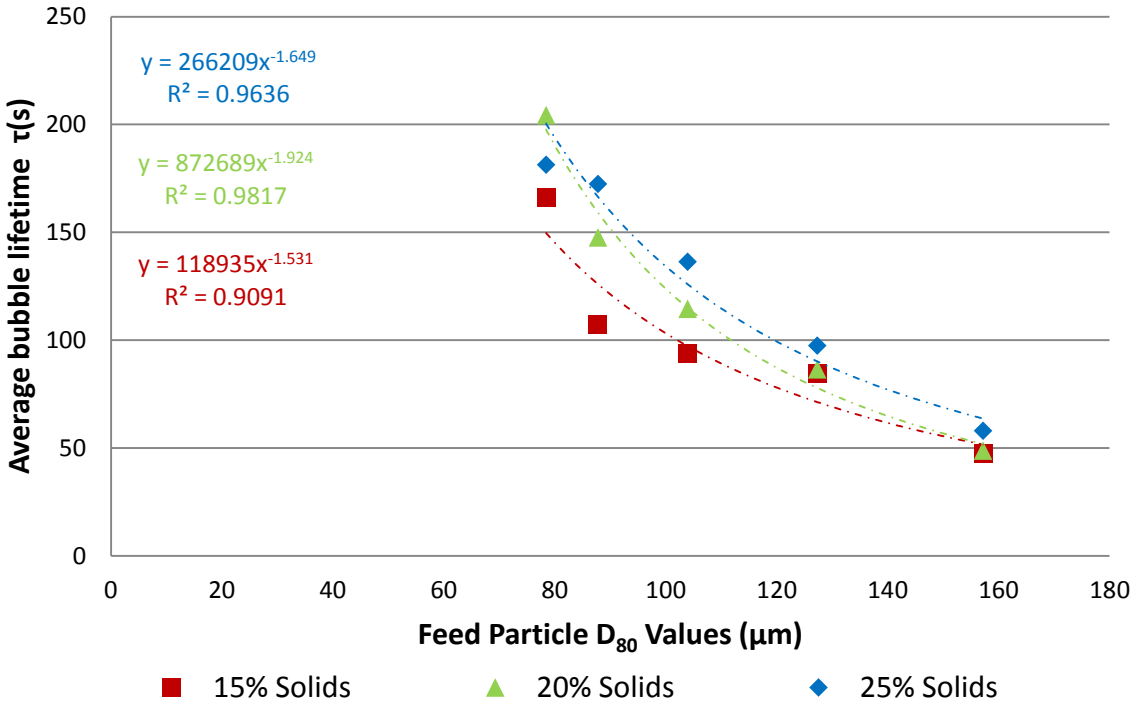

Figure 46: Froth growth rate (average bubble lifetime) as a function of feed particle size for UG2 ore.

c. Froth Decay Rate

The stability of the froth as assessed by the froth decay rate was investigated using the froth decay half-life which is defined as the time it takes for the froth in equilibrium to collapse to half of its maximum equilibrium height. A more stable froth phase can be illustrated by a longer froth half-life as the froth phase takes more time to collapse.

Analysis of the stability of the froth phase using the froth half-life as a proxy also showed that the finer the particle, the higher the froth half-life and thus a more stable froth as illustrated in Figure 47. The finest grind with a D_{80} of 78 µm had the longest half-life over all three solids concentrations tested with the coarsest grind with D_{80} of 157 µm having the shortest half-life. A reducing power law was shown to be the best model to fit the data set for the half-life data set and this was also according to the R-

squared values. From the analysis of the trend, it was shown that the impact of changing particle size had a more significant effect over the finer size range with the greatest impact in the 78 µm to 128 µm size ranges, with reference to the feed particle size.

As illustrated in Figure 47, the solids concentration had an effect on the froth half-life over the solids concentration range of 15% - 25% investigated. An increase in the solids concentration resulted in an increase in the froth half-life thus increasing the stability of the froth. The solids concentration however had less of an impact on the froth half-life in comparison to particle size.

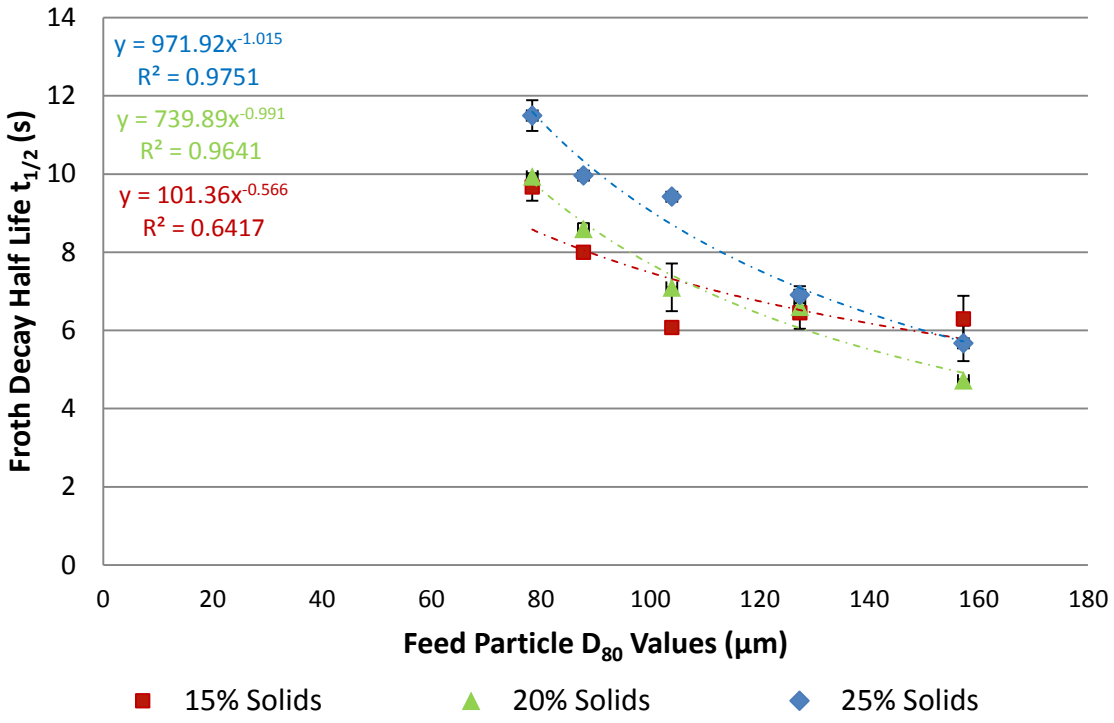

Figure 47: Froth decay rate as a function of feed particle size for UG2 ore.

Froth stability was also shown to follow an increasing linear relationship with increasing feed weighted specific area shown in Figure 48, with an increase in the surface area resulting in an increase of the froth half-life.

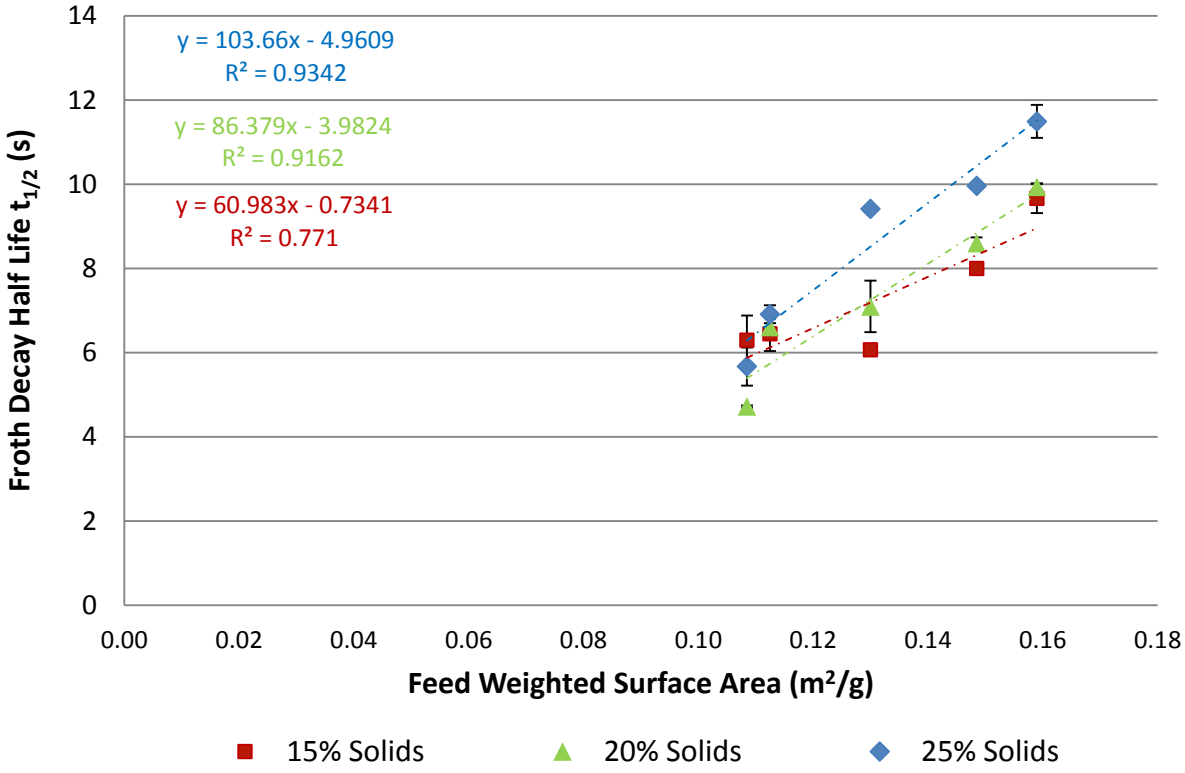

Figure 48: Froth decay rate as a function of feed weighted particle surface area for UG2 ore.

4.3.2. Iron Ore Results

a. Float Test Conditions

Froth decay rates for the iron ore were not determined due to visibility limitations in the column. No weighted surface area calculations were performed due to the limitations of the Malvern sizer in measuring the iron ore.

b. Froth Stability Factor

As for the UG2 ore the stability of the froth phase for the iron ore was assessed using the froth stability factor and from Figure 49 it is evident that finer particles resulted in a more stable froth. The maximum froth stability values were obtained at the finest grind which had a feed D_{80} of 48 µm. A general decrease in the froth stability factor with increasing feed particle size was observed for the iron ore. A decreasing power law trend was also observed for the stability factor as a function of feed particle size following the same trend as that shown for the UG2 ore. It should be noted, that the trend is the same, however, the magnitude is higher for the iron ore as compared to the UG2 ore which is a sparsely mineralised ore.

Figure 49 also shows that an increase in the solids concentration had a positive effect on the froth stability factor for the solids concentration tested. The highest solids concentration tested viz. 25% resulted in the highest froth stability factor values. A decreasing power law with feed particle size was observed at all the solids concentrations tested.

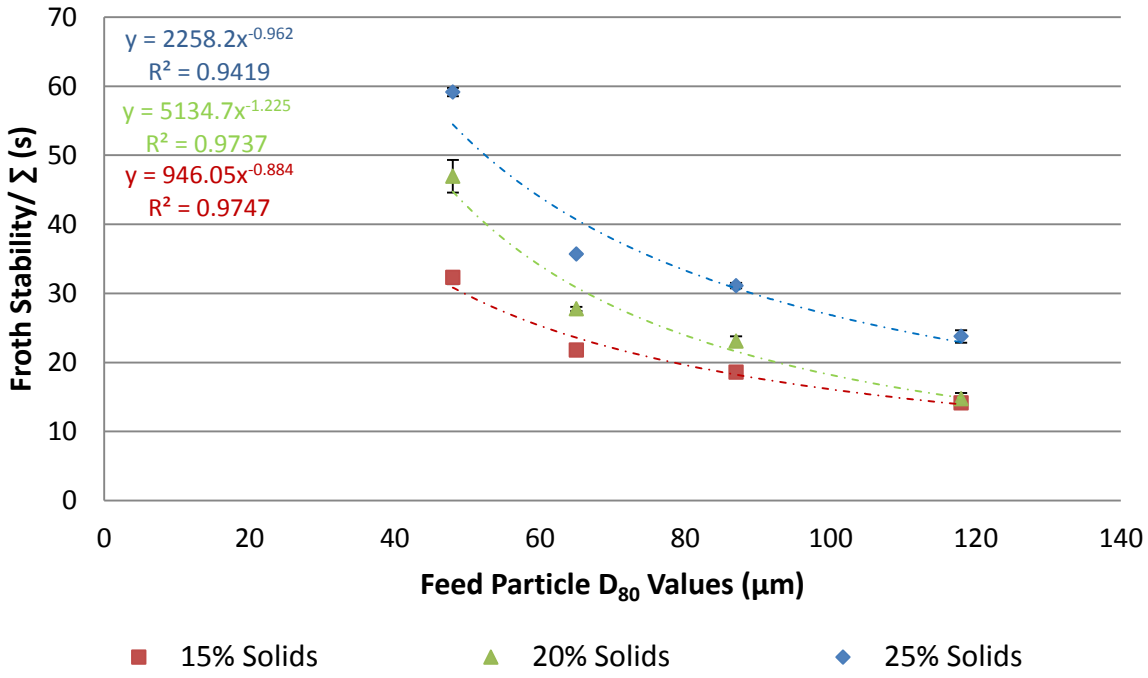

Figure 49: Dynamic froth stability as a function of feed particle size for iron ore.

The dynamic froth stability factor for the test work done using iron ore was also assessed as a function of the reciprocal of feed particle size which has been shown to be proportional to particle surface area according to the BET (assuming spherical particles). A linear relationship was observed for the stability factor with increasing froth stability as a function of the surface area proxy as shown in Figure 50, thereby following the same trend as that observed for the UG2 ore.

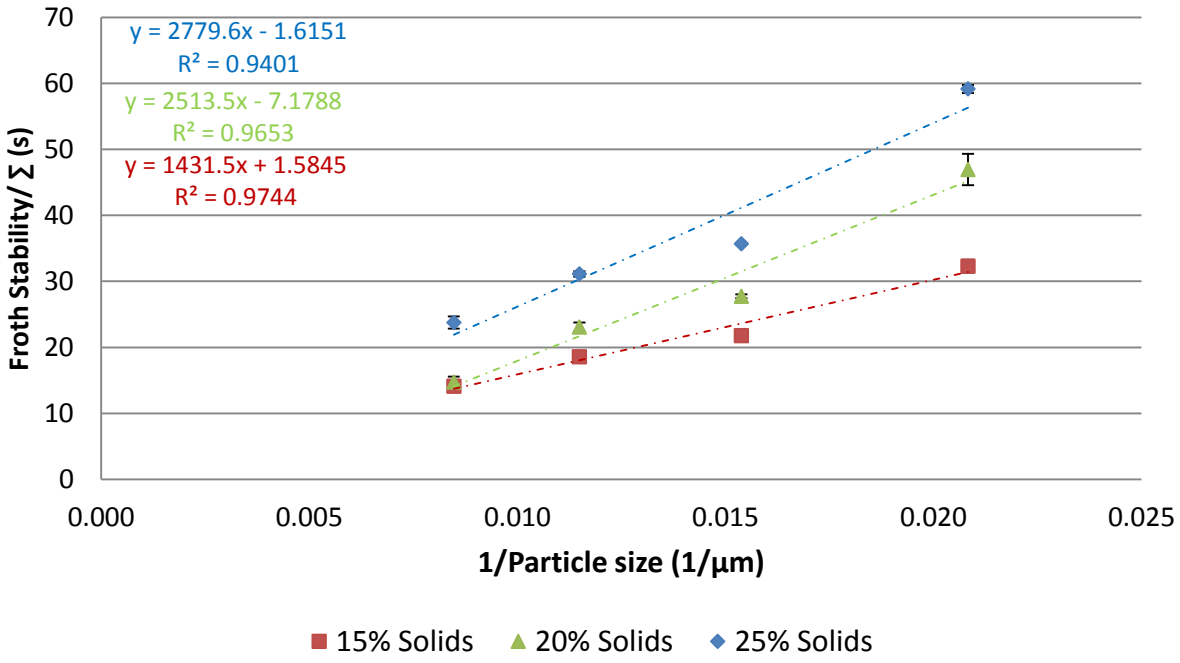

Figure 50: Dynamic froth stability as a function of reciprocal feed size for iron ore

Froth Growth Rate

Figure 51 shows the average bubble lifetime τ, as a function of feed particle D_{80}. An increase in the particle size resulted in a decrease in the τ values which means the bubbles had a shorter lifespan and thus the froth was less stable. A decreasing power law trend was also observed with feed particle size. The finest grind with a D_{80} of 48 µm resulted in the highest τ values and thus the finest grind had the highest froth stability for the iron ore. The coarsest grind with a D_{80} of 118 µm on the other hand had the lowest τ values. A linear relationship between froth stability and weighted specific surface area proxy was also displayed for the iron ore as assessed by froth growth rate.

Solids concentration was shown to have a very significant effect on the froth stability as assessed by average bubble life as shown in Figure 51. An increase in the solids concentration resulted in higher average bubble lifetime values and thus higher froth stabilities.

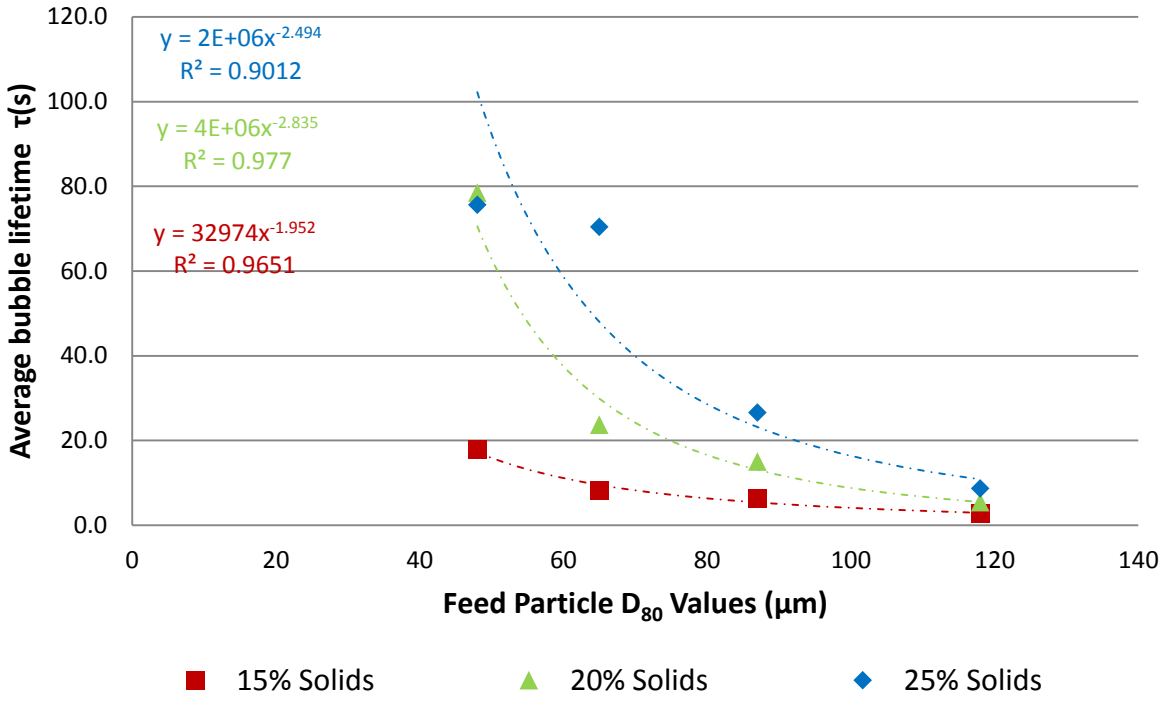

Figure 51: Froth growth rate as a function of feed particle size for iron ore.

4.3.3. Ore Mineralogy Effects on Froth Stability

The effect of the difference in the mineralogy of the two ores assessed in this project was analysed by a comparison of the froth stability factor and the froth growth rate results obtained for the two ores. Due to limitations in visibility through the column of the equipment, tests on the froth decay half-life for the iron ore were unable to be performed due to visibility constraints on the column as the iron ore stained the Perspex.

Figure 52 shows that iron ore had a somewhat higher froth stability factor values than the UG2 ore. The iron ore did have a finer overall particle size range, but the size range that overlapped with that of the UG2 ore illustrated higher froth stability factors. From the stability column tests, it was then shown that iron ore resulted in a more stable froth phase as compared to UG2 ore as shown in Figure 52.

The effect of solids concentration was shown to be more pronounced on the froth stability factor and average bubble lifetime for the iron ore as compared to the UG2 ore as shown in Figure 52.

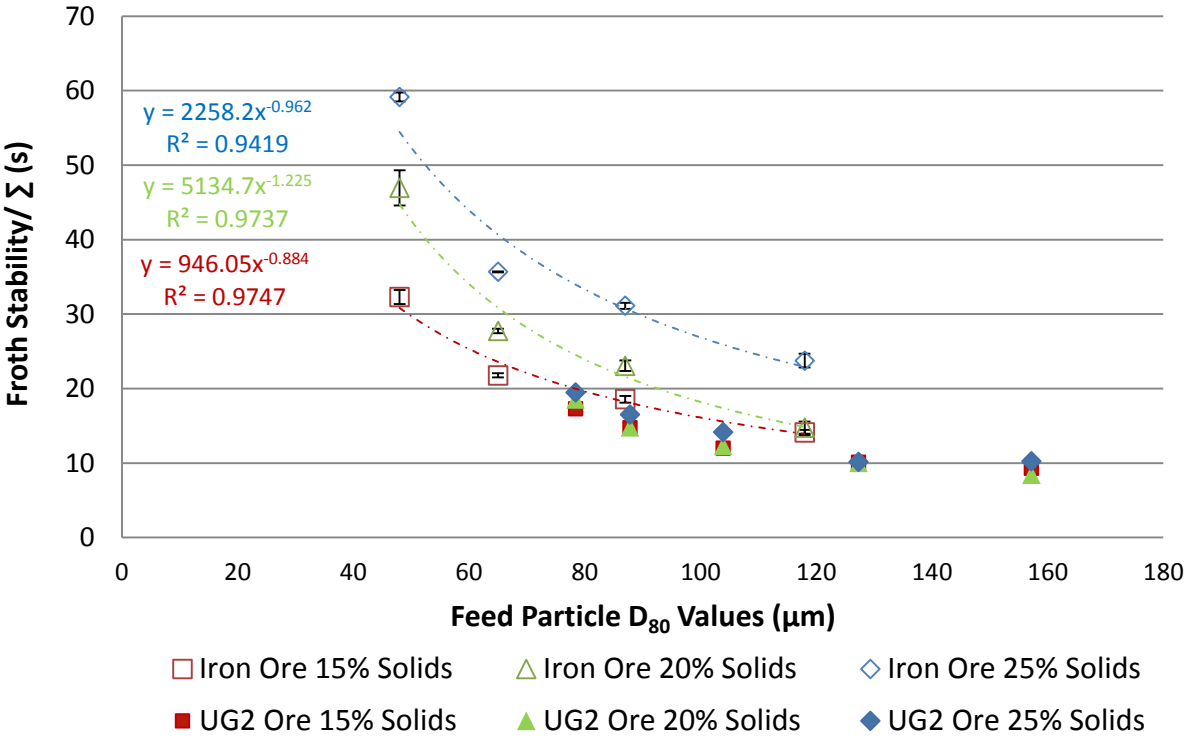

Figure 52: Dynamic froth stability as a function of feed particle size for UG2 and iron ore.

4.4. Agitated Hybrid Cell Results

4.4.1. Float Test Conditions

The UG2 ore tests were performed at a solids concentration of 25% in the presence of a guar gum depressant, Sendep 348 at a dosage of 100 g/t based on the ore mass. The collector used was SIBX at a dosage of 80 g/t based on the ore mass, and the frother was DOW 200 at a dosage of 25 ppm based on the water mass. The tests for UG2 ore were all performed at a constant superficial gas velocity of 1.7 cm/s. A lower frother dosage was used than that used in the frothing column in order to correlate more closely with plant operations, and also to prevent froth from overflowing the launder.

The iron ore tests were performed at a solids concentration of 25% in the presence of starch depressant at a dosage of 750 g/t based on the ore mass. The collector used was EDA at a dosage of 50 g/t based on the ore mass and because the collector possessed frothing properties no frother was used. The tests on iron ore were also all performed at constant superficial gas velocity of 1.7 cm/s. For the iron ore tests, a lower collector dosage and higher depressant dosage were used for the hybrid cell in comparison to the frothing column so as to counteract froth overflowing the launder.

4.4.2. Effect of Particles Size on Water Recovery

The amount of water recovered to the concentrate has been used as an indicator of the stability of the froth phase with a higher water recovery used as an indicator for a more stable froth phase. From Figure 53, it is evident that there was an increase in the amount of water recovered with a decrease in the particle size. The same trend was observed for both the ores tested and at all the column heights evaluated. For UG2 ore from a feed particle size of 160 μm down to 120 μm water recovery was relatively constant, but there was a dramatic increase in the amount of water recovered when the feed particles were finer than 120 μm. The same trend was observed for iron ore, with a dramatic increase in water recovery for feed particles less than 120 μm in size. The water recovery data as a function of feed particle size was fitted to a reducing power law trend line according to the residual values, and the data was shown to follow the model closely.

Minimal difference was observed for the water recovered at the various column heights for the iron ore tests in the column range of 10 cm to 25 cm. A more significant difference in the water recoveries was observed for the UG2 ore tests as shown in Figure 53 with an increase in water recovery with decreasing column height. The shortest column height of 10cm resulted in the maximum water recovery for both UG2 ore and iron ore tests. UG2 ore flotation tests were also shown to have resulted in higher amounts of water recovered in comparison to the iron ore tests at the respective reagent conditions.

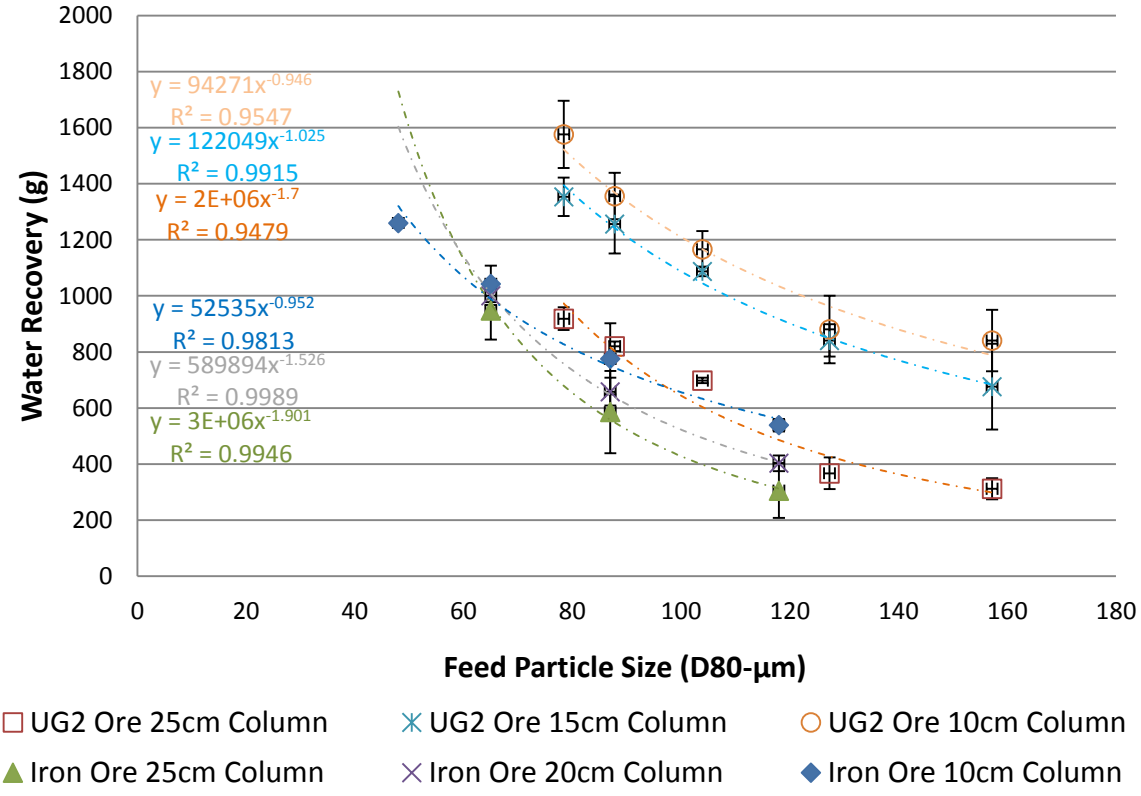

Figure 53: Water recovered as a function of feed particle size for UG2 ore and iron ore.

The amount of water recovered was also assessed as a function of the concentrate particle size. Figure 54 shows that an increase in the concentrate particle size resulted in a reduction in the amount of water recovered for tests conducted on the UG2 ore. The trend observed for the effect of concentrate particle size was similar to that for the feed particle size. The water recovery data was also shown to best follow a reducing power law trend-line, with a sharp increase in the amount of water recovered for concentrate particle sizes roughly less than 60 µm. The decrease in the amount of water recovered with an increase in the concentrate particle size was

observed for all the three column heights tested viz. 10cm, 15cm and 25cm. The shortest column height of 10 cm resulted in the highest amount of water recovered with the 25 cm column resulting in the lowest.

The results for the amount of water recovered from iron ore tests were assessed as a function of concentrate particle percentage passing 38 µm. From Figure 55, it is evident that an increase in the percentage of particles passing 38 µm generally resulted in an increase in the amount of water recovered. This in turn means that a decrease in the concentrate particle size resulted in an increase in the amount of water recovered.

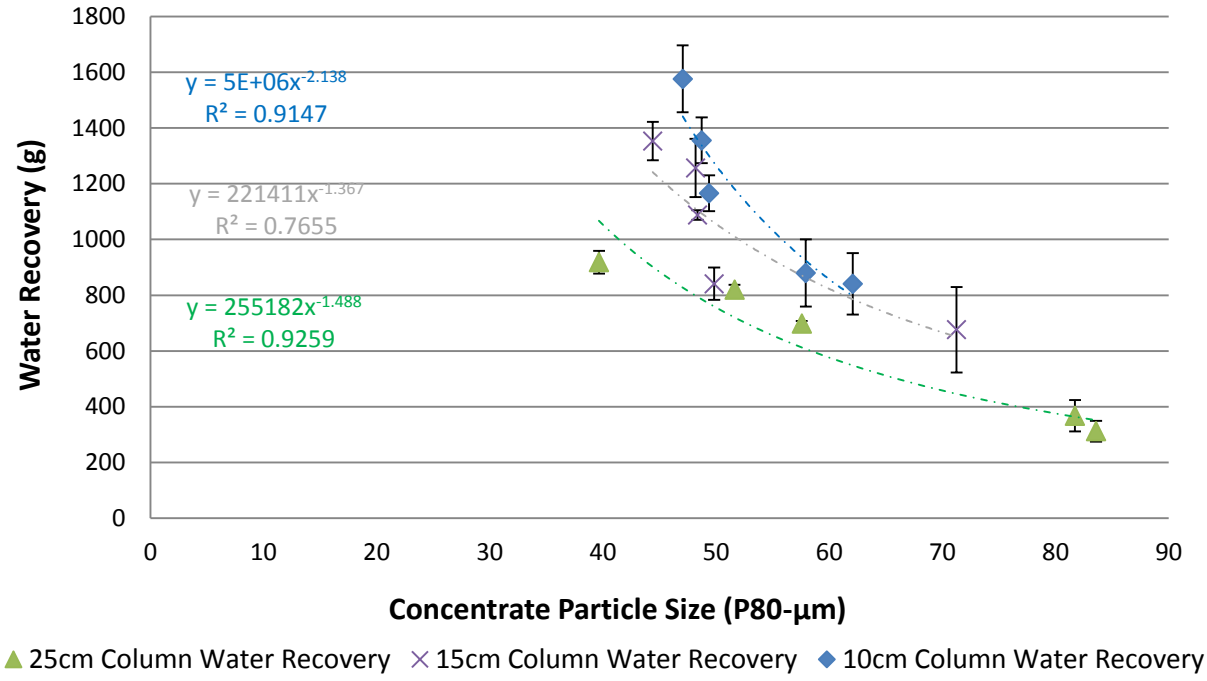

Figure 54: Amount of water recovered as a function of concentrate particle size for UG2 ore.

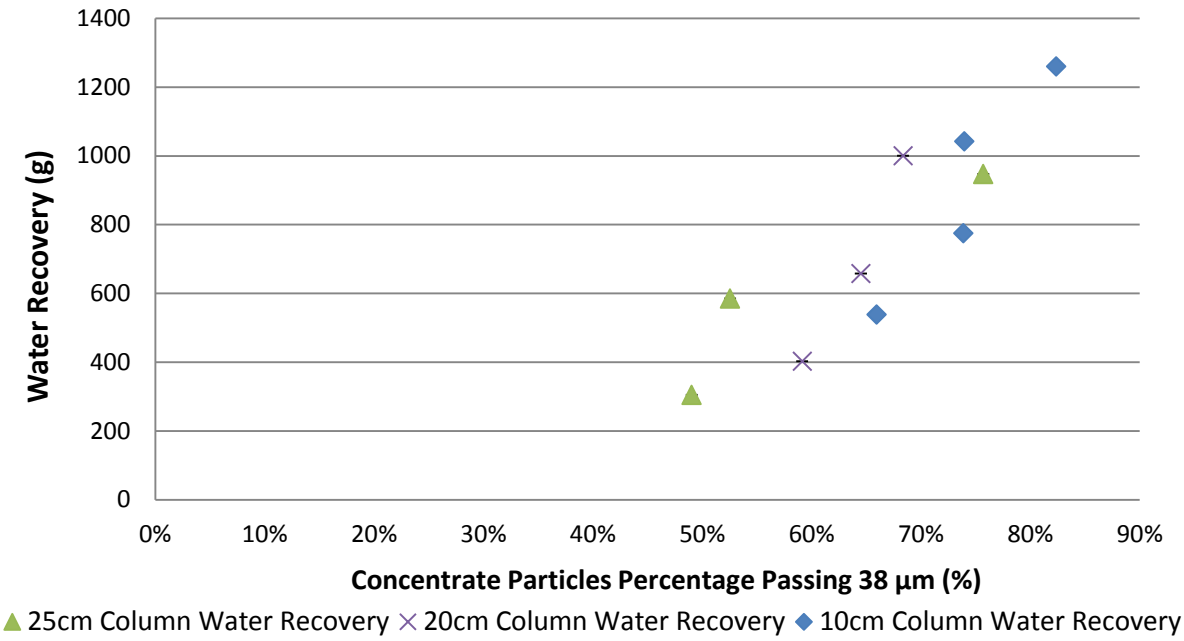

Figure 55: Amount of water recovered as a function of concentrate particle size for iron ore.

The amount of water recovered which is a proxy for froth stability was also evaluated as a function of feed specific surface area for the UG2 ore tests. The amount of water recovered was shown to have a linear dependence with feed specific surface area for all the column heights tested as shown in Figure 56. The amount of water recovered was shown to increase with increasing specific surface area.

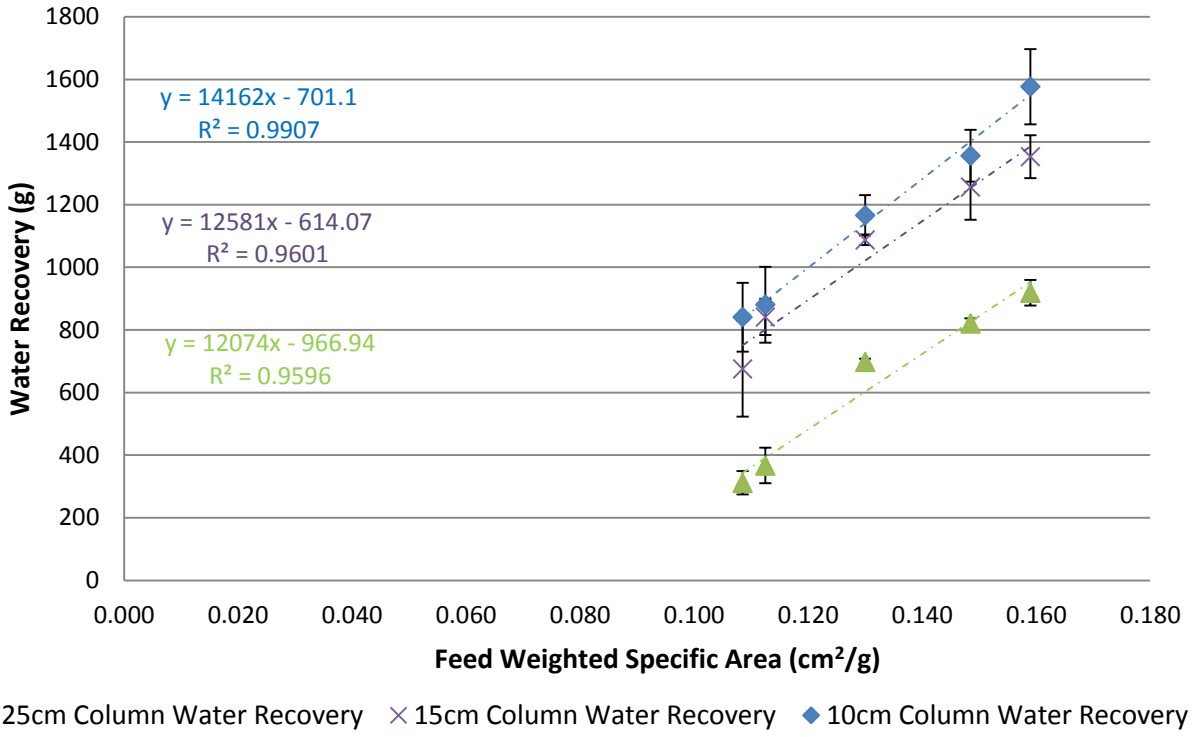

Figure 56: Amount of water recovered as a function of feed specific area for UG2 ore.

The water recovered in the iron ore flotation tests was also evaluated as a function of the reciprocal of feed particle size, which is a proxy of specific surface area. A linear dependence of the amount of water recovered with surface area was also illustrated for the iron ore as shown in Figure 57. The same linear trend was observed at all the column heights tested.

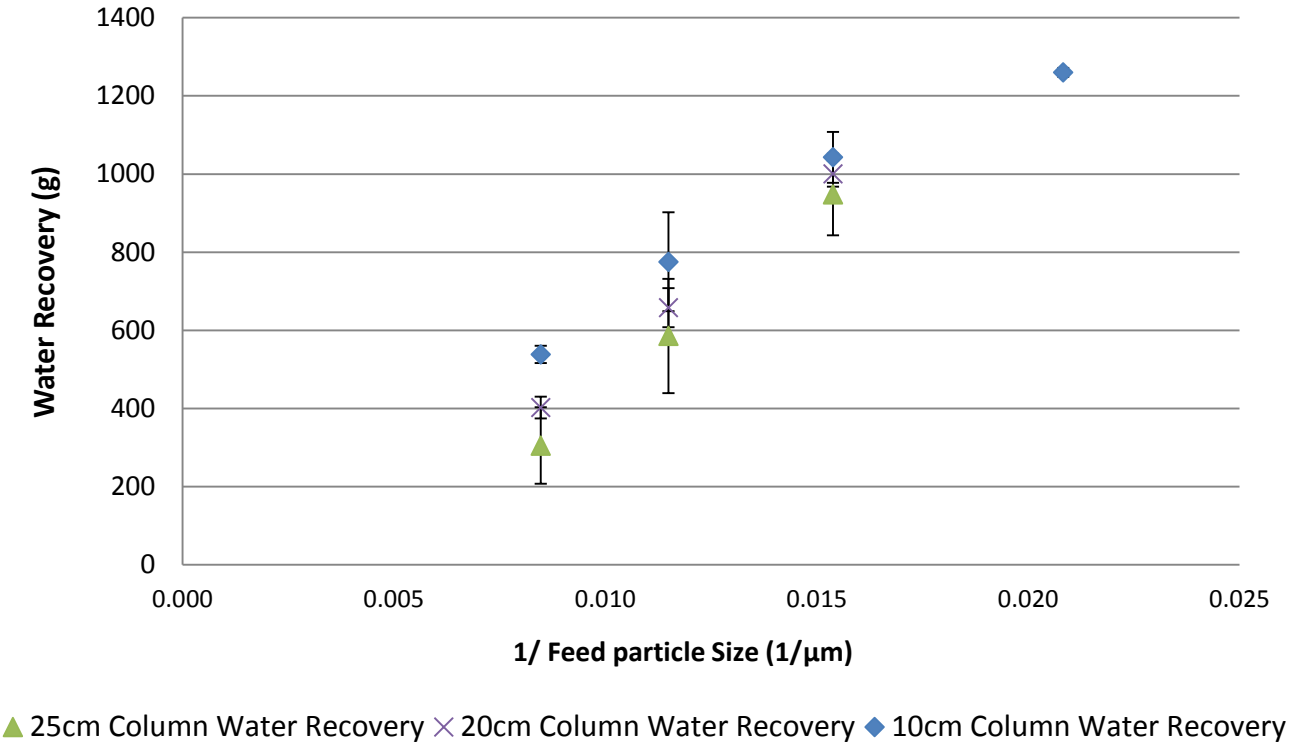

Figure 57: Amount of water recovered as a function of the reciprocal of feed particle size for iron ore.

The amount of solids reporting to the launder was also analysed and as shown in Figure 58, there was an increase in the amount of solids recovered with decreasing feed particle size. The same trend was observed in tests performed on both the UG2 ore and the iron ore. A reducing power law trend was fitted to the data showing the decrease in the amount of solids recovered with increasing feed particle size. The variation in the amount of solids recovered followed the same trend as the amount of water recovered for all the tests performed, with the amount of water recovered as a function of solids particle size also following a reducing power law.

A significant difference in the amount of solids recovered was found with a change in the flotation cell column height, viz. 10 cm, 15 cm and 25 cm for the tests performed on the UG2 ore. Minimal difference in the amount of solids recovered to the launder was observed as the column height was changed for the tests performed on the iron ore as shown in Figure 58. The highest amount of solids recovery was obtained for test work performed with the shortest column height for both ore types.

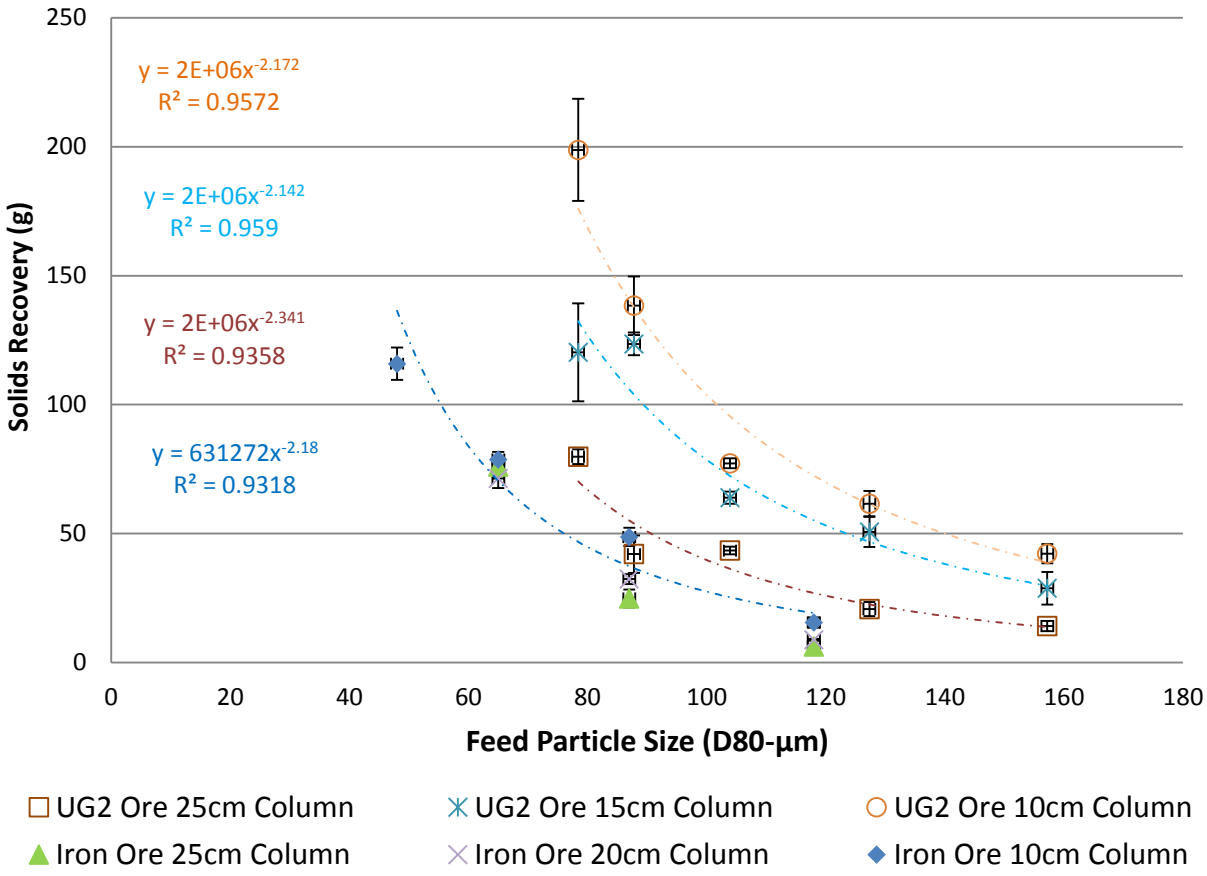

Figure 58: Solids recovered as a function of feed particle size for the UG2 ore and iron ore.

With the amount of water recovered is shown to follow a more linear relationship as a function of feed specific weighted surface area for both ores (Figure 56 and Figure 57) and the amount of solids reporting to the concentrate is shown to considerably differ with froth height (Figure 58), the total amount of surface area imparted by the concentrate particles was then used to decouple the effect of particle amount in assessing froth stability. Figure 59 shows that froth stability, as assessed by the amount of water recovered, had an increasing linear relationship with the total amount of surface area imparted by the concentrate particles. The froth stabilities obtained at the different froth heights were more importantly shown to overlap, thereby showing that the same trend is followed with respect to total surface area despite the different froth heights. The highest froth height tests viz. 25 cm, which resulted in the lowest total surface area, resulted in froth stability measurements that are situated mostly on the lower end of the overall curve. The shortest froth height with the greater total surface area of the concentrate on the other hand, resulted in froth stability measurements which are situated on the higher end of the overall froth

stability curve. The overlapping of the curves signifies that the total surface area of the concentrate particles might be the underlying factor governing froth stability.

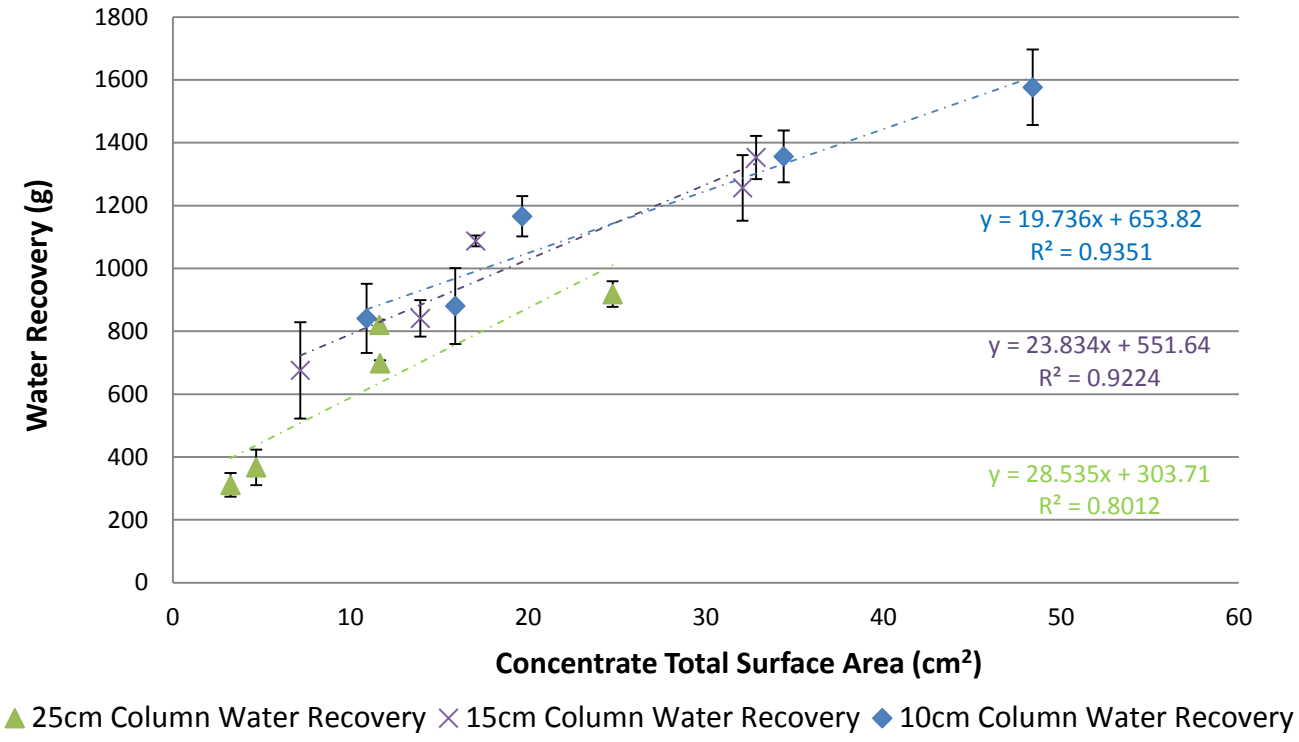

Figure 59: Water recovered as a function of concentrate total surface area for the UG2 ore.

4.4.3. Effect of Particle Size on Top of Froth Average Bubble Diameter

The stability of the froth, as previously stated, was also assessed by using the top of froth sauter-mean bubble size as a proxy for froth stability with an increase in the bubble size depicting a decrease in the stability of the froth phase.

Upon examination of Figure 60, it is evident that an increase in the feed particle size resulted in an increase in the sauter-mean bubble size. This increase in bubble size was observed for all the column heights investigated and for both ore types. There was minimal increase in the average top of froth bubble size in the two coarsest grinds for the UG2 ore viz. D_{80} 127 µm and D_{80} 157 µm illustrating that any further increase in the particle size may result in an insignificant increase in the bubble size.

Minimal differences were observed in the bubble size for tests performed at different column sizes used and this was shown for both ores.

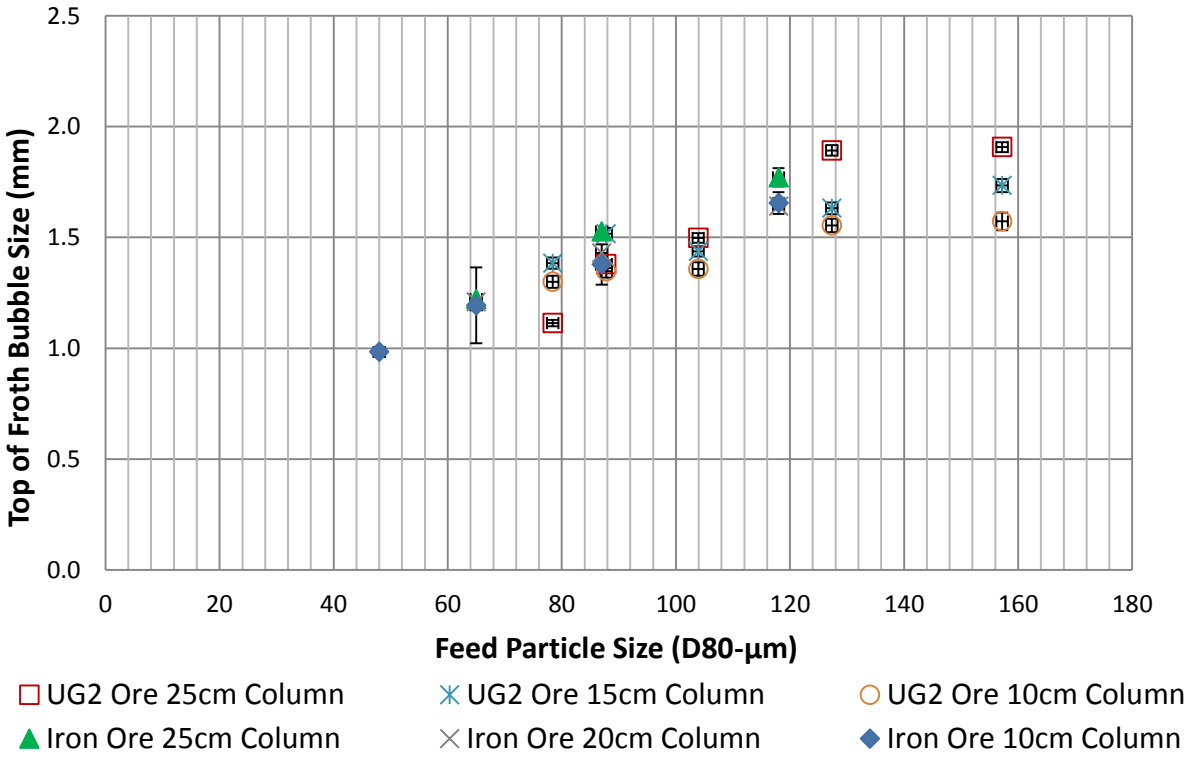

Figure 60: Top of froth sauter-mean bubble size as a function of feed particle size for UG2 ore and iron ore.

4.4.4. Effect of Particle Size on Axial Sauter-mean Bubble Diameter Profile

The stability of the froth was also evaluated by assessing the rate of growth of the bubbles as they moved up the froth in the column. This was evaluated for test work performed on the 25 cm column.

Figure 61 and Figure 62 show the various bubble size profiles for test work performed on UG2 ore and iron ore respectively. The figures illustrate that the coarser the grind, the steeper the gradient of the profile and thus the less stable the froth. The same trend was observed for both the ores.

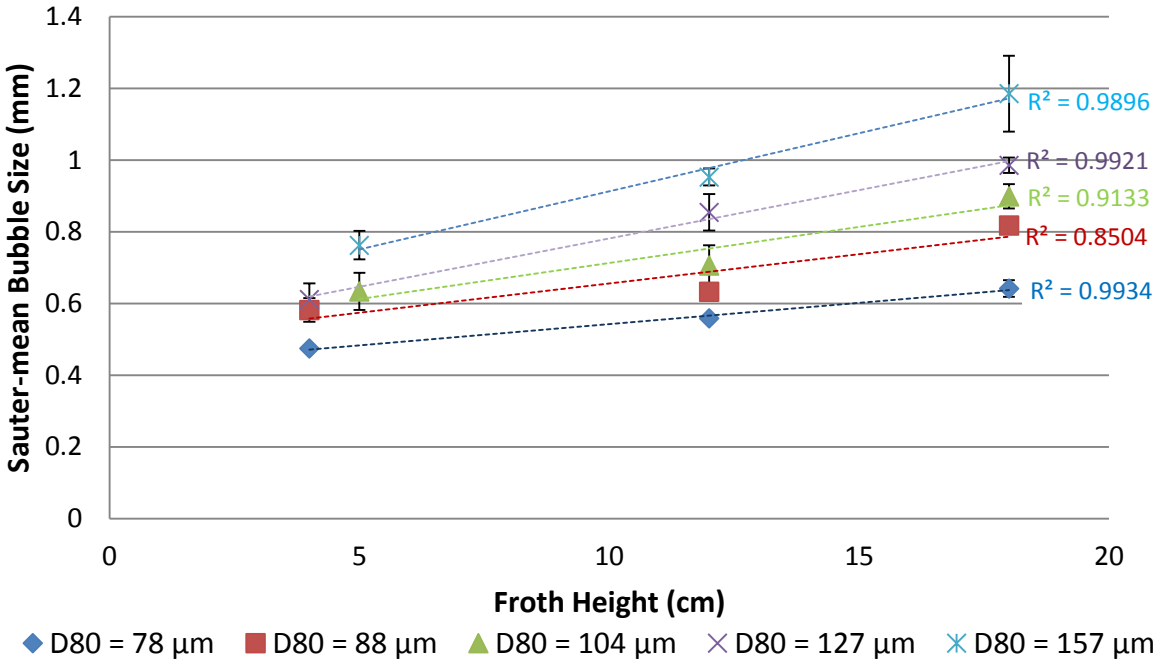

Figure 61: Bubble size as a function of height in the froth phase for UG2 ore.

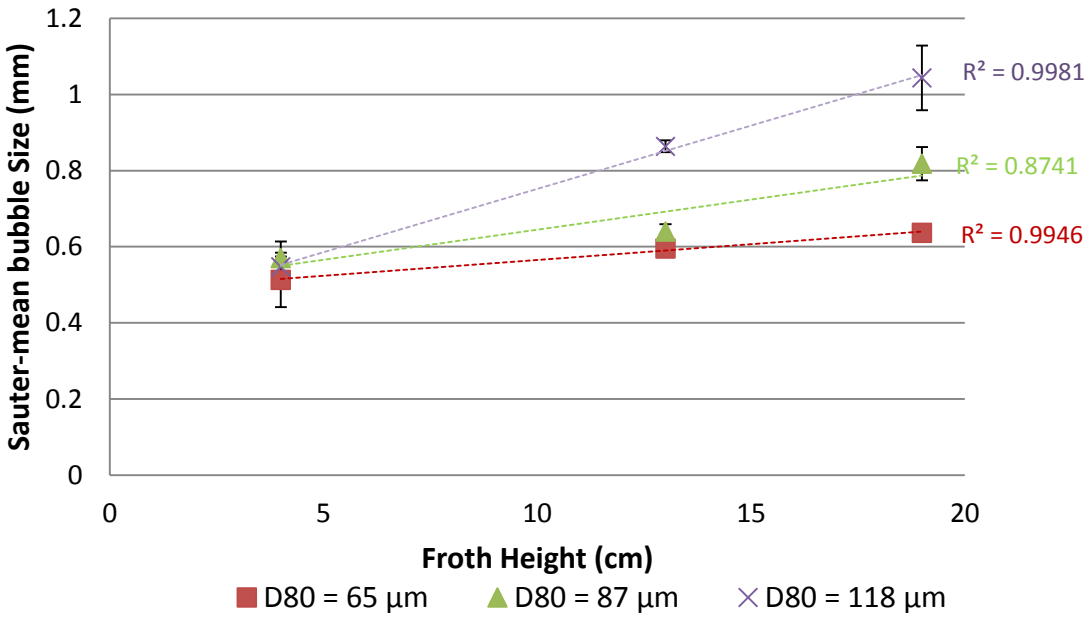

Figure 62: Bubble size as a function of height in the froth phase for iron ore.

The respective gradients from these results were then plotted as a function of the feed particle size as shown in Figure 63. An increase in the feed particle size resulted in an increase in the average bubble size growth rate showing bubble coalescence to form larger bubbles. The trend is shown for both the ore types and thus an increase in particle size resulted in a decrease in froth stability. For the feed size range tested, the UG2 ore bubble growth rate trend showed that the relative effect of particle size was plateauing potentially reaching a maximum value when further increase in particle size would not result in any change in the growth rate.

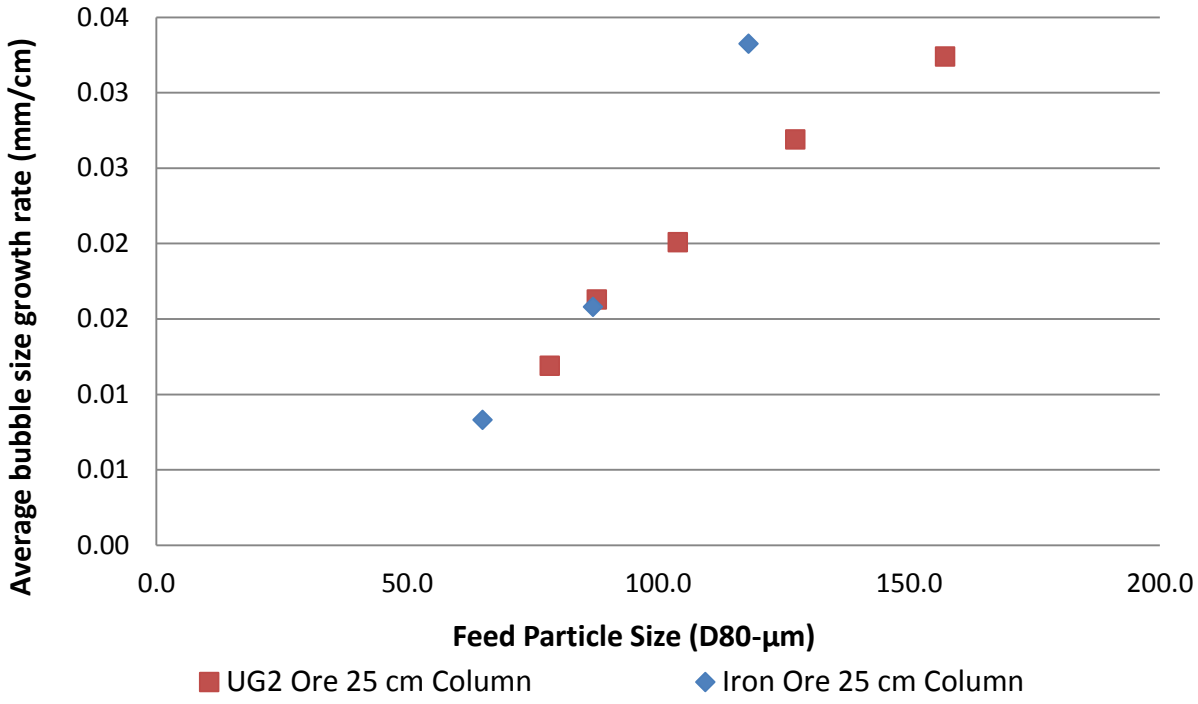

Figure 63: Average bubble size growth rate as a function of feed particle size for UG2 ore and iron ore.

4.4.5. Effect of Particle Size on Froth Recovery

Flotation tests were carried out at different froth heights so as to determine froth recovery according to the technique proposed by Feteris et al. (1987). The froth recovery was determined by using a ratio of the flotation rate constant to that of the collection zone rate constant. The collection zone rate constant was determined by extrapolating a linear flotation rate constant – froth height relationship to the zero froth height.

Froth Recovery

The effect of feed particle size on froth recovery was assessed for the UG2 ore and iron ore as shown in Figure 64 and Figure 65 respectively. Upon examination of the equations for the curves in Figure 64, it is evident that there is no particular trend with respect to flotation rate constant or the collection zone rate constant for the recoveries of PGMs in the flotation of UG2 ore. On the other hand, analysis of the flotation rate constant with froth height relationships for the iron ore yielded linear relationships as shown in Figure 65. From the extrapolation of the linear relationships, the collection zone rate constants were determined with the finest grind with a D_{80} of 65 µm having the highest rate constant and vice versa. The coarsest grind with a D_{80} of 118 µm had the lowest flotation rate at all the three froth heights tested, but all in all were very low as expected (Crosbie, 2009).

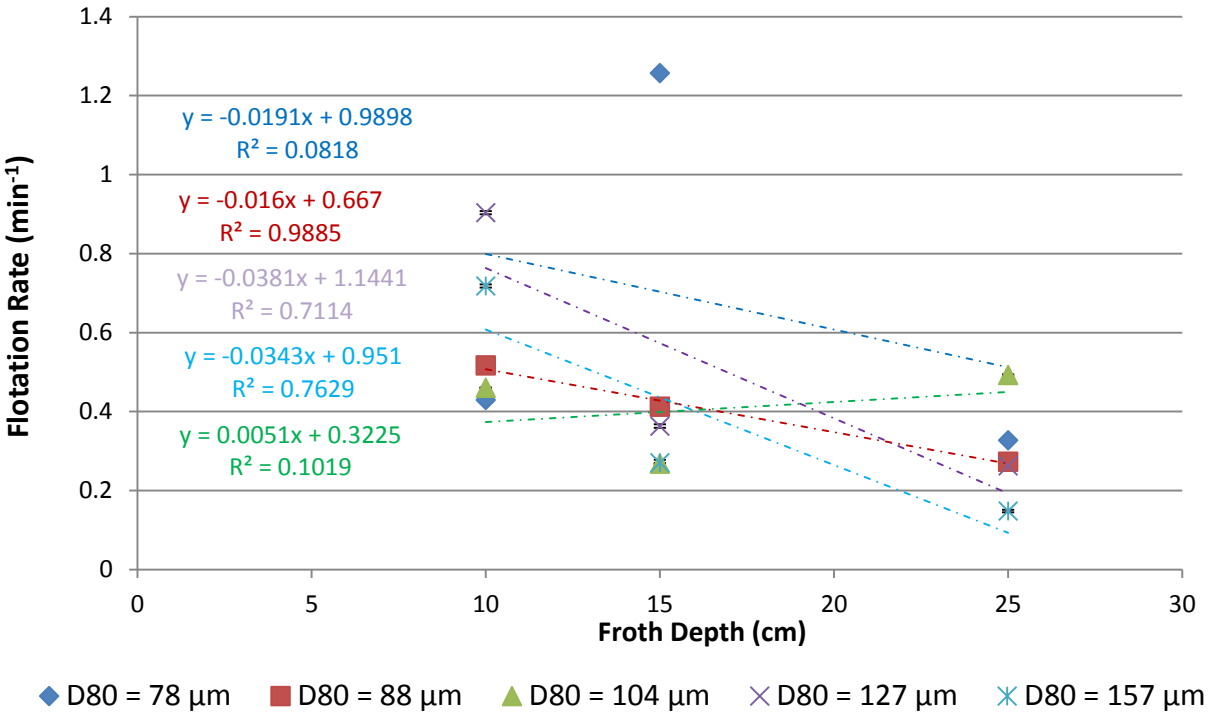

Figure 64: Variation in flotation rate constant as a function of froth height for UG2 ore.

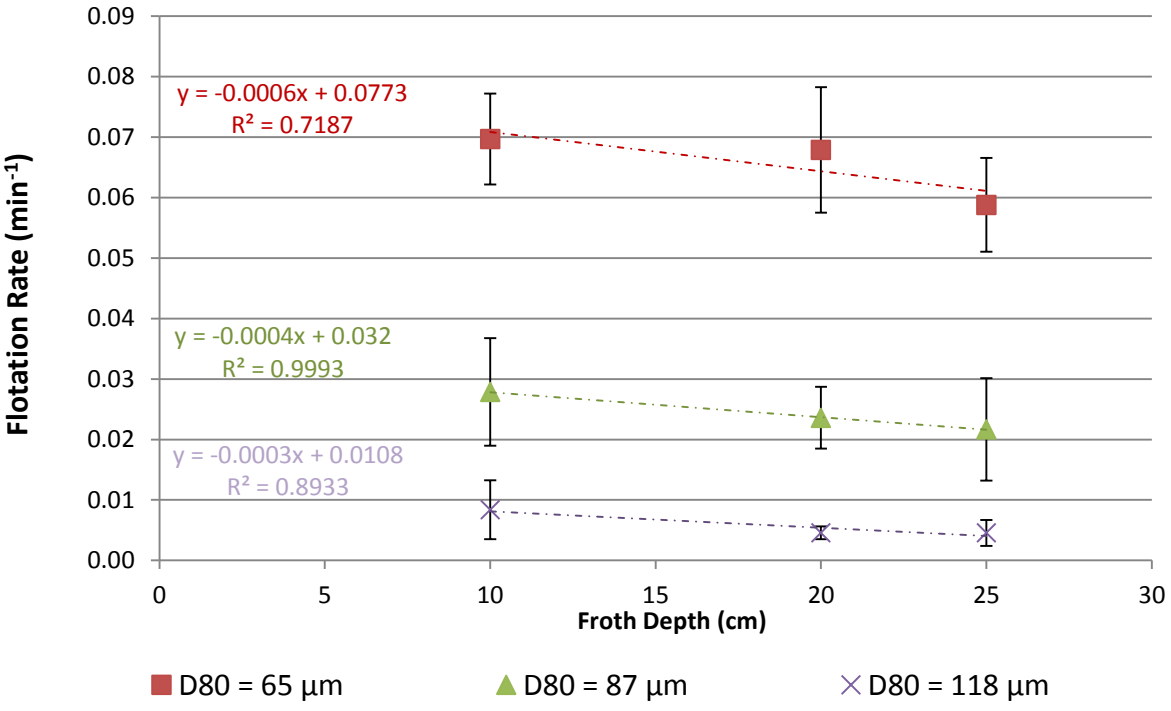

Figure 65: Variation in flotation rate constant as a function of froth height for iron ore.

Further analysis of the flotation rate constants resulted in the froth recovery results as a function of feed particle size for the UG2 ore and iron ore as shown in Figure 66. No clear trend was exhibited for the tests on UG2 ore with respect to the effect of particle size on froth stability. Froth recovery increased with decreasing feed particle size and then a large decrease was observed for the finer size range and this could be attributed to inaccurate assaying of samples. Iron ore froth recovery showed a clear trend for froth recovery with a decrease in the feed particle size resulting in an increase in the froth recovery at all the froth heights tested viz. 10 cm, 15 cm and 25 cm. Froth recovery can thus be used as a supporting proxy for froth stability, with an increase in froth recovery signifying an increase in froth stability and therefore a decrease in particle size resulted in increased froth stability following the same trend observed for water recovery and the stability column results.

The shortest froth height of 10 cm resulted in the highest froth recoveries for all the grinds tested with a higher fraction of the desired mineral ore that reports to the froth phase reporting to the overhead launder as shown in Figure 66.

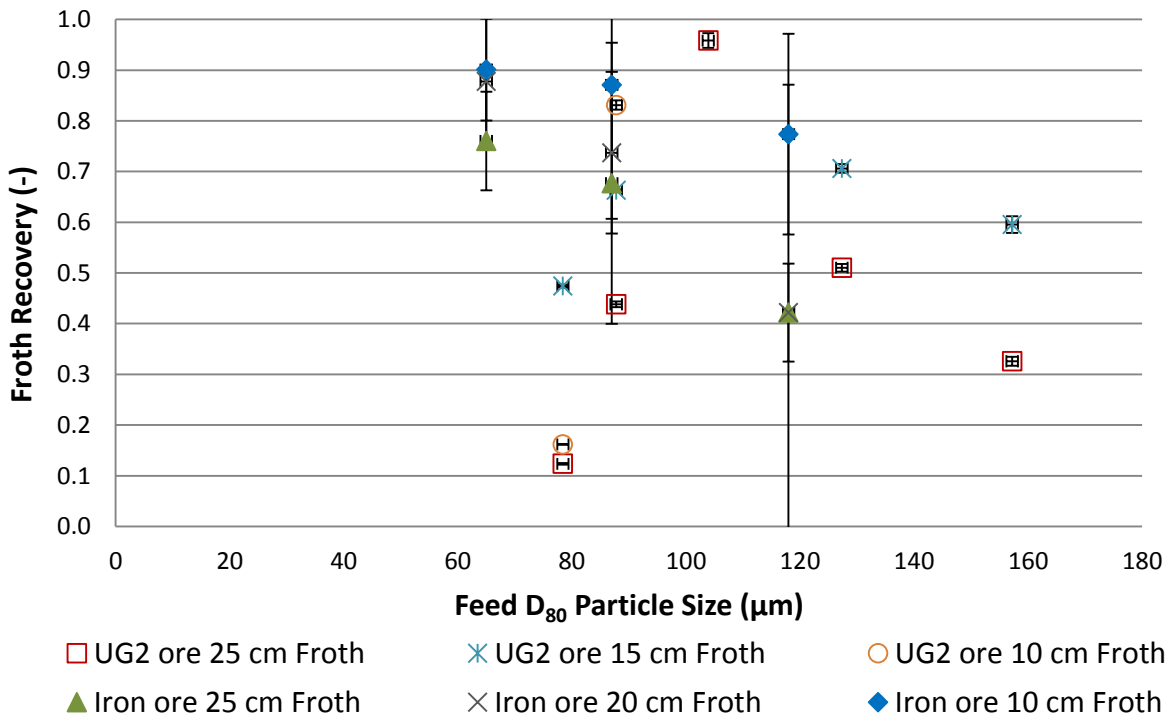

Figure 66: Variation in froth recovery with feed particle size for UG2 and iron ore.

Entrainment Factor

The amount of hydrophilic material that is recovered in the concentrate per unit amount of water recovered can be used as an indication of the degree of entrainment occurring in a flotation system. For the UG2 ore tests, chromite was used as the hydrophilic component indicator. Iron was used as the hydrophilic component for the iron ore as silica is recovered by true flotation in the process.

For the assessment of the effect of particle size, the entrainment factor was analysed as shown in Figure 67 for both ores. The entrainment factor data was fitted to decreasing power law trend lines, with drastic increases in the entrainment factor with reducing feed particle size shown over the finer size ranges for both the UG2 and iron ore tests. The same general trend was observed for all the froth heights tested showing consistent effects of particle size on entrainment as fine particles are expected to report to the froth mainly due to entrainment. It is to be noted that the entrainment factors for the UG2 ore and iron ore tests were not being compared in Figure 67 as entrainment factor is surfactant dependent (Kracht et al., 2016).

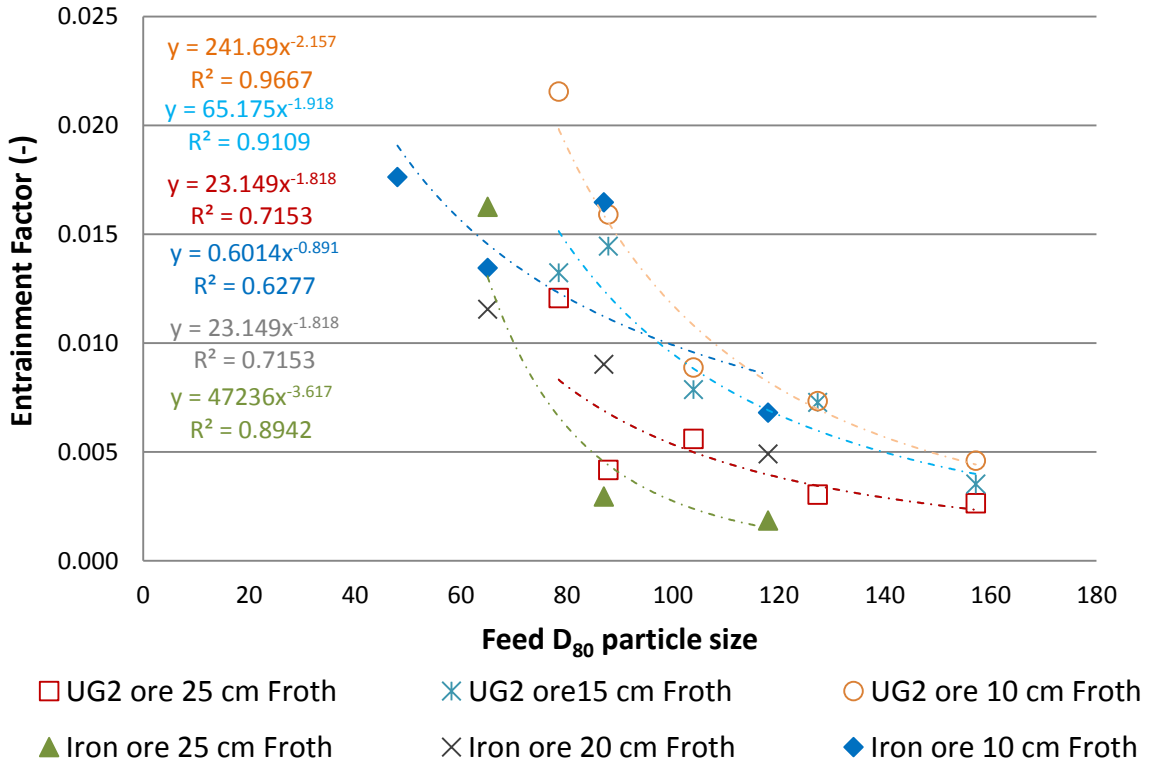

Figure 67: Entrainment factor as a function of feed particle size for UG2 and iron ore.

The chromite based entrainment factor for the UG2 ore was also assessed as a function of concentrate particle size as shown in Figure 68. The entrainment factor was also shown to increase drastically with a decrease in the concentrate particle size. The drastic increase in the entrainment factor became more significant for concentrate particle sizes less than approximately 60 µm for all the column heights tested. The shortest froth height resulted in the highest entrainment factor with the opposite true for the maximum froth height as shown in Figure 67 and Figure 68.

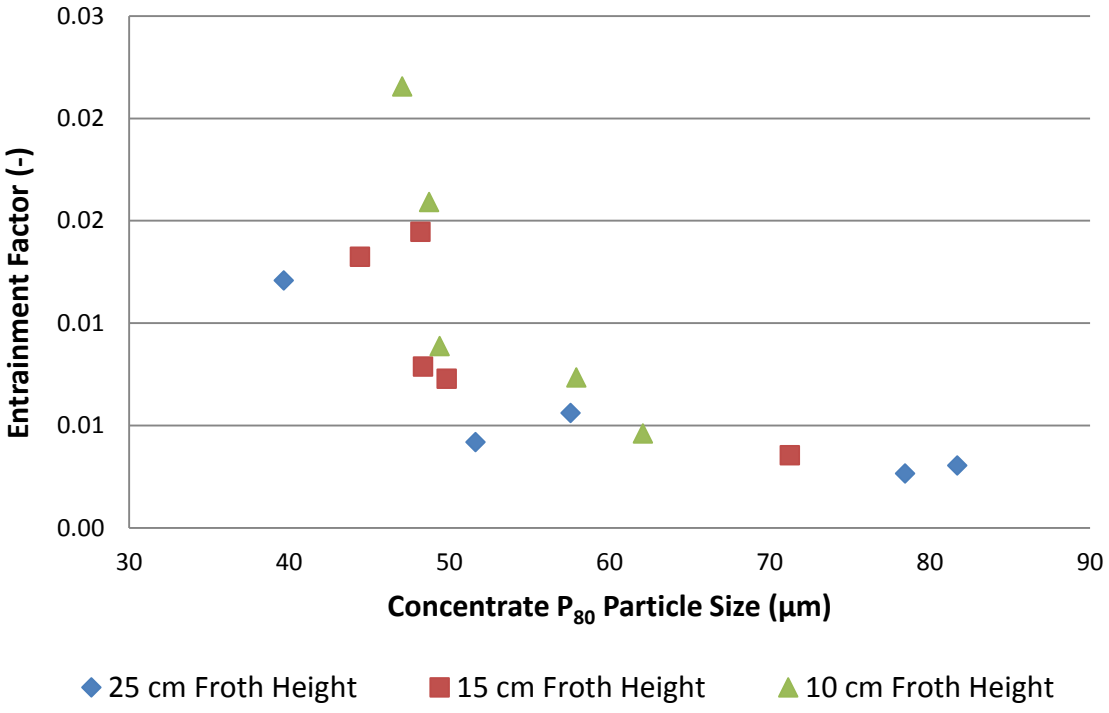

Figure 68: Variation in entrainment factor with concentrate particle size for UG2 ore.

Flotation Performance

The overall performance of the flotation tests conducted was also assessed using the desired mineral recovery and grade as the performance proxies. PGM recovery and grade were used for the assessment of the UG2 ore flotation tests. A general increase in the PGM recovery was observed with a decrease in the feed particle size and this was shown at a froth height of 25 cm and 15 cm as illustrated in Figure 69. It was also shown that an increase in the froth height resulted in a reduction in the overall recovery of PGMs. The maximum froth height of 25 cm resulted in the lowest PGM recovery as there is more time for the particles to drain back into the pulp phase.

The variation in PGM grade as a function of feed particle size was assessed as shown in Figure 69. An increase in the particle size resulted in an increase in the PGM grade. This is in line with the normal flotation trends, which suggest that an increase in recovery results in a compromise in the grade of the desired mineral. The maximum froth height resulted in the maximum PGM grades for all the particle sizes tested, with lowest froth height resulting in the lowest PGM grade as shown in Figure 69. This is in line with the general understanding that a higher froth height allows for more time for drainage of the unwanted gangue material from the froth phase back into the pulp phase.

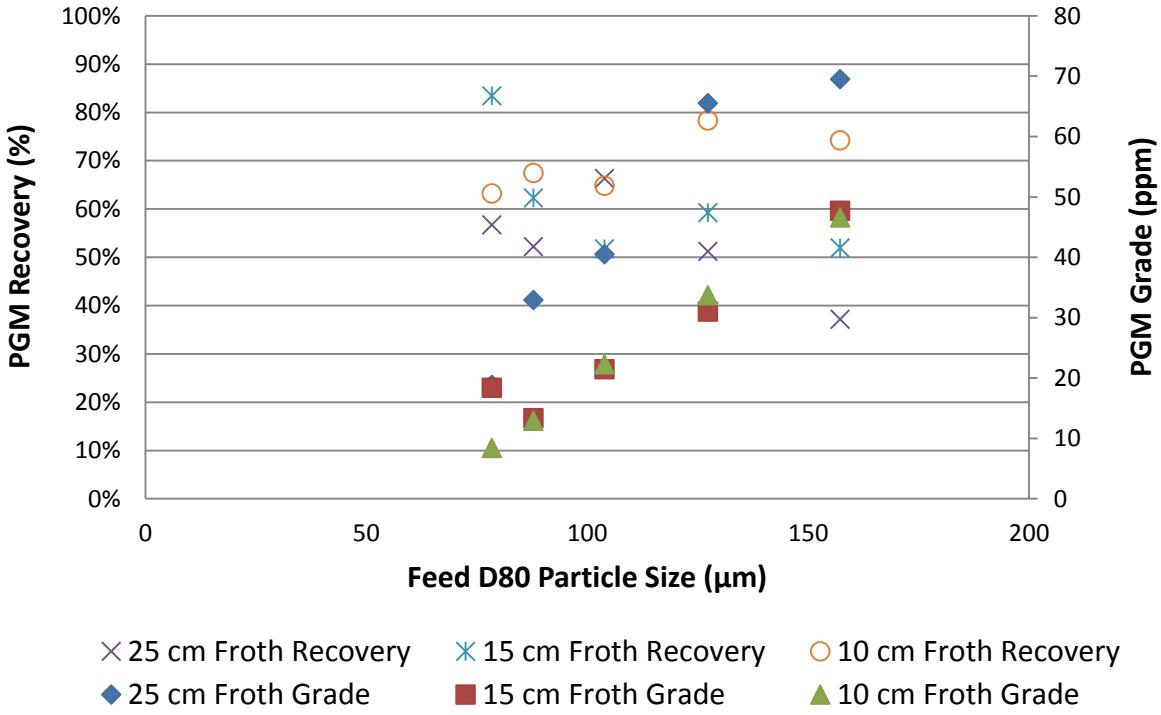

Figure 69: Variation in PGM recovery and grade as a function of feed particle size for the UG2 ore.

Flotation performance of the iron ore floatation tests was also assessed with the recovery of silica used as the hydrophobic, desired mineral performance proxy. Figure 70 shows that an increase in the feed particle size resulted in a decrease in the silica recovery. Significantly lower recoveries were obtained for the iron ore tests as compared to the UG2 ore tests as significantly lower than standard plant reagent conditions were used for the iron ore tests.

A slight decrease in the silica grade was observed with an increase in the feed particle size for tests performed at the 10 cm and 20 cm froth heights. The largest froth height of 25cm resulted in the highest grade for tests performed on the iron ore as shown in Figure 70.

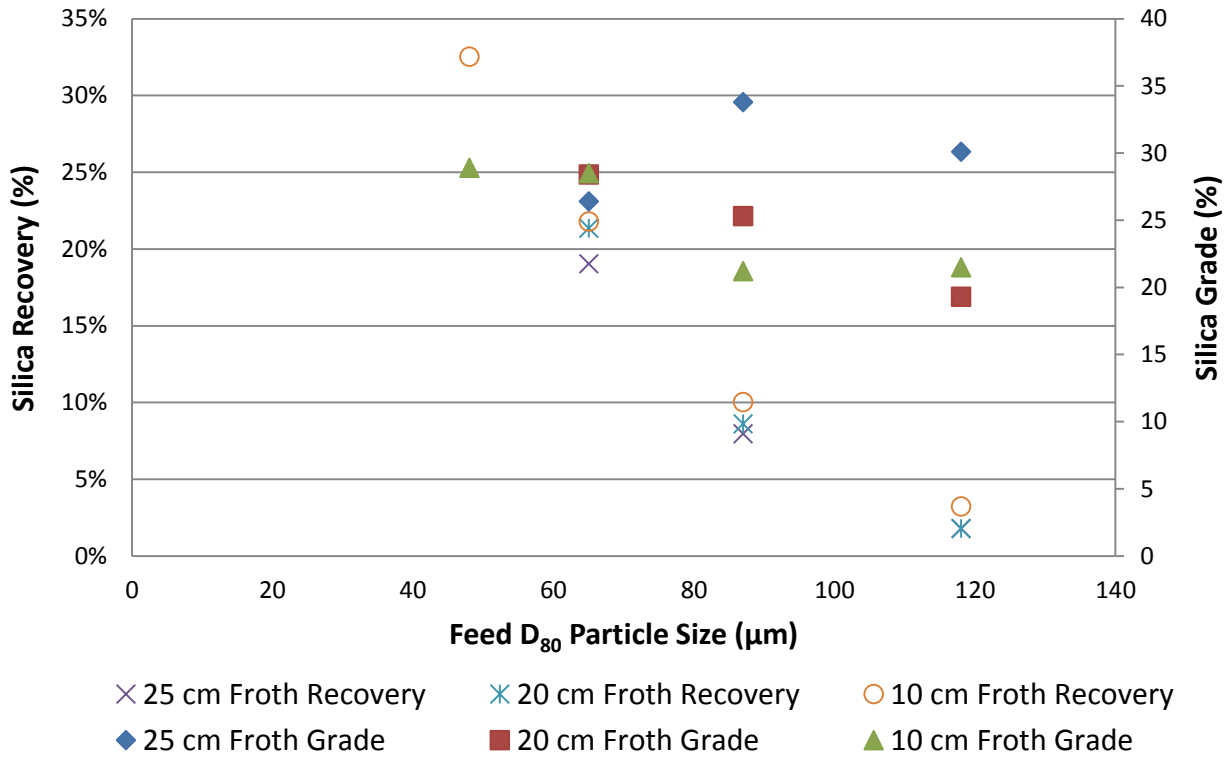

Figure 70: Silica recovery and grade as a function of feed particle size for iron ore.

Chapter 5. DISCUSSION

The aim of this study was to investigate the effect of particle size and solids concentration on the stability of the froth phase. The study's main focus was developing a quantitative relationship between particle size and froth stability. The study was also aimed at assessing the viability of using image processing techniques (namely top of froth and side of froth bubble sizes) in measuring froth stability defined as the ability to resist coalescing.

The experimental approach taken to investigate the proposed hypotheses was fully described in Chapter 3 and the corresponding results shown in Chapter 4. This chapter provides a full discussion of the results presented in Chapter 4.

5.1. The effect of pulp particle size distribution on the froth phase particle size distribution

For this study, the pulp zone particle size distribution was altered by changing the feed particle size distribution. A fine particle size range was defined as feed particle size with a D_{80} less than 100 µm, and the latter as the coarse feed particle size. The change in pulp particle size distribution was expected to result in a change in the particle size distribution reporting to the froth phase. The resultant concentrate particle size was then used to assess the particle size distribution reporting to the froth phase to a reasonable extent. The concentrate particle size was not expected to be an accurate measurement of the actual particle size in the froth phase as some of the particles drain back into the pulp phase before overflowing into the launder due to bubble coalescence (Garibay et al., 2002). The particles are transferred back to the pulp as entrained particles draining with the interfilm fluid due to gravity or as released particles after detaching from rising bubbles due bubble coalescence and turbulence in the froth phase (Farrokhpay, 2011; Ata et al., 2003).

The concentrate particle size was expected to have a slightly finer particle size distribution as compared to the feed size distribution as a larger fraction of the coarse particles will not report to the froth phase as they are less likely to be attached to the rising bubbles in the pulp zone. The residence time associated with particle attachment to bubbles has been shown to decrease in proportion to the particle's size and density. Heavier particles are expected to report less frequently

than fine particles to the froth phase and subsequently to the concentrate due to gravity effects (Harris et al., 1992). Also, due to particle weight, coarser particles drain faster than finer particles after becoming detached from rising bubbles due to coalescence or as entrained particles in the interfilm fluid and as a result, the larger heavier particles will be available in lesser proportions as height in the froth phase increases (Soto, 1992). A considerable amount of coarse particles are however expected to report to the concentrate, as the presence of fine particles stabilises the froth phase resulting in improved coarse particle recovery (Moudgil, 1992; Aktas et al. 2008; Rahman *et al.*, 2012).

The test results presented in Figure 39 and Figure 43, show that the concentrate particle size distribution was significantly finer than the feed particle size distribution for test work performed on both the UG2 ore and the iron ore. The concentrate particle size was shown to be far finer for the UG2 ore as compared to the iron ore. This was expected as the ore is a sparsely mineralized PGM ore forming a less stable froth phase. This then resulted in more of the larger particles draining back to the pulp due to a higher coalescence rate. The finer concentrate size distribution was in accordance with literature which states that finer particles are more readily floated than coarser particles (Soto, 1992; Moudgil & Gupta, 1989; Viera & Peres, 2007). This might contradict some of the literature which states both coarse and fine particles do not float very well as fine particles are less likely to collide with the rising bubbles thereby streamlining back into the pulp with the draining interfilm fluid (Trahar, 1981). Fine particles also tend to have large specific areas which can lead to excessive adsorption of reagents, and other effects associated with chemically active particles that inhibit the floating of fine particles (Feng & Adrich, 1998).

Changing the feed particle size was also shown to result in a change in the concentrate particle size distribution as shown in Table 12 and Table 13. The apparent relationship enabled for alterations in the feed particle size to be used to effect a change in the size distribution of particles reporting to the froth phase. The intention of the study was to investigate what effect the size of particles in the froth phase had on the stability of the froth, and changing the feed particle size had been conclusively shown to effect a change in the froth zone particle size distribution.

5.2. The effect of particle size on froth stability

Literature shows that a qualitative consensus exist on the effect of particle size on froth stability, stating that a decrease in particle size will result in increased froth stability (Johansson & Pugh, 1992; Aktas et al., 2008; Hunter et al., 2008; Farrokhpay, 2011). On the other hand, limited quantitative relationships have been postulated for the relationship of particle size and froth stability. An inverse linear relationship between particle size and froth stability was, however, shown by Ip et al., (1999) investigating aluminium metal foams which showed an increase in froth stability imparted by a decrease in particle size. Johansson and Pugh demonstrated that the 26 – 44 μm size had a higher stability (maximum froth height) than the 74 – 106 μm size range for the same frother concentration. In the present study, results from both the stability column and the agitated hybrid cell show a general increase in the froth stability with decreasing particle size over a feed size range of D_{80} 78 – 157 μm for the UG2 ore and 48 – 118 μm for the iron ore.

5.2.1. Non-continuous system

From the results obtained from test work on the stability column, froth stability was shown to increase with decreasing particle size as assessed by the froth stability factor, average bubble lifetime and froth half-life. The froth stability factor which is based on the maximum equilibrium froth height was shown to follow a decreasing power law trend as a function of feed particle size as shown in Figure 44 and Figure 49 for both the UG2 ore and iron ore respectively. Since an inverse relationship exists between the maximum capillary pressure and the particle size with a decrease in particle size resulting in an increase in the maximum capillary pressure according to Equation 2-3, it can be postulated that, decreasing the feed particle size resulted in an increase in the maximum capillary pressure and as a result reduced the pressure difference between the plateau borders and the bubble film. This in turn resulted in reduced capillary drainage and thus a more stable froth phase since it was postulated by Dippenaar (1982b) that film drainage rate was the rate determining step in bubble coalescence. The decrease in particle size can also be postulated to have resulted in finer particles entrained in the lamellae fluid; this then affected the fluid rheology by increasing the viscosity of the fluid. The increased fluid viscosity reduced the fluid drainage rate, thereby increasing the stability of the froth phase shown by an increase in the maximum equilibrium froth height. The trend

shown did not follow the inverse linear relationship with particle size as observed by Ip et al. (1999).

The effect of feed particle size on froth stability was also shown to follow a decreasing power law trend as assessed by the average bubble lifetime, which is a stability proxy based on the froth growth rate. The decreasing power law relationship was clearly demonstrated for both the UG2 ore and iron ore as shown in Figure 46 and Figure 51 respectively. A decrease in the feed particle size was shown to result in an increase in the average lifetime of each bubble and hence an increased froth stability. This followed the trend shown by Feng and Adrich (1999) with water recovery which can has been used widely as a froth stability proxy. The tests were performed using discrete sizes from 20 µm to 90 µm. A gradual increase in froth stability was observed with decreasing particle size in the coarser size range (particles with feed D_{80} greater than 100 µm) and then a steep increase in froth stability is shown for the finer particle size range (particles with feed D_{80} less than 100 µm), hence the decreasing power law trend. This trend suggests that finer particles had a significantly greater influence on the stability of the froth as compared to coarse particles. The same trend is also observed with the analysis of froth stability using the froth half-life as a stability proxy for the UG2 ore as shown in Figure 47. Finer particles resulted in longer froth lives and thus a more stable froth phase. This suggests that froth stability follows a decreasing power law trend as a function of feed particle size for a non-continuous system as tested by a frothing stability column.

The stability of the froth phase was also investigated as a function of particle specific surface area and froth stability was shown to increase with increasing specific surface area. A more linear relationship was shown between froth stability as measured by the froth stability factor and the particle specific surface area as shown in Figure 45. A decrease in the particle size, which in turn results in an increase in the particle specific area, resulted in an increase in the stability of the froth phase. The linear dependency of the froth stability on feed particle surface area was also shown with the evaluation of froth stability according to average bubble life-time and the static froth half-life proxy. The more linear trend with feed specific area was consistently observed in all the stability column tests performed. The results from the

non-continuous flotation tests suggest that froth stability has an increasing linear dependency on the feed particle specific surface area.

5.2.2. Continuous System

The effect of particle size on froth stability was also assessed in a continuous floatation system, using an agitated hybrid cell. The continuous system provided a more comprehensive assessment of the effect of interest, as it is more representative of plant operations which are also continuous. Froth stability was evaluated using water recovery (Aktas *et al.*, 2008) and a decrease in particle size was shown to result in an increase in froth stability as shown in Figure 53. The trend was also postulated to be as a result of the same mechanism discussed in the non-continuous system stability column tests. Decreasing the particle size resulted in an increase in the maximum capillary pressure and viscosity of the lamellae fluid in the continuous system, which in-turn caused an increase in the stability of the froth phase. This follows the trend observed in earlier studies by Feng and Aldrich (1999) which also showed a decrease in the amount of water recovered with increasing particle size.

A quantitative relationship between the water recovered and feed particle size was determined with a decreasing power law trend shown between the water recovered and feed particle size as shown in Figure 53. The feed particle size was used to determine a relationship with froth stability as it allows for a more accessible variable in plant operations. The decreasing power law relationship findings followed the same trend illustrated by froth stability proxies from the non-continuous system. This followed the trend shown by Feng & Adrich 1999 using discrete size ranges between 20 µm and 90 µm for tests on the UG2 ore and Merensky ore. The trend was observed at all the column heights tested, with the amount of water recovered conclusively shown to gradually increase with decreasing feed size over the coarser size range (particles with feed D_{80} greater than 100 µm corresponding to concentrate particle size greater than 50 µm). A steep increase in the amount of water recovered was achieved with decreasing particle size over the fine particle size range (particles with feed D_{80} less than 100 µm corresponding to concentrate particle size less than 50 µm) which is typically associated with particles reporting to the froth phase through entrainment (Smith & Warren, 1989; Savassi et al., 1997). The decreasing power law trend did not follow the trend presented in earlier research by Ip et al.

(1999) which showed a linear decrease in froth stability with increasing particle size. In order to obtain a more direct relationship with the postulated stabilising mechanism, froth stability was also assessed as a function of concentrate particle size as shown in Figure 54 and Figure 55. The sharp increase in froth stability for the UG2 ore was shown to occur for particle sizes less than 50 μm. This then suggests that the entrainment of fine particles might have a more significant effect on the stability of the froth phase by increasing the inter-film fluid viscosity which in-turn reduces the drainage rate.

Froth stability was also assessed as a function of the feed specific surface area and a linear relationship was observed with the amount water recovered increasing with increasing particle specific area as shown in Figure 56 and Figure 57. These findings confirmed the results obtained for the non-continuous system which exhibited a linear dependence of froth stability on particle specific surface area. The linear dependence was observed at all the column heights tested and for both ores thus increasing the surface area for reactions results in increased froth stability.

Froth recovery was also used as a proxy for froth stability (Finch & Dobby,1990). A higher froth recovery shows that a higher fraction of the solids reporting to the froth phase are being recovered to the launder. This in turn means the froth is more stable, as fewer bubbles are bursting releasing the attached material, allowing it to drain back into the pulp zone. Froth recovery was then used to assess the effect of particle size on froth stability as shown in **Error! Reference source not found.**Figure 66, for both ores. From the examination of the figure, it was shown qualitatively that a decrease in feed particle size resulted in an increase in froth recovery and thus increased froth stability. The results suggest that a decrease in the feed particle size will result in reduced bubble coalescence and bursting thereby allowing for a higher fraction of the bubble attached particles and entrained particles to be recovered to the launder. A distinct quantitative relationship between particle size and froth recovery was not observed for both ores.

Since the size of the particles that are reporting to the froth phase and the amount of particles recovered has been shown to change with particle size, total surface area imparted by the particles was used to assess froth stability as shown in Figure 58. The amount of solids recovered to the concentrate was shown to increase with

decreasing particle size following generally the decreasing power law trend for froth stability. This was expected as an increase in froth stability will result in less of the attached particles detaching and draining back into the pulp zone as there is less bubble coalescence. The amount of solids recovered was also shown to vary with froth height and therefore the total surface area imparted by the concentrate particles was then used as the factor to assess froth stability. Froth stability was shown to increase with increasing total concentrate surface area as shown in Figure 59. Froth stability followed a more linear trend at the three column heights tested and the respective particle size range for UG2 ore. The froth stability curves were also shown to almost overlap for the different froth heights suggesting that the effect of froth height on froth stability was heavily outweighed by the overall effect of the total particle surface area on froth stability which follows a linear trend over the size range investigated.

5.3. The major contributing particle froth stabilising mechanism

There is no consensus in literature as to which particle froth stabilising mechanism has a greater influence on froth stability. The particle stabilising properties are either affected by the inter-film layer, with particles affecting the rheology and drainage of the inter-film fluid or in the particle-interface steric barrier formed, altering the maximum capillary pressure (Hunter et al., 2008). From the froth stability proxies discussed, it was shown that there was a gradual increase in the froth stability with decreasing particle size over the coarser size range. This followed the trend shown by Ip et al. (1999), with particles attached to the interface resulting in the flattening of the bubble curvature around the plateau borders altering the maximum capillary pressure. A decrease in the particle size results in an increase in the maximum capillary pressure and thus a more stable froth. A sharp increase in froth stability was shown with decreasing particle size in the finer size range. Figure 54 showed that the steep increase was exhibited for concentrate particles of less than 50 μm and particles in this size range report to the froth phase mainly through entrainment (Smith & Warren, 1989). Decreasing the particle size in the inter-film fluid will result in increased viscosity and it has been shown by Gergely and Clyne (2004) that increasing the inter-film fluid viscosity will inhibit drainage thereby increasing froth stability.

The entrainment factor results suggest that the amount of entrained material also followed a decreasing power law trend with feed particle size as shown in Figure 67**Error! Reference source not found.**. Froth stability followed the same trend as the amount of entrainment, thereby showing that the amount of entrainment has a significant correlation with froth stability for the size range investigated. The entrainment factor was also shown to spike with decreasing particle size for sizes less than 50 µm. This follows the proposed trend in literature which states that particle less than 50 µm in size are more prone to entrainment (Smith & Warren, 1989; Neethling & Cilliers, 2002). Therefore the particle-interface steric barrier stabilising method can be suggested to have a less pronounced effect on froth stability. The sharp increase in froth stability following the same trend as the entrainment factor can then lead to a postulation that particle entrainment in the fine size range resulting in particles affecting the rheology and drainage of the inter-film fluid has a more significant effect on the stability of the froth phase in the particle size range tested.

5.4. The effect of solids concentration on froth stability

Gergely and Clyne (2004) showed that high particle concentration could increase the viscosity of the inter-film fluid and inhibit liquid drainage thus increasing froth stability. An increase in solids concentration results in increased bubble surface coverage which results in a reduced coalescence rate and thus increased froth stability. The increased bubble loading will on the other hand reduce froth mobility increasing the time for froth drainage thereby reducing the stability of the froth (Gergely and Clyne, 2004).

Figure 46 and Figure 51 illustrated that an increase in solids concentration resulted in an increase in the stability of the froth phase as assessed by the average bubble lifetime. This followed the same trend shown in literature by Sun and Gao, 2001, were the froth height of ethanol-60% water solution was shown to increase against TEFLON powder concentration. The foam volume increases approximately linearly with particle concentration. During the growth of the froth, an increase in the solids concentration will result in an increase in the amount of available particles that can be attached to the bubbles increasing the surface coverage. The same trend was also observed by Ip et al., 1999 in the study of aluminium froths. The increase in solids concentration will also increase the amount of available fine particles that can

be entrained into the froth phase and change the rheology of the inter-film fluid. This will then result in an increase in froth stability.

Solids concentration was shown to have minimal effect on froth stability as evaluated by the froth stability factor for UG2 ore as shown in Figure 44. Since the froth stability factor is based on the equilibrium maximum froth height, the system reaches its equilibrium amount of particles that can be supported at a given reagent dosage and equipment. An increase in the solids concentration therefore resulted in minimal increase in the maximum froth height for the sparsely mineralised PGM-bearing ore. An increase in the solids concentration for the iron ore which is naturally floating resulted in increased bubble loading thereby increasing froth stability as shown in Figure 49.

Solids concentration was also shown to have a minimal effect on froth stability as assessed by the froth half-lives for UG2 ore. Since the half-lives are measured from the equilibrium maximum height, the maximum equilibrium heights at the different solids concentration have been shown to be the same, with also roughly the same amount of particles in the froth phase. As a result, minimal differences in the half-lives were shown for the different solids concentrations as shown in Figure 47.

5.5. The effect of ore mineralogy affect froth stability

The iron ore which has a large silica fraction as its hydrophobic component resulted in higher froth stability values as compared to the UG2 ore as shown in Figure 52. The iron ore is therefore more hydrophobic as compared to the sparsely mineralised PGM-bearing UG2 ore and this was evident from the higher froth stability values obtained for the work done in the stability column. Platinum-bearing ores with fragile, poorly mineralised froths are known to have froth recoveries that are routinely less than 10% (Crosbie et al, 2009)as compared to the iron ore which was supplied at 36% hydrophobic SiO_2. The iron ore tests resulted in higher stability factor values and average bubble lives as compared to the UG2 ore tests and this is postulated to be due to the increased bubble loading that occurs with the iron ore as there is more of the desired hydrophobic component in the froth of silica in the reverse-flotation process of the iron ore. Lower froth stability values and recoveries were also shown for the sparsely mineralised UG2 ore in tests by Feng and Adrich (1999), which was

being compared to the Merensky ore which has its PGMs associated with pentlandite that is approximately 32%.

UG2 ore tests conducted on the continuous hybrid cell resulted in higher water recoveries and thus greater froth stability than iron ore tests which was un-expected. This was due to the very high depressant dosage that was used in the hybrid cell tests which was more than 3 times the standard plant operation conditions and lower the collector dosage used. The reagent dosages were adjusted significantly to combat the over-flowing of the froth in the launder as the froth bubbles resisted collapsing. This in-turn resulted in a less stable froth phase as compared to the UG2 ore tests.

5.6. The use of image analysis techniques to assess froth stability

The top of froth bubble size and side of froth bubble coalescence profile were investigated as proxies to measure froth stability as they can be considered as true froth stability indicators that vary due to the changes in the stability of the froth. Water recovery which is a more robust proxy that has been widely used as a froth stability proxy (Wiese et al., 2011) and hence the trends exhibited by the water recovery were then used to compare with the trends shown by image analysis techniques which measures bubble coalescence.

5.6.1. Top of froth phase Sauter-mean bubble size

The top of froth bubble size has been proposed as a tool to evaluate froth stability. The larger the average bubble size at the top of the froth, the less stable the froth as the bubbles would have coalesced more in the froth phase forming larger bubbles (Ventura-Medina et al., 2002; Lin et al. 2008). The top of froth bubble size can be applied to plant operation as it allows for non-intrusive froth stability measurements. From Figure 60, it was shown that an increase in the particle size resulted in an increase in the top of froth bubble size for both the UG2 ore and iron ore with the trend exhibited at all the column heights tested. The top of froth bubble size trend showed that the bubble size plateaued with increasing particle size. The trend corroborated with the other froth stability proxies, which also showed relative decreases in the effect of particle size on froth stability. The image analysis technique showed similar trend to earlier research by Ventura-Medina et al., (2002) were the least stable froth corresponded to the largest bubbles. The top of froth

bubble size can then be used to measure froth stability with caution as the analysis techniques used were not accurate as bubbles were measured individually by hand.

5.6.2. Side of froth axial Sauter-mean bubble size

The rate of bubble coalescence measured from the pulp-froth interface to the froth surface can be used to assess froth stability. Ata et al., (2003) used the method to evaluate the effect of hydrophobicity on froth stability. Figure 61 and Figure 62 show the variation in average bubble size up the column for the UG2 ore and iron ore respectively. The slopes of the curves are shown to increase with increasing particle size for both ores. The increase in the slopes demostrated that an increase in the particle size resulted in higher bubble coalescence rates since the slopes were higher indicating a less stable froth. This provided a robust qualitative assessment of the effect of particle size on the stability of the froth. A plot of the slopes of the various curves as a function of particle size is shown in Figure 63. The coalescence rate was shown to increase with increasing particle size for both ores. This suggests that an increase in particle size resulted in higher coalescence of bubbles, meaning that the stability of the froth decreased with increasing particle size following the same trend shown by water recovery. The increasing axial bubble size profile corresponding with water recovery was also shown by Ata et al. (2003) were the effect of particle contact angle was being investigated. The relative effect of changing particle size on the coalescence rate was shown to be decreasing with increasing particle size showing that coarser particles had a less signficant influence on froth stability. The trend exhibited by the variation in coalescence rate with feed particle size corroborated the earlier trends from the other froth stability proxies. The image analysis technique can then be used with caution to measure froth stability as further image processing would be required to make the technique more accurate.

Chapter 6. CONCLUSIONS and RECOMMENDATIONS

This chapter summarizes the main findings obtained from the test work performed to investigate the effect of particle size and concentration on froth stability. It also summarizes the main findings on the applicability of image analysis techniques in the measurement on froth stability. Conclusions drawn from the work are stated and recommendations for future work made.

6.1. Conclusions

The conclusions drawn from this study are addressed by answering the key questions posed in Chapter One. Since froth stability has been shown to be very significant to the efficiency of a flotation process with an unstable froth will result in poor valuable mineral recovery as these desired hydrophobic particles are detached from air bubbles and drain with the water back into the pulp phase due to bubble coalescence. On the other hand, a very stable froth may result in poor concentrate grade as the unwanted gangue materials are unselectively entrained to the concentrate. As a result, understanding and being able to manipulate the stability of the froth phase is paramount to future optimisation of flotation circuits and particle size has been shown to have one of the most significant impacts on froth stability, hence the study.

I. What is the effect of changing pulp particle size on the froth particle size?

The concentrate particle size distribution was shown to be significantly finer than the pulp particle size distribution during the flotation process. The decrease in particle size was ascribed to a higher drainage rate of the heavier coarse particles due to gravity in the froth phase as bubbles coalesce and lamellae fluid drains back into the pulp zone. The presence of fine particles increases the recovery of coarse particles due to increased froth stability, but the final concentrate particle size will still reflect a finer size distribution as coarser particles will drain at a faster rate as compared to fine particles. The hydrodynamic conditions in the cell could have also affected the particle size distribution in the froth as high turbulence in the cell would have resulting in the heavier coarser particles detaching from the bubbles at a faster rate

than the finer particles, hence a finer concentrate particle size distribution. Changing the feed particle size was also shown to evidently result in a change in the concentrate particle size distribution. This indicates that not only a specific size range reports to the concentrate, but a wider range depending on the feed particle size distribution utilised.

II. What is the effect of particle size on froth stability?

Froth stability was shown conclusively to increase with decreasing particle size as evidently exhibited in both a non-continuous and continuous flotation system. The decrease in particle size results in an increase in the maximum capillary pressure of coalescence thereby increasing the stability of the froth. The decrease in particle size also results in an increase in the amount of entrained material in the froth phase. It also results in an increase in the interfilm fluid rheology. The combined effect of the increased amount of particles and increased viscosity due to the decrease in particle size reduces the drainage rate thereby increasing froth stability.

Froth stability was shown to follow a decreasing power law trend as a function of feed particle size. Froth stability increased rapidly with decreasing feed particle sizes less than 100 μm which corresponded to concentrate particle sizes less than 50 μm, which is in the region where particles are expected to be recovered by entrainment. Froth stability was also shown to follow a linear dependency with feed particle specific surface area. Increasing the specific area of the particles which increased the area for reactions with particles to occur resulted in an increase in froth stability. The decreasing power law trend as a function of feed particle size and the linear dependency with particle specific surface area were shown conclusively in both a non-continuous and continuous flotation systems.

Froth stability follows a more linear relationship as a function of the total surface area imparted by the concentrate particles. A decrease in the particle size distribution of the feed will result in a decrease in the size of particles reporting to the froth phase and the amount of the respective particles that are actually transferred to the froth. The increased amount and reduced size of particles then translates into increased particle surface area for interactions between the particles and the foam. The increased area in conjunction with the increased maximum capillary pressure and

increased interfilm fluid viscosity will result in an increase in the stability of the froth phase.

Particle properties in the inter-film layer affecting the rheology and drainage of the inter-film fluid, was shown to have a more significant contribution to froth stability as compared to the particle-interface steric barrier effect. The stability of the froth was shown to increase sharply with decreasing particle size when the concentrate particle size range was in the entrainment zone. The inter-film layer particle properties that stabilise the froth occur as a result of the presence of entrained particles and thus the interfilm layer particle properties are concluded to have a major contributing role.

III. What is the effect of solids concentration on froth stability?

Increasing solids concentration was shown to increase the froth growth rates in a non-continuous flotation system due to an increase in surface coverage of the bubble films and increased amount of material in the inter-film fluid which increased the fluid viscosity thereby reducing drainage rates. The effect of solids concentration on froth stability with reference to the maximum froth height and decay rates in a non-continuous system was shown to be greatly dependent on ore mineralogy. An increase in solids concentration was shown to have a significant effect on froth stability in a naturally floating ore, with such increases resulting in an increase in froth stability. In the other ore, minimal effect was observed as the equilibrium maximum froth height was not altered by changes in the solids concentration.

For continuous flotation systems, increases in solids concentration were shown to have a positive effect on froth stability, with increased water recoveries observed for both ores. The increased solids concentration did increase surface coverage on the particle-interface steric barrier formed and also resulted in an increased amount of particles in the inter-film fluid layer which affects the rheology to a greater extent. The combined effect of the increased maximum capillary pressure and the reduced inter-film fluid drainage rate resulted in greater froth stability.

IV. Can image analysis techniques be used to measure froth stability?

The top of froth average bubble size was shown to be a viable quantitative froth stability measurement proxy. A decrease in froth stability was represented as an

increase in the average bubble size and this is as a result of bubbles coalescing to a greater extent thereby forming larger bubbles. The top of froth bubble size may provide a non-intrusive online method to analyse froth stability for plant operations. The two image analysis methods can then be used as an indicator to evaluate froth stability either as assessed as the ability to resist coalescence rate.

6.2. Aims and Objectives Overview

The aims and objectives set out for this project were achieved, as a relationship between froth stability and particle size, which translates into the total surface area imparted, was obtained. The effect of solids concentration was determined with stability increasing with increasing solids concentration and also the effect of particle surface wettability assessed for the two ores. A procedure for the operation of the agitated hybrid cell was also developed and the image processing method of assessing froth stability (Sauter-mean bubble size and the side of froth axial Sauter-mean bubble size profile) was shown to be a potentially non-invasive method to evaluate froth stability.

- The first hypothesis that stated that, “Froth stability increases with a decrease in solids particle size per unit mass during a flotation process.” was accepted based on the discussion presented in section 5.2. and the conclusions drawn in section 6.1.ii.

- The second hypothesis that stated that, “An increase in the solids concentration between 15 – 25% will result in an increase in froth stability.” Was also accepted based on the discussion presented in section 5.4. and the conclusions drawn in section 6.1.iii.

6.3. Recommendations

Based on the above stated key findings of this research, recommendations for future test work are outlined as follows:

- From the study, it was shown that all particle froth stabilising properties, namely the particle-interface steric barrier properties and particle properties in the inter-film layer have some effect on froth stability. With the trends shown from results, it suggests that the particle properties in the inter-film layer might have the major contribution to froth stability as compared to the steric barrier properties. It is imperative that more studies be carried out on the isolated effects of the two properties, so as to comprehensively conclude if the interfilm fluid properties do indeed have the major contributing role in particle froth stabilisation.
- Future study should also include the assessment of froth rheology in conjunction with the presently measured variables in evaluating froth stability as it is critical to the drainage rates of the inter-film fluid which controls the stability of the froth.
- This study focused on assessing if the top of froth bubble size and bubble coalescence rate are viable in measuring froth stability. A higher resolution camera should be used for future studies to allow for more accurate measurements of bubble sizes. Flat sided columns can be used to reduce the distortion of images caused by the curvature of the cylindrical column during analysis of the side of froth bubble size. A more robust method of measuring the bubble sizes is also required to have a more accurate assessment of the viability of image processing in measuring froth stability.
- Explore froth stability studies in larger diameter columns that allow development of froth structures that resemble more of plant operations due to reduced wall effects.

Chapter 7. REFERENCES

Aktas, Z., Cilliers, J.J. & Banford, A.W. 2008. Dynamic froth stability: Particle size, airflow rate and conditioning time effects. *International Journal of Mineral Processing.* 87(1–2):65-71. DOI:http://dx.doi.org/10.1016/j.minpro.2008.02.001.

Ata, S. 2009. The detachment of particles from coalescing bubble pairs. *Journal of Colloid and Interface Science.* 338(2):558-565. DOI:http://dx.doi.org/10.1016/j.jcis.2009.07.003.

Ata, S., Ahmed, N. & Jameson, G.J. 2003. A study of bubble coalescence in flotation froths. *International Journal of Mineral Processing.* 72(1–4):255-266. DOI:http://dx.doi.org/10.1016/S0301-7516(03)00103-0.

Ata, S. 2012. Phenomena in the froth phase of flotation-A review. *International Journal of Mineral Processing*, (102-103): 1-12.

Banford, A.W., Aktas, Z. & Woodburn, E.T. 1998. Interpretation of the effect of froth structure on the performance of froth flotation using image analysis. *Powder Technology.* 98(1):61-73. DOI:http://dx.doi.org/10.1016/S0032-5910(98)00032-1.

Barbian, N., Hadler, K., Ventura-Medina, E. & Cilliers, J.J. 2005. The froth stability column: linking froth stability and flotation performance. *Minerals Engineering.* 18(3):317-324. DOI:http://dx.doi.org/10.1016/j.mineng.2004.06.010.

Barbian, N., Ventura-Medina, E. & Cilliers, J.J. 2003. Dynamic froth stability in froth flotation. *Minerals Engineering.* 16(11):1111-1116. DOI:http://dx.doi.org/10.1016/j.mineng.2003.06.010.

Barbian, N., Hadler, K. & Cilliers, J.J. 2006. The froth stability column: Measuring froth stability at an industrial scale. *Minerals Engineering.* 19(6–8):713-718. DOI:http://dx.doi.org/10.1016/j.mineng.2005.09.021.

Bıçak, Ö., Ekmekçi, Z., Can, M., Öztürk, Y., 2012. The effect of water chemistry on froth stability and surface chemistry of the flotation of a Cu–Zn sulfide ore. *International Journal of Mineral Processing.* 102–103: 32–37.

Bikerman, J., 1953. Foam*. Applied Physics and Engineering.* 10 ed. Berlin: Springer-Verlag.

Bradshaw, D., Harris, P. & O'Connor, C. 2005. The effect of collectors and their interactions with depressants on the behaviour of the froth phase in flotation. *Centenary of Flotation Symposium.* 2005. Brisbane: Centenary of flotation symposium. AusIMM The Minerals Institute.

Brunauer, S., Emmett, P. H., Teller, E., Adsorption of Gases in Multimolecular Layers. *Journal of the American Chemical Society*. 60(2):309-319

Chen, C. 2012. Development of measurement of froth characteristics. Master of Science thesis in the master degree program. Advanced engineering materials. Department of Chemical and Biological Engineering Chalmers University of Technology Gothenburg, Sweden

Cho, Y. & Laskowski, J., 2002. Effect of flotation frothers on bubble size and foam stability. *International Journal of Mineral Processing,* (64): 69-80.

Corin, K.C. & Wiese, J.G., 2014. Investigating froth stability: A comparative study of ionic strength and frother dosage. *Minerals Engineering*, (66-88): 130-34.

Crosbie, R., Runge, K., McMaster, J., Rivett, T., Peaker, R. (2009). The impact of the froth zone on metallurgical performance in a 3m^3 RCS flotation cell. *Flotation '09*, Cape Town.

Dippenaar, A. 1982. The destabilization of froth by solids. I. The mechanism of film rupture. *International Journal of Mineral Processing.* 9(1):1-14. DOI:http://dx.doi.org/10.1016/0301-7516(82)90002-3.

Dippenaar, A. 1982. The destabilization of froth by solids. II. The rate-determining step. *International Journal of Mineral Processing.* 9(1):15-22. DOI:http://dx.doi.org/10.1016/0301-7516(82)90003-5.

Falutsu, M. 1994. Column flotation froth characteristics — stability of the bubble-particle system. *International Journal of Mineral Processing.* 40(3–4):225-243. DOI:http://dx.doi.org/10.1016/0301-7516(94)90045-0.

Farrokhpay, S. 2011. The significance of froth stability in mineral flotation — A review. *Advances in Colloid and Interface Science.* 166(1–2):1-7. DOI:http://dx.doi.org/10.1016/j.cis.2011.03.001.

Feng, D., & Aldrich, C. (1999). Effect of particle size on flotation performance of complex sulphide ores. *Minerals Engineering, 12*(7), 721-731.

Feteris, S.M., Frew, J.A. & Jowett, A. 1987. Modelling the effect of froth depth in flotation. *International Journal of Mineral Processing.* 20(1):121-135.

Finch, J.A. & Dobby, G.S., 1990. *Column Flotation*. 1st ed. Oxford: Pergamon Press.

Fuerstenau, M. & Han, K., 2003. *Principles of Mineral Processing.* Colorado : Society for Mining,Metallurgy and Exploration,Inc.

Fuerstenau, M., Jameson G. and Yoon R. 2007. Froth Flotation A Century of Innovation*. USA: Society for Mining, Metallurgy, and Exploration, Inc.*

Garibay, R.P., Gallegos A, P.M., Uribe S, A. & Nava A, F. 2002. Effect of collection zone height and operating variables on recovery of overload flotation columns. *Minerals Engineering.* 15(5):325-331. DOI:http://dx.doi.org/10.1016/S0892-6875(02)00035-3.

Gaudin, A.M., 1957. Flotation. 2nd Edition. New York. McGraw-Hill

Gence, N. 2005. Wetting behavior of magnetite and dolomite surfaces. Applied Surface Science, vol 252: 3744-3750.

Gergely V. & Clyne, T.W. 2004. Drainage in standing liquid metal foams: modelling and experimental observations. Acta Materialia. 52:3047–3058.

Gorain, B.K., Franzidis, J.P. and Manlapig, E.V. 1997. Studies on impeller type; impeller speed and air flow rate in an industrial scale flotation cell. Part 4: Effect of bubble surface area flux on flotation kinetics. Minerals Engineering. 10: 367-379.

Grau, R.A., Laskowski, J.S. & Heiskanen, K. 2005. Effect of frothers on bubble size. *International Journal of Mineral Processing.* 76(4):225-233. DOI:http://dx.doi.org/10.1016/j.minpro.2005.01.004.

Hadler, K., Cilliers, J.J. 2009. The relationship between peak in air and flotation bank performance. *Minerals Engineering.* 22(5): 451-455.

Hadler, K., Smith, C.D., Cilliers, J.J. 2010. Recovery vs. mass pull: The link to air recovery, *Minerals Engineering*. 23(11-13): 994-1002.

Hadler, K., Greyling, M., Plint, N. & Cilliers, J.J. 2012. The effect of froth depth on air recovery and flotation performance. *Minerals Engineering.* 36–38(0):248-253. DOI:http://dx.doi.org/10.1016/j.mineng.2012.04.003.

Harris, M.C., Franzidis, J., O'Connor, C.T. & Stonestreet, P. 1992. An evaluation of the role of particle size in the flotation of coal using different cell technologies. *Minerals Engineering.* 5(10–12):1225-1238. DOI:http://dx.doi.org.ezproxy.uct.ac.za/10.1016/0892-6875(92)90161-2.

Harris, G.H.,& Jia, R. 2000. An improved class of flotation frothers. *International Journal for Mineral Processing*, 58 (1-4):35-43.

Hay, M.P. & Roy, R. 2010. A case study of optimising UG2 flotation performance. Part 1: Bench, pilot and plant scale factors which influence Cr2O3 entrainment in UG2 flotation. *Minerals Engineering.* 23(11–13):855-867. DOI:http://dx.doi.org/10.1016/j.mineng.2010.05.002.

Hunter, T.N., Pugh, R.J., Franks, G.V. & Jameson, G.J. 2008. The role of particles in stabilising foams and emulsions. *Advances in Colloid and Interface Science.* 137(2):57-81. DOI:http://dx.doi.org/10.1016/j.cis.2007.07.007.

Ip, S. W., Wang, Y., & Toguri, J. M. 1999. Aluminium foam stabilisation by solid particles. *Canadian Metallurgical Quarterly, 38*: 81-92.

Iglesias, E., Anderez, J., Forgiarini, A. & Salager, J. 1995. A new method to estimate the stability of short-life foams. *Colloids and Surfaces A: Physicochemical and Engineering Aspects.* 98(1–2):167-174. DOI:http://dx.doi.org/10.1016/0927-7757(95)03101-I.

Johansson, G. & Pugh, R.J. 1992. The influence of particle size and hydrophobicity on the stability of mineralized froths. *International Journal of Mineral Processing.* 34(1–2):1-21. DOI:http://dx.doi.org/10.1016/0301-7516(92)90012-L.

Kaptay, G. 2006. On the equation of the maximum capillary pressure induced by solid particles to stabilize emulsions and foams and on the emulsion stability diagrams. *Colloids and Surfaces A: Physicochem. Eng. Aspects, 282-283*, 387-401.

Kirjavainen, V.M., 1996. Review and analysis of factors controlling the mechanical flotation of gangue minerals. *International Journal of Mineral Processing*, 46: 21-34.

Kracht, W., Orozco, Y., Acuna, C. 2016. Effect of surfactant type on the entrainment factor and selectivity of flotation at laboratory scale. *International Journal of Minerals Engineering*, 92: 216-220.

Levine, S., Bowen, B.D., Partridge, S.J., 1989. Stabilization of emulsions by fine particles I. Partitioning of particles between continuous phase and oil/water interface. Colloids and Surfaces. 38:325–343.

Lin, B., Recke, B., Knudsen, J.K.H. & Jørgensen, S.B. 2008. Bubble size estimation for flotation processes. *International Journal of Minerals Engineering.* 21(7):539-548. DOI:http://dx.doi.org/10.1016/j.mineng.2007.11.004.

Livshits, A.K. & Dudenkov, S.V. 1965. Some factors in flotation froth stability. 1965. New York: Proc. VII th International Mineral Processing Congress. 367.

Lu S, Pugh RJ, Forssberg E. 2005. Interfacial separation of particles. *Studies in interface science series. Elsevier*; (20): 1383-7303.

Macias-Garcia, A., Cuerda-Correa. Eduardo M., Diaz-Diez. M.A. 2004. Application of the Rosin-Rammler and Gates-Gaudin-Schuhmann models to the particle size distribution analysis of agglomerated cork. *Materials Characterisation.*52(1):159-164.

Mathe, Z.T., Harris, M.C., O'Connor, C.T. & Franzidis, J. 1998. Review of froth modelling in steady state flotation systems. *International Journal of Minerals Engineering.* 11(5):397-421. DOI:http://dx.doi.org/10.1016/S0892-6875(98)00020-X.

McLaren, C.H., & De Villiers, J.P.R., 1982. The Platinum-Group Chemistry and Mineralogy of UG-2 Chromitite Layer of the Bushveld Complex. *Economic Geology* 77, 1348-1366.

Melo, F., 2001. Fundamental Properties of Flotation Frothers and Their Effect On Flotation. MSc Thesis. Concepcion: The University Of British Columbia University of Concepcion.

Moolman, D.W., Aldrich, C., Van Deventer, J.S.J. & Bradshaw, D.J. 1995. The interpretation of flotation froth surfaces by using digital image analysis and neural networks. *Chemical Engineering Science.* 50(22):3501-3513. DOI:http://dx.doi.org/10.1016/0009-2509(95)00190-G.

Morar, S.H., Bradshaw, D.J. & Harris, M.C. 2012. The use of the froth surface lamellae burst rate as a flotation froth stability measurement. *International Journal of Minerals Engineering.* 36–38(0):152-159. DOI:http://dx.doi.org/10.1016/j.mineng.2012.03.018.

Moyo, P., 2005. Characterization Of Frothers By Water Carrying Rate. *PhD Thesis. Montreal: Canada Heritage McGill University.*

Moys, M.H., 1984. Residence time distributions and mass transport in the froth phase of the flotation process. *International Journal of Mineral Processing* 13: 117–142.

Moudgil, B. 1992. Enhanced recovery of coarse particles during phosphate flotation. *Florida Institute of Phosphate Research.* University of Florida.

Neethling, S.J., Cilliers, J.J., 2002. The entrainment of gangue into a flotation froth. *International Journal of Mineral Processing*, 64(2-3):123-34.

Neethling, S.J., Cilliers, J.J. 2009. The entranment factor in froth flotation:Model for particle size and other operating parameter effects. *International Journal of Mineral Processing.* 93(2):141-148. DOI;http://dx.doi:10.1016/j.minpro.2009.07.004.

Nelson, M.G. & Lelinski, D. 2000. Hydrodynamic design of self-aerating flotation machines. *International Journal of Minerals Engineering.* 13(10–11):991-998. DOI:http://dx.doi.org/10.1016/S0892-6875(00)00085-6.

Pugh, R.J. 2005. Experimental techniques for studying the of foams and froths, *Advanced Colloid Interface Science*, 114–115:239.

Qu, X., Wang, L., Nguyen, A.V. 2013. Correlation of air recovery with froth stability and separation efficiency in coal flotation. *International Journal of Minerals Engineering.* 41: (25:30).

Roberts, W.M. 1965. Geology and Mineral Resources of the Pico de Itabirito District Minas Gerais, Brazil. *Geology and Mineral Resources of Parts of Minas Gerais, Brazil.*

Rosin, P. & Rammler, E. 1933. The laws governing the fineness of powdered coal. Journal of the Institute of Fuel. 7 :29− 36.

Runge, K. C., Seaman, B. A. & Seaman, D. R., 2007. Optimising down the bank flotation froth performance in Metso's 3m3 RCSTM test cell, in *Proceedings of the Minerals Engineering Flotation '07 Conference*.

Runge, K., Crosbie, R., Rivett, T. & McMaster, J., 2010. An evaluation of froth recovery measurement techniques. In *XXV International Mineral Processing Congress*. Brisbane, 2010. IMPC.

Savassi, O.N., Alexander, D.J., Franzidis, J.P. & Manlapig, E.V., 1997. An Empirical Model for Entrainment in Industrial Flotation Plants. *International Journal of Minerals Engineering*, 11(3), pp.243-56.

Schubert, H., 2008. *On the optimisation of hydrodynamics in fine particle*. *International Journal of Minerals Engineering*, 21(12-14), pp.930-936.

Sheludko, A. 1967. Thin Liquid Films. Advances in Colloid and Interface Science. 1(4): 391-464.

Shumba, T., C. 2014. Relationship between flotation operational factors and froth behaviour. MSc Eng Chemical. University of Cape Town.

Soto, H. S. (1992). *Development of novel flotation-elutriation method for coarse phosphate beneficiation*: Final report to Florida Institute of Phosphate Research; Publication number 02-070-098.

Smith, C.D., Hadler, K., Cilliers, J.J., 2009. The benefits of flotation bank air profiling. *Australian Institute of Mining and Metallurgical Publication* 11: 229− 232

Smith, P.G. & Warren, L.J., 1989. Entrainment of particles into flotation froths. *Minerals Processing and Extractive Metallurgy Review*, 5, pp.123-45.

Subrahmanyam, T.V. & Forssberg, E. 1988. Froth stability, particle entrainment and drainage in flotation — A review. *International Journal of Mineral Processing.* 23(1−2):33-53. DOI:http://dx.doi.org/10.1016/0301-7516(88)90004-X.

Sun, Y. Q. & Gao, T. 2002. The Optimum Wetting Angle for the Stabilization of Liquid-Metal Foams by Ceramic Particles: Experimental Simulations. *Metallurgical and Material Transactions A.* 33A: 3285.

Tang, D., Wightman, E., Franzidis, J. & Montes-Atenas, G. 2010. Assessment of the consistency between different laboratory froth stability measurements. *International Mineral Processing Conference, Brisbane.*

Tang, F., Xiao, Z., Tang, J. & Jiang, L. 1989. The effect of SiO2 particles upon stabilization of foam. *Journal of Colloid and Interface Science.* 131(2):498-502. DOI:http://dx.doi.org/10.1016/0021-9797(89)90192-6.

Tao, D., Luttrell, G.H. & Yoon, R.-. 2000. A parametric study of froth stability and its effect on column flotation of fine particles. *International Journal of Mineral Processing.* 59(1):25-43. DOI:http://dx.doi.org/10.1016/S0301-7516(99)00033-2.

Triffett, B. & Cilliers, J., 2004. Measuring froth stability. Technological Resources Pty Limited, University Of Manchester. WO/2004080600 (2004).

Ventura-Medina, E. & Cilliers, J.J. 2000. Calculation of the specific surface area in flotation. *Minerals Engineering.*13(3):265-275. DOI:http://dx.doi.org/10.1016/S0892-6875(00)00006-6.

Ventura-Medina, E. & Cilliers, J.J. 2002. A model to describe flotation performance based on physics of foams and froth image analysis. *International Journal of Mineral Processing.* 67(1–4):79-99. DOI:http://dx.doi.org/10.1016/S0301-7516(02)00038-8.

Vera, M.A. et al., 2002. The modelling of froth zone recovery in batch and continuously operated laboratory flotation cells. *International Journal of Mineral Processing*, 64(1): 135-51.

Vermaak, C.F., 1995. The Platinum Group Metals: A global Perspective. Mintek, Randburg, 247pp.

Vieira, A.M. & Peres, A.E.C. 2007. The effect of amine type, pH, and size range in the flotation of quartz. *Minerals Engineering.* 20(10):1008-1013. DOI:http://dx.doi.org/10.1016/j.mineng.2007.03.013.

Wiese, J., Harris, P. & Bradshaw, D. 2005. The influence of the reagent suite on the flotation of ores from the Merensky Reef. *International Journal of Minerals Engineering.* 18(1): 189.

Wiese, J., Harris, P. & Bradshaw, D., 2011. The effect of the reagent suite on froth stability in laboratory scale batch flotation tests. *Minerals Engineering ,* Volume 24, pp. 995-1003.

Wills, B. Ed. 2006. *Mineral Processing Technology: An Introduction to the Practical Aspects of Ore Treatment and Mineral Recovery.* 7th ed.: Pergamon Press.

Wuebben, T. & Odenbach, S. 2005. Stabilisation of liquid metallic foams by solid particles *Colloids and Surfaces A: Physicochemical Engineering Aspects*; 266(1-3):207–13.

Yianatos, J. Contreras, F. 2010. Particle entrainment model for industrial flotation cells. *Powder Technology*. 197 : 260−267

Yianatos, J.B., Moys, M.H., Contreras, F. & Villanueva, A. 2008. Froth recovery of industrial flotation cells. *Minerals Engineering.* 21(12−14):817-825. DOI:http://dx.doi.org/10.1016/j.mineng.2007.12.012.

Chapter 8. APPENDICES

A1. Feed Particle Sizes

Table A14: UG2 ore feed size classes used for flotation tests.

	Particle Size Classes						Specific Surface Area (m2/g)
Milling Time	D_{10} (µm)	D_{20} (µm)	D_{50} (µm)	D_{80} (µm)	D_{90} (µm)	D_{98} (µm)	
30 minutes	5.5	12.4	38.3	78.4	103.9	154.1	0.159
25 minutes	6.0	13.6	43.4	87.8	115.3	168.1	0.149
20 minutes	7.1	16.1	52.7	103.9	135.7	198.0	0.130
15 minutes	8.5	19.3	66.1	127.3	165.6	240.9	0.113
10 minutes	8.2	18.8	71.3	157.2	213.3	327.4	0.109

Table A15: Iron ore feed size classes used for flotation tests.

	Fraction passing size class								
Milling Times	25 (µm)	38 (µm)	53 (µm)	75 (µm)	106 (µm)	125 (µm)	150 (µm)	212 (µm)	300 (µm)
15 Minutes	0.47	0.76	0.90	1.00	1.00	1.00	1.00	1.00	1.00
10 Minutes	0.37	0.62	0.78	0.96	1.00	1.00	1.00	1.00	1.00
5 Minutes	0.31	0.42	0.61	0.84	0.98	1.00	1.00	1.00	1.00
2 Minutes	0.21	0.31	0.49	0.69	0.88	0.98	1.00	1.00	1.00
0 Minutes	0.20	0.29	0.46	0.63	0.78	0.85	0.89	0.95	0.99

A2. Concentrate Particle Sizes

Table A16: UG2 ore concentrate size classes for the 10 cm column agitated hybrid cell tests.

					Particle Size Classes	
Milling Time	D_{10} (µm)	D_{20} (µm)	D_{50} (µm)	D_{80} (µm)	D_{90} (µm)	D_{98} (µm)
30 minutes	3.1	6.8	20.8	47.0	66.6	110.8
25 minutes	3.0	6.5	20.4	48.7	71.3	131.6
20 minutes	2.9	6.2	19.6	49.4	76.8	150.1
15 minutes	2.8	6.1	20.2	57.9	91.5	169.5
10 minutes	2.8	6.0	20.3	62.1	102.4	202.4

Table A17: UG2 ore concentrate size classes for the 15 cm column agitated hybrid cell tests.

Milling Time	Particle Size Classes					
	D_{10} (µm)	D_{20} (µm)	D_{50} (µm)	D_{80} (µm)	D_{90} (µm)	D_{98} (µm)
30 minutes	2.7	5.7	18.3	44.4	64.8	111.5
25 minutes	2.8	6.1	19.6	48.2	71.3	125.1
20 minutes	2.7	5.9	19.1	48.3	72.9	131.3
15 minutes	2.6	5.5	18.4	49.8	79.3	158.3
10 minutes	2.9	6.3	22.4	71.3	115.1	228.9

Table A18: UG2 ore concentrate size classes for the 25 cm column agitated hybrid cell tests.

Milling Time	Particle Size Classes					
	D_{10} (µm)	D_{20} (µm)	D_{50} (µm)	D_{80} (µm)	D_{90} (µm)	D_{98} (µm)
30 minutes	2.3	4.9	16.0	39.7	59.2	104.5
25 minutes	2.5	5.5	20.7	51.6	87.9	153.8
20 minutes	2.7	5.8	19.5	57.6	89.0	160.9
15 minutes	3.2	7.3	28.6	81.7	119.4	204.2
10 minutes	3.1	7.3	29.1	83.6	125.1	222.7

A3. Experimental Conditions

Table A19: Experimental conditions used for the flotation tests.

Ore Type	Stability Column		Hybrid Cell	
UG2 Ore	Frother - DOW 200 - ppm (Water) =	60	Frother - DOW 200 - ppm (Water) =	60
	Collector -SIBX - g/t (Solids) =	80	Collector -SIBX - g/t (Solids) =	80
	Depressant - Sendep 348 - g/t (Solids) =	100	Depressant - Sendep 348 - g/t (Solids) =	100
	Air Rate (Jg - cm/s) =	1.27	Air Rate (Jg - cm/s) =	1.73
Iron Ore	Frother - N/A =	N/A	Frother - N/A =	N/A
	Collector -EDTA - g/t (Solids) =	150	Collector -EDTA - g/t (Solids) =	50
	Depressant - Starch Solution (Potato) - g/t (Solids) =	500	Depressant - Starch Solution (Potato) - g/t (Solids) =	750
	Air Rate (Jg - cm/s) =	1.27	Air Rate (Jg - cm/s) =	1.73

A4. Stability Column Results

a. A3.1. UG2 Ore tests at 15% solids concentration

Table A20: Froth rise rate experimental data for the 30 minute grind UG2 ore at 15% solids.

	30 Minute Grind Froth Height (mm)			
Time (s)	Run 1	Run 2	Run 3	Run 4
5	78	82	61	70
10	115	113	98	103
15	138	140	123	123
20	156	155	137	137
25	166	166	147	146
30	175	176	155	154
35	182	184	159	159
40	189	189	159	164
45	194	189	166	164
50	199	199	166	171
55	199	203	174	171
60	204	203	174	184
65	204	208	182	191
70	207	208	182	191
75	207	214	186	198
80	214	214	186	198
85	214	218	189	205
90	218	223	189	205
95	218	223	189	205
100	218	223	194	210
105	223	223	194	210
110	223	223	199	210
115	223	223	199	210
120	228	223	205	215
125	228	223	205	215
130	228	223	210	215
135	228	223	210	215
140	228	223	215	215
145	228	223	215	215
150	228	223	215	215
155	228	223	215	215

Table A21: Froth decay rate experimental data for the 30 minute grind UG2 ore at 15% solids.

	30 Minute Grind Froth Height (mm)			
Time (s)	Run 1	Run 2	Run 3	Run 4
0	228	223	215	215
2	211	214	206	193
4	191	196	182	170
6	168	170	153	140
8	144	137	124	114
10	117	110	95	89
12	81	78	61	57
14	46	51	38	36
16	38	39	28	30

Table A22: Froth rise rate experimental data for the 25 minute grind UG2 ore at 15% solids.

	25 Minute Grind Froth Height (mm)			
Time (s)	Run 1	Run 2	Run 3	Run 4
5	58	59	52	59
10	90	85	87	84
15	105	104	107	102
20	118	112	120	114
25	126	120	126	119
30	131	126	126	119
35	137	131	130	126
40	137	135	135	132
45	142	135	135	132
50	142	143	140	138
55	142	143	140	138
60	142	151	140	143
65	142	151	140	143
70	142	159	144	149
75	148	159	144	155
80	148	168	150	161
85	153	168	150	161
90	153	174	156	167
95	158	174	156	167
100	158	180	160	174
105	163	180	160	174
110	163	185	160	181
115	168	185	168	181
120	173	189	168	187
125	181	189	175	187
130	181	189	175	189
135	186	189	181	189
140	186	189	181	189
145	186	189	188	189
150	186	189	188	189
155	186	189	188	189

Table A23: Froth decay rate experimental data for the 25 minute grind UG2 ore at 15% solids.

	25 Minute Grind Froth Height (mm)			
Time (s)	Run 1	Run 2	Run 3	Run 4
0	186	189	188	189
2	170	156	174	166
4	147	127	155	143
6	112	96	127	114
8	93	66	94	79
10	56	41	50	45
12	25	23	25	25

Table A24: Froth rise rate experimental data for the 20 minute grind UG2 ore at 15% solids.

	20 Minute Grind Froth Height (mm)			
Time (s)	Run 1	Run 2	Run 3	Run 4
5	54	56	46	45
10	82	92	77	72
15	100	108	91	86
20	108	116	97	91
25	112	121	97	96
30	112	121	102	96
35	116	121	102	96
40	116	127	102	101
45	116	127	108	101
50	120	131	108	101
55	120	131	108	107
60	126	131	113	107
65	126	134	113	114
70	126	134	113	114
75	126	138	118	118
80	129	138	118	118
85	129	144	118	118
90	129	144	118	126
95	129	144	124	126
100	133	150	124	132
105	133	150	128	132
110	133	155	128	139
115	133	155	133	139
120	139	155	133	147
125	139	159	133	147
130	139	159	140	153
135	143	159	145	153
140	143	162	150	153
145	143	162	150	153
150	143	162	154	153
155	143	162	154	153

Table A25: Froth decay rate experimental data for the 20 minute grind UG2 ore at 15% solids.

	20 Minute Grind Froth Height (mm)			
Time (s)	Run 1	Run 2	Run 3	Run 4
0	143	162	154	153
2	129	134	142	128
4	107	108	120	97
6	70	68	82	65
8	34	36	42	36
10	20	21	18	17

Table A26: Froth rise rate experimental data for the 15 minute grind UG2 ore at 15% solids.

	15 Minute Grind Froth Height (mm)			
Time (s)	Run 1	Run 2	Run 3	Run 4
5	46	48	43	45
10	69	71	65	62
15	84	86	77	75
20	92	88	82	82
25	97	88	82	82
30	97	102	82	82
35	102	102	82	82
40	107	102	87	86
45	107	108	87	86
50	111	108	87	90
55	111	108	87	90
60	117	114	87	90
65	117	114	87	90
70	117	114	92	96
75	122	121	92	96
80	122	121	92	101
85	122	121	96	101
90	122	128	96	101
95	122	128	96	105
100	127	133	96	105
105	127	133	101	105
110	127	133	101	110
115	132	133	101	110
120	132	133	107	110
125	132	133	107	117
130	137	133	107	117
135	137	133	107	117
140	137	133	114	124
145	137	133	114	124
150	137	133	114	124
155	137	133	114	132

Table A27: Froth decay rate experimental data for the 15 minute grind UG2 ore at 15% solids.

	15 Minute Grind Froth Height (mm)			
Time (s)	Run 1	Run 2	Run 3	Run 4
0	114	132	114	132
2	103	125	103	125
4	86	100	86	100
6	55	68	55	68
8	27	30	27	30
10	16	13	16	13

Table A28: Froth rise rate experimental data for the 10 minute grind UG2 ore at 15% solids.

	10 Minute Grind Froth Height (mm)			
Time (s)	Run 1	Run 2	Run 3	Run 4
5	49	53	41	38
10	76	82	59	57
15	94	98	72	72
20	104	107	77	77
25	110	110	77	77
30	110	110	77	77
35	110	110	77	82
40	114	110	77	82
45	114	110	77	82
50	114	116	77	82
55	114	116	77	82
60	118	116	77	87
65	118	116	77	87
70	118	122	77	87
75	118	122	82	87
80	122	122	82	87
85	122	126	88	87
90	122	126	88	92
95	122	126	88	92
100	122	132	88	92
105	129	132	92	96
110	129	132	92	96
115	129	132	92	96
120	129	137	92	96
125	129	137	96	101
130	129	137	96	101
135	129	137	96	101
140	129	141	96	101
145	129	141	96	108
150	129	141	96	108

Table A29: Froth decay rate experimental data for the 10 minute grind UG2 ore at 15% solids.

	10 Minute Grind Froth Height (mm)			
Time (s)	Run 1	Run 2	Run 3	Run 4
0	129	141	96	108
2	123	128	86	96
4	107	106	70	74
6	82	80	40	41
8	50	42	15	16
10	21	18	6	8

b. UG2 Ore tests at 20% solids concentration

Table A30: Froth rise rate experimental data for the 30 minute grind UG2 ore at 20% solids.

	30 Minute Grind Froth Height (mm)			
Time (s)	Run 1	Run 2	Run 3	Run 4
5	83	77	64	62
10	131	121	99	97
15	158	146	120	118
20	177	165	129	127
25	190	180	139	137
30	201	189	147	145
35	210	198	156	154
40	216	207	162	160
45	222	214	169	167
50	227	223	172	170
55	233	229	172	170
60	239	234	172	170
65	243	238	176	174
70	243	238	176	174
75	250	244	176	174
80	250	244	182	180
85	255	244	182	180
90	255	250	189	187
95	259	250	189	187
100	259	255	193	191
105	259	255	193	191
110	265	255	206	204
115	265	260	206	204
120	265	260	211	209
125	265	260	211	209
130	265	260	211	209

Table A31: Froth decay rate experimental data for the 30 minute grind UG2 ore at 20% solids.

	30 Minute Grind Froth Height (mm)			
Time (s)	Run 1	Run 2	Run 3	Run 4
0	265	260	259	254
2	245	244	239	238
4	223	223	217	217
6	193	198	187	192
8	160	170	154	164
10	129	135	123	129
12	94	101	88	95
14	67	74	61	68
16	48	52	42	46
18	39	35	33	29
20	33	30	27	24

Table A32: Froth rise rate experimental data for the 25 minute grind UG2 ore at 20% solids.

	25 Minute Grind Froth Height (mm)			
Time (s)	Run 1	Run 2	Run 3	Run 4
5	54	64	54	64
10	96	97	96	97
15	117	112	117	112
20	127	120	127	120
25	132	126	132	126
30	137	130	137	130
35	142	134	142	134
40	147	138	147	138
45	151	144	151	144
50	156	149	156	149
55	160	153	160	153
60	165	158	165	158
65	170	164	170	164
70	170	168	170	168
75	178	174	178	174
80	182	174	182	174
85	182	174	182	174
90	186	178	186	178
95	186	178	186	178
100	192	184	186	178
105	192	184	186	178
110	196	187	186	178
115	196	187	186	178
120	196	187	186	178
125	196	187	186	178
130	196	194	186	178
135	196	194	186	178
140	196	194	186	178
145	196	194	186	178
150	196	194	186	178

Table A33: Froth decay rate experimental data for the 25 minute grind UG2 ore at 20% solids.

	25 Minute Grind Froth Height (mm)			
Time (s)	Run 1	Run 2	Run 3	Run 4
0	196	194	186	178
2	192	166	192	166
4	170	144	170	144
6	147	122	147	122
8	109	97	109	97
10	84	62	84	62
12	52	36	52	36
14	32	26	32	20
16	23	20	23	20

Table A34: Froth rise rate experimental data for the 20 minute grind UG2 ore at 20% solids.

	20 Minute Grind Froth Height (mm)			
Time (s)	Run 1	Run 2	Run 3	Run 4
5	61	46	46	49
10	98	80	75	80
15	118	101	94	97
20	126	107	104	104
25	130	110	109	110
30	134	110	109	114
35	134	114	116	114
40	140	114	116	118
45	140	117	122	118
50	143	117	122	125
55	143	122	126	125
60	143	122	126	130
65	143	122	132	130
70	148	129	132	137
75	148	129	138	137
80	151	135	138	145
85	151	135	144	145
90	151	135	144	151
95	151	141	150	151
100	154	141	150	155
105	154	141	154	155
110	154	147	154	159
115	154	147	154	159
120	154	150	154	159
125	154	150	159	159
130	154	150	159	164
135	154	150	159	164
140	154	150	159	164
145	154	150	159	164
150	154	150	159	164

Table A35: Froth decay rate experimental data for the 20 minute grind UG2 ore at 20% solids.

	20 Minute Grind Froth Height (mm)			
Time (s)	Run 1	Run 2	Run 3	Run 4
0	154	150	159	164
2	133	137	154	144
4	110	116	134	123
6	81	94	108	95
8	55	60	80	63
10	32	39	53	39
12	16	17	26	23
14	11	10	14	15

Table A36: Froth rise rate experimental data for the 15 minute grind UG2 ore at 20% solids.

	15 Minute Grind Froth Height (mm)			
Time (s)	Run 1	Run 2	Run 3	Run 4
5	46	45	46	45
10	77	70	77	70
15	90	85	90	85
20	94	92	94	92
25	94	92	94	92
30	94	97	94	97
35	94	97	94	97
40	94	97	94	97
45	100	97	100	97
50	100	102	100	102
55	100	107	100	107
60	100	107	100	107
65	100	107	100	107
70	111	113	111	113
75	116	118	116	118
80	116	118	116	118
85	116	118	116	118
90	116	122	116	122
95	116	122	116	122
100	122	122	122	122
105	122	127	122	127
110	128	127	128	127
115	128	127	128	127
120	128	127	128	127
125	128	127	128	127
130	128	127	128	127

Table A37: Froth decay rate experimental data for the 15 minute grind UG2 ore at 20% solids.

	15 Minute Grind Froth Height (mm)			
Time (s)	Run 1	Run 2	Run 3	Run 4
0	128	127	128	127
2	121	105	121	105
4	107	87	107	87
6	79	66	79	66
8	48	41	48	41
10	26	24	26	24
12	12	14	12	14

Table A38: Froth rise rate experimental data for the 10 minute grind UG2 ore at 20% solids.

	10 Minute Grind Froth Height (mm)			
Time (s)	Run 1	Run 2	Run 3	Run 4
5	40	36	42	37
10	63	59	65	60
15	74	72	76	73
20	74	76	76	77
25	74	76	76	77
30	74	76	76	77
35	78	76	80	77
40	78	82	80	83
45	78	82	80	83
50	83	82	85	83
55	83	82	85	83
60	83	86	85	87
65	88	86	90	87
70	88	86	90	87
75	88	90	90	91
80	88	90	90	91
85	88	90	90	91
90	95	96	97	97
95	95	96	97	97
100	95	100	97	101
105	95	100	97	101
110	99	100	101	101
115	99	104	101	105
120	105	104	107	105
125	105	104	107	105
130	105	108	107	109
135	105	108	107	109
140	105	108	107	109

Table A39: Froth decay rate experimental data for the 10 minute grind UG2 ore at 20% solids.

	10 Minute Grind Froth Height (mm)			
Time (s)	Run 1	Run 2	Run 3	Run 4
0	105	108	107	109
2	87	90	89	91
4	61	65	63	66
6	34	38	36	39
8	14	20	16	21
10	2	3	4	4

c. UG2 Ore tests at 25% solids concentration

Table A40: Froth rise rate experimental data for the 30 minute grind UG2 ore at 25% solids.

	30 Minute Grind Froth Height (mm)			
Time (s)	Run 1	Run 2	Run 3	Run 4
5	81	76	55	55
10	134	118	101	100
15	157	148	129	130
20	171	164	151	148
25	182	176	169	160
30	192	184	180	170
35	199	191	188	180
40	206	198	194	188
45	213	203	200	195
50	217	203	206	201
55	217	212	210	207
60	224	215	214	210
65	230	215	217	214
70	230	221	217	214
75	230	221	224	220
80	237	227	224	225
85	242	227	227	229
90	242	233	227	229
95	248	233	231	229
100	248	237	231	232
105	251	242	231	232
110	251	242	236	232
115	251	242	236	232
120	251	242	241	240
125	251	242	241	240
130	251	242	241	246
135	251	242	247	246
140	251	242	247	252
145	251	242	247	252

Table A41: Froth decay rate experimental data for the 30 minute grind UG2 ore at 25% solids.

	30 Minute Grind Froth Height (mm)			
Time (s)	Run 1	Run 2	Run 3	Run 4
0	251	242	247	252
2	233	222	236	237
4	219	206	222	220
6	203	187	199	190
8	168	164	171	161
10	141	136	146	130
12	107	101	125	99
14	78	70	83	73
16	51	48	57	51
18	31	31	34	32

Table A42: Froth rise rate experimental data for the 25 minute grind UG2 ore at 25% solids.

	25 Minute Grind Froth Height (mm)			
Time (s)	Run 1	Run 2	Run 3	Run 4
5	59	52	75	65
10	93	86	106	109
15	115	111	120	129
20	128	123	138	143
25	136	128	146	149
30	142	128	152	159
35	148	138	158	164
40	152	143	162	169
45	158	143	168	175
50	164	151	173	180
55	164	151	178	187
60	169	158	178	190
65	169	158	186	193
70	177	164	186	193
75	177	164	198	201
80	177	170	203	201
85	182	170	203	209
90	182	173	209	209
95	182	173	209	209
100	188	173	213	211
105	194	179	213	211
110	194	179	217	216
115	194	179	217	216
120	201	183	217	216
125	201	183	223	221
130	201	183	223	221
135	204	193	223	221
140	204	193	223	221
145	204	193	223	221
150	204	193	223	221

Table A43: Froth decay rate experimental data for the 25 minute grind UG2 ore at 25% solids.

	25 Minute Grind Froth Height (mm)			
Time (s)	Run 1	Run 2	Run 3	Run 4
0	204	193	226	225
2	189	161	215	214
4	171	134	196	199
6	147	110	171	171
8	126	85	145	121
10	101	61	113	78
12	65	38	84	56
14	42	23	58	38
16	16	16	36	22

Table A44: Froth rise rate experimental data for the 20 minute grind UG2 ore at 25% solids.

	20 Minute Grind Froth Height (mm)			
Time (s)	Run 1	Run 2	Run 3	Run 4
5	55	44	53	41
10	95	82	93	84
15	114	103	112	105
20	126	115	124	118
25	131	120	129	125
30	131	127	129	133
35	139	127	137	133
40	139	130	137	141
45	149	130	147	146
50	156	138	154	153
55	156	142	154	159
60	162	142	160	164
65	162	148	160	164
70	162	148	160	170
75	162	154	160	170
80	164	154	162	170
85	164	161	162	174
90	164	161	162	174
95	172	164	170	174
100	172	164	170	178
105	172	168	170	178
110	179	168	177	182
115	179	168	177	182
120	179	175	177	186
125	179	175	177	189
130	179	175	177	189
135	179	175	177	189
140	179	175	177	189

Table A45: Froth decay rate experimental data for the 20 minute grind UG2 ore at 25% solids.

	20 Minute Grind Froth Height (mm)			
Time (s)	Run 1	Run 2	Run 3	Run 4
0	179	175	177	189
2	174	158	172	173
4	156	138	154	160
6	136	113	134	140
8	112	84	110	111
10	81	59	79	182
12	58	35	56	158
14	35	15	33	33
16	15	11	13	14

Table A46: Froth rise rate experimental data for the 15 minute grind UG2 ore at 25% solids.

	15 Minute Grind Froth Height (mm)			
Time (s)	Run 1	Run 2	Run 3	Run 4
5	45	47	39	38
10	79	75	73	72
15	94	94	88	87
20	105	104	99	98
25	112	109	106	105
30	118	116	112	111
35	118	116	112	111
40	125	122	119	118
45	131	122	125	124
50	131	122	125	124
55	131	129	125	124
60	131	129	133	124
65	131	129	133	124
70	131	129	133	124
75	131	129	133	124
80	131	129	133	124
85	131	129	133	124
90	131	129	133	124
95	131	129	133	124
100	131	129	133	124
105	131	129	133	124
110	131	129	133	124
115	131	129	133	124
120	131	129	133	124
125	131	129	133	124
130	131	129	133	124
135	131	129	133	124
140	131	129	133	124

Table A47: Froth decay rate experimental data for the 15 minute grind UG2 ore at 25% solids.

	15 Minute Grind Froth Height (mm)			
Time (s)	Run 1	Run 2	Run 3	Run 4
0	131	129	133	132
2	124	116	118	117
4	109	92	103	102
6	80	77	74	73
8	57	55	51	50
10	33	37	27	26
12	15	12	9	8
14	6	4	0	-1

Table A48: Froth rise rate experimental data for the 10 minute grind UG2 ore at 25% solids.

	10 Minute Grind Froth Height (mm)			
Time (s)	Run 1	Run 2	Run 3	Run 4
5	45	43	44	48
10	73	70	72	68
15	90	86	88	85
20	93	91	88	90
25	93	91	93	97
30	93	91	93	97
35	93	96	93	97
40	98	96	100	97
45	98	101	100	101
50	103	101	105	101
55	103	101	105	107
60	111	106	105	107
65	111	106	111	113
70	117	113	111	113
75	117	113	116	113
80	123	120	116	120
85	123	120	116	120
90	123	120	120	125
95	123	120	120	125
100	128	125	120	131
105	128	125	125	131
110	128	125	125	131
115	128	125	125	135
120	128	125	130	135
125	128	125	130	135

Table A49: Froth decay rate experimental data for the 10 minute grind UG2 ore at 25% solids.

	10 Minute Grind Froth Height (mm)			
Time (s)	Run 1	Run 2	Run 3	Run 4
0	128	125	134	135
2	107	105	124	123
4	82	83	104	94
6	47	60	72	66
8	20	38	40	34
10	6	17	17	15
12	1	5	9	8

d. Iron Ore tests at 15% solids concentration

Table A50: Froth rise rate experimental data for the 10 minute grind iron ore 15% solids.

	10 Minute Grind Froth Height (mm)			
Time (s)	Run 1	Run 2	Run 3	Run 4
5	99	89	118	89
10	148	143	170	143
15	185	187	217	187
20	228	235	263	235
25	258	268	337	268
30	284	297	359	297
35	308	321	391	321
40	326	333	418	333
45	344	348	418	348
50	356	363	440	363
55	356	363	464	363
60	365	371	464	371
65	365	371	479	371
70	365	383	479	383
75	379	383	479	383
80	379	383	479	383
85	379	392	479	392
90	382	392	479	392
95	382	392	479	392
100	382	392	479	392
105	382	392	479	392
110	382	392	479	392
115	382	392	479	392
120	382	392	479	392
125	382	392	479	392
130	382	392	479	392

Table A51: Froth rise rate experimental data for the 5 minute grind iron ore 15% solids.

	5 Minute Grind Froth Height (mm)			
Time (s)	Run 1	Run 2	Run 3	Run 4
5	87	92	75	80
10	118	108	107	114
15	147	133	131	136
20	166	159	150	156
25	184	167	167	172
30	201	181	167	185
35	212	194	184	185
40	212	194	200	197
45	233	209	200	197
50	233	209	211	208
55	249	209	211	208
60	249	223	224	208
65	249	223	224	218
70	266	240	233	218
75	266	240	233	218
80	284	240	233	231
85	284	250	246	231
90	284	250	246	245
95	298	250	257	245
100	298	263	257	245
105	298	263	257	256
110	298	271	269	256
115	298	271	269	256
120	298	271	269	256
125	298	271	284	256
130	298	271	284	256
135	298	271	284	256
140	298	271	284	256

Table A52: Froth rise rate experimental data for the 2 minute grind iron ore 15% solids.

	2 Minute Grind Froth Height (mm)			
Time (s)	Run 1	Run 2	Run 3	Run 4
5	75	59	79	70
10	89	78	103	92
15	100	97	125	113
20	119	115	138	134
25	129	134	153	154
30	143	148	170	171
35	154	159	182	188
40	160	168	193	204
45	170	177	201	217
50	170	188	209	224
55	178	188	209	224
60	178	200	215	238
65	188	200	215	238
70	188	209	225	244
75	197	209	225	244
80	197	209	225	244
85	204	209	233	250
90	204	217	233	250
95	204	217	239	250
100	211	223	239	250
105	211	223	246	250
110	219	231	246	250

Table A53: Froth rise rate experimental data for the 0 minute grind iron ore 15% solids.

	0 Minute Grind Froth Height (mm)			
Time (s)	Run 1	Run 2	Run 3	Run 4
5	56	53	55	63
10	69	69	71	80
15	77	88	85	100
20	88	104	97	116
25	96	116	108	133
30	105	128	120	149
35	110	137	128	155
40	116	144	135	168
45	121	148	142	168
50	127	156	142	173
55	127	161	150	173
60	135	161	150	183
65	135	161	150	183
70	135	167	154	191
75	140	167	154	191
80	140	172	154	191
85	140	172	154	199
90	140	178	162	199
95	140	178	162	199
100	147	178	162	199
105	147	183	162	199
110	147	183	162	204
115	147	183	167	204
120	153	189	167	204
125	153	189	167	210
130	153	189	167	210

e. Iron Ore tests at 20% solids concentration

Table A54: Froth rise rate experimental data for the 10 minute grind iron ore 20% solids.

	10 Minute Grind Froth Height (mm)			
Time (s)	Run 1	Run 2	Run 3	Run 4
5	122	131	170	143
10	173	186	246	215
15	220	256	298	275
20	268	323	349	340
25	319	364	399	403
30	352	405	446	444
35	387	436	476	488
40	420	463	507	523
45	435	463	528	544
50	454	475	552	559
55	465	475	552	572
60	474	488	563	588
65	474	488	563	588
70	491	504	580	608
75	491	504	580	625
80	503	513	608	635
85	503	513	608	635
90	514	513	624	651
95	514	534	624	651
100	514	534	641	651
105	524	534	641	661
110	524	534	655	661
115	524	551	655	661
120	524	551	655	661
125	524	551	655	661

Table A55: Froth rise rate experimental data for the 5 minute grind iron ore 20% solids.

	5 Minute Grind Froth Height (mm)			
Time (s)	Run 1	Run 2	Run 3	Run 4
5	86	91	98	106
10	118	126	130	151
15	148	162	158	181
20	177	181	193	202
25	205	207	218	218
30	205	225	232	233
35	244	242	247	243
40	262	257	258	243
45	274	257	258	261
50	293	282	280	261
55	293	282	280	261
60	309	302	301	277
65	309	302	301	277
70	324	320	301	293
75	324	320	316	293
80	324	337	316	306
85	339	337	316	306
90	339	353	335	320
95	349	353	335	320
100	349	353	347	320
105	359	363	347	333
110	359	363	347	333
115	359	363	358	333
120	359	363	358	333

Table A56: Froth rise rate experimental data for the 2 minute grind iron ore 20% solids.

	2 Minute Grind Froth Height (mm)			
Time (s)	Run 1	Run 2	Run 3	Run 4
5	75	79	92	79
10	99	103	119	107
15	123	131	146	138
20	144	149	175	161
25	160	170	201	188
30	176	193	222	210
35	187	210	237	228
40	196	226	254	243
45	196	240	268	262
50	208	240	268	275
55	208	251	284	275
60	218	257	284	288
65	218	257	291	288
70	226	268	291	299
75	226	268	291	299
80	236	277	299	305
85	236	277	299	305
90	244	283	307	312
95	244	283	307	312
100	252	292	312	312
105	252	292	312	312

Table A57: Froth rise rate experimental data for the 0 minute grind iron ore 20% solids.

	0 Minute Grind Froth Height (mm)			
Time (s)	Run 1	Run 2	Run 3	Run 4
5	38	56	0	61
10	46	67	52	80
15	54	80	82	101
20	60	93	94	121
25	66	105	107	136
30	74	115	119	151
35	80	124	128	165
40	80	128	136	177
45	85	137	145	177
50	85	143	150	186
55	93	149	150	193
60	93	154	161	198
65	98	154	161	198
70	98	159	166	204
75	98	159	166	204
80	105	165	171	209
85	105	165	171	209
90	110	172	171	216
95	110	172	177	216
100	125	172	177	220
105	125	172	177	220
110	135	182	183	220
115	135	182	183	227
120	148	186	183	227
125	148	186	190	227
130	148	186	190	227

f. Iron Ore tests at 25% solids concentration

Table A58: Froth rise rate experimental data for the 10 minute grind iron ore 25% solids.

	10 Minute Grind Froth Height (mm)			
Time (s)	Run 1	Run 2	Run 3	Run 4
5	183	185	174	180
10	243	256	243	259
15	304	331	307	335
20	366	395	374	408
25	425	437	443	478
30	478	490	491	521
35	528	525	543	562
40	570	547	582	590
45	605	547	607	604
50	630	574	626	628
55	630	574	648	645
60	673	596	663	668
65	673	596	663	668
70	673	628	691	678
75	705	628	691	678
80	705	662	721	693
85	734	662	721	693
90	734	694	721	713
95	734	694	748	713
100	740	694	748	740
105	740	736	748	740
110	740	736	762	740
115	740	736	762	764
120	740	736	762	764
125	740	736	762	775
130	740	736	762	775

Table A59: Froth rise rate experimental data for the 5 minute grind iron ore 25% solids.

	5 Minute Grind Froth Height (mm)			
Time (s)	Run 1	Run 2	Run 3	Run 4
5	98	124	111	154
10	136	169	151	188
15	189	211	190	227
20	232	255	231	250
25	272	283	266	285
30	308	313	296	285
35	338	331	323	310
40	360	331	334	310
45	384	355	351	345
50	402	370	370	345
55	402	370	370	366
60	425	392	401	366
65	425	392	401	385
70	438	402	416	400
75	438	402	416	400
80	453	416	426	415
85	453	416	426	415
90	453	427	437	433
95	472	427	437	433
100	472	427	451	433
105	472	440	451	442
110	472	440	451	442
115	472	440	463	442

Table A60: Froth rise rate experimental data for the 2 minute grind iron ore 25% solids.

	2 Minute Grind Froth Height (mm)			
Time (s)	Run 1	Run 2	Run 3	Run 4
5	93	97	78	71
10	150	148	125	120
15	200	192	169	164
20	241	241	215	206
25	264	272	243	246
30	281	304	275	271
35	294	332	297	307
40	321	360	322	334
45	342	381	341	349
50	342	380	350	360
55	355	380	350	360
60	355	396	360	376
65	372	396	360	376
70	372	396	380	392
75	387	403	380	392
80	387	403	380	392
85	400	403	380	392
90	410	403	380	392
95	410	403	380	392

Table A61: Froth rise rate experimental data for the 0 minute grind iron ore 25% solids.

	0 Minute Grind Froth Height (mm)			
Time (s)	Run 1	Run 2	Run 3	Run 4
5	99	76	80	90
10	116	96	98	113
15	131	121	127	147
20	140	141	146	170
25	150	156	162	190
30	162	170	180	209
35	167	182	194	230
40	176	198	206	243
45	182	206	214	256
50	187	206	227	270
55	187	212	238	270
60	193	219	244	283
65	193	226	244	291
70	198	226	255	299
75	198	238	255	308
80	204	238	264	308
85	204	244	264	316
90	204	244	264	316
95	210	251	273	324
100	210	251	273	332
105	210	256	278	332
110	214	256	278	332
115	222	264	282	332
120	222	264	282	341
125	256	271	289	341
130	256	271	289	341
135	276	276	295	341
140	276	276	295	350
145	276	282	302	350
150	276	282	302	350

A5. Agitated Hybrid Results

a. UG2 ore metallurgical assay results

Table A62: Assay results for the UG2 ore tests performed on the agitated hybrid cell.

	Sample Name	Sample Type	Rep	ICP15	MINPGM4E_S			
				Cr2O3	Au	Pd	Pt	Rh
				%	ppm	ppm	ppm	ppm
Sample 1	25 cm Column, 30 min grind	Concentrate	1	13.9	0.14	6.43	12.4	2.54
Sample 2	25 cm Column, 25 min grind	Concentrate	1	8.17	0.17	11	21.9	4.52
Sample 3	25 cm Column, 20 min grind	Concentrate	1	9.01	0.18	13.8	26.7	5.29
Sample 4	25 cm Column, 15 min grind	Concentrate	1	5.39	0.32	22.7	42.8	8.84
Sample 5	25 cm Column, 10 min grind	Concentrate	1	5.82	0.34	23.3	46.2	8.87
Sample 6	15 cm Column, 30 min grind	Concentrate	1	14.9	<0.1	6.19	12.2	2.24
Sample 7	15 cm Column, 25 min grind	Concentrate	1	14.7	<0.1	4.72	8.64	1.88
Sample 8	15 cm Column, 20 min grind	Concentrate	1	13.4	0.19	6.96	14.5	2.66
Sample 9	15 cm Column, 15 min grind	Concentrate	1	12.1	0.18	9.5	21.5	4.04
Sample 10	15 cm Column, 10 min grind	Concentrate	1	8.29	0.26	16.1	31.6	6.33
Sample 11	10 cm Column, 30 min grind	Concentrate	1	17.1	<0.1	3.06	5.37	1.15
Sample 12	10 cm Column, 25 min grind	Concentrate	1	15.6	<0.1	4.41	8.51	1.8
Sample 13	10 cm Column, 20 min grind	Concentrate	1	13.4	0.11	6.83	15.4	2.69
Sample 14	10 cm Column, 15 min grind	Concentrate	1	10.5	0.19	11.4	22.3	4.54
Sample 15	10 cm Column, 10 min grind	Concentrate	1	9.18	0.24	15.8	30.8	6.32
Sample 16	F-1	Feed	1	20.6	<0.1	1.69	2.73	0.13

b. Iron ore metallurgical assay results

Table A63: Assay results for the UG2 ore tests performed on the agitated hybrid cell.

Sample Name	Description	Sample Name	Sample Type	Rep	ICP1	
					Fe	Si
					%	%
INT15586/1	Sample 1	10 cm Column, No min grind	Concentrate	1	35.9	21.5
INT15586/2	Sample 2	10 cm Column, 2 min grind	Concentrate	1	35.5	21.2
INT15586/3	Sample 3	10 cm Column, 2 min grind	Tails	1	46.7	16.3
INT15586/4	Sample 4	10 cm Column, 5 min grind	Concentrate	1	24.1	28.5
INT15586/5	Sample 5	10 cm Column, 5 min grind	Tails	1	51.1	14.4
INT15586/6	Sample 6	10 cm Column, 10 min grind	Concentrate	1	23.3	28.9
INT15586/7	Sample 7	10 cm Column, 10 min grind	Tails	1	55	14.1
INT15586/8	Sample 8	10 cm Column, F-1-A	Feed	1	44.9	17.2
INT15586/9	Sample 9	20 cm Column, No min grind	Concentrate	1	38	19.3
INT15586/10	Sample 10	20 cm Column, No min grind	Tails	1	43.3	16.2
INT15586/11	Sample 11	20 cm Column, 2 min grind	Concentrate	1	28.5	25.3
INT15586/12	Sample 12	20 cm Column, 2 min grind	Tails	1	46.9	15.7
INT15586/13	Sample 13	20 cm Column, 5 min grind	Concentrate	1	23.7	28.4
INT15586/14	Sample 14	20 cm Column, 5 min grind	Tails	1	51.5	13
INT15586/15	Sample 15	20 cm Column, F-2-A	Feed	1	46.9	15.5
INT15586/16	Sample 16	25 cm Column, No min grind	Concentrate	1	18.5	30.1
INT15586/17	Sample 17	25 cm Column, No min grind	Tails	1	46.5	16.4
INT15586/18	Sample 18	25 cm Column, 2 min grind	Concentrate	1	13.3	33.8
INT15586/19	Sample 19	25 cm Column, 2 min grind	Tails	1	46	15.7
INT15586/20	Sample 20	25 cm Column, 5 min grind	Concentrate	1	26.8	26.4
INT15586/21	Sample 21	25 cm Column, 5 min grind	Tails	1	54	14.9
INT15586/22	Sample 22	25 cm Column, F-3-A	Feed	1	42.9	16.8

c. UG2 ore flotation performance results

i. 10 cm Column Height

Table A64: Cumulative water and solids recovery over a 4 minute float with UG2 ore, using a 10 cm column height.

Cumulative Recoveries over a 4 minute float (g)

	30 min grind		25 min grind		20 min grind		15 min grind		10 min grind	
	Water	Solids	Water	Solids	Water	Solids	Water	Solids	Water	Solids
C1	399	49	349	36	298	18	234	17	234	10
C2	789	98	708	73	592	37	463	32	427	20
C3	1202	151	1021	104	888	57	647	47	659	31
C4	1577	199	1356	138	1166	77	880	62	841	42

Table A65: Cumulative water and solids recovery error over a 4 minute float with UG2 ore, using a 10 cm column height.

Cumulative Error in Recoveries over a 4 minute float (g)

	30 min grind		25 min grind		20 min grind		15 min grind		10 min grind	
	Water	Solids	Water	Solids	Water	Solids	Water	Solids	Water	Solids
C1	40	11	22	2	12	1	13	2	30	2
C2	52	12	44	4	28	1	39	3	50	2
C3	64	12	48	6	32	1	69	3	57	3
C4	120	20	83	11	65	2	121	5	110	4

ii. 15 cm Column Height

Table A66: Cumulative water and solids recovery over a 4 minute float with UG2 ore, using a 15 cm column height.

Cumulative Recoveries over a 4 minute float (g)

	30 min grind		25 min grind		20 min grind		15 min grind		10 min grind	
	Water	Solids	Water	Solids	Water	Solids	Water	Solids	Water	Solids
C1	346	35	314	29	281	16	229	21	217	9
C2	674	67	627	60	569	31	438	32	387	16
C3	1018	93	947	93	852	48	637	41	522	22
C4	1353	120	1256	124	1088	64	841	51	676	29

Table A67: Cumulative water and solids recovery error over a 4 minute float with UG2 ore, using a 15 cm column height.

Cumulative Error in Recoveries over a 4 minute float (g)

	30 min grind		25 min grind		20 min grind		15 min grind		10 min grind	
	Water	Solids	Water	Solids	Water	Solids	Water	Solids	Water	Solids
C1	13	6	29	0	1	0	14	2	30	1
C2	29	8	65	2	4	0	23	4	42	2
C3	67	12	91	3	5	1	40	5	111	5
C4	69	19	105	4	17	2	58	6	153	6

iii. 25 cm Column Height

Table A68: Cumulative water and solids recovery over a 4 minute float with UG2 ore, using a 25 cm column height.

Cumulative Recoveries over a 4 minute float (g)

	30 min grind		25 min grind		20 min grind		15 min grind		10 min grind	
	Water	Solids	Water	Solids	Water	Solids	Water	Solids	Water	Solids
C1	233	21	200	13	176	11	112	6	54	3
C2	460	41	411	25	352	22	177	10	123	6
C3	684	60	616	35	523	32	285	16	217	10
C4	919	80	820	42	698	43	367	21	312	14

Table A69: Cumulative water and solids recovery error over a 4 minute float with UG2 ore, using a 25 cm column height.

Cumulative Error in Recoveries over a 4 minute float (g)

	30 min grind		25 min grind		20 min grind		15 min grind		10 min grind	
	Water	Solids	Water	Solids	Water	Solids	Water	Solids	Water	Solids
C1	9.9	0.4	0.2	1.0	0.7	0.3	23.5	1.0	1.8	0.4
C2	26.6	1.5	2.0	1.9	2.8	0.6	29.3	1.2	15.8	1.5
C3	33.5	1.8	6.3	3.6	3.8	0.8	33.1	1.6	23.0	1.7
C4	40.6	2.8	16.8	7.2	9.9	1.5	56.6	2.8	37.5	2.0

d. Iron ore flotation performance results

i. 10 cm Column

Table A70: Cumulative water and solids recovery over a 4 minute float with iron ore, using a 10 cm column height.

Cumulative Recoveries over a 4 minute float (g)

	10 min grind		5 min grind		2 min grind		0 min grind	
	Water	Solids	Water	Solids	Water	Solids	Water	Solids
C1	318	34	252	19	183	13	136	4
C2	639	63	531	39	382	24	266	8
C3	953	89	789	58	588	36	412	11
C4	1260	116	1043	79	776	49	539	16

Table 71: Cumulative water and solids recovery error over a 4 minute float with iron ore, using a 10 cm column height.

Cumulative Error in Recoveries over a 4 minute float (g)

	10 min grind		5 min grind		2 min grind		0 min grind	
	Water	Solids	Water	Solids	Water	Solids	Water	Solids
C1	6.6	4.2	29.3	0.1	49.5	0.2	5.7	0.8
C2	7.1	4.2	40.5	0.5	68.2	2.5	8.8	1.5
C3	10.3	4.3	47.1	0.7	103.1	3.5	12.4	1.9
C4	11.6	6.2	64.9	3.0	126.9	3.5	22.0	2.0

ii. 20 cm Column

Table A72: Cumulative water and solids recovery over a 4 minute float with iron ore, using a 20 cm column height.

Cumulative Recoveries over a 4 minute float (g)

	10 min grind		5 min grind		2 min grind		0 min grind	
	Water	Solids	Water	Solids	Water	Solids	Water	Solids
C1	-	-	245	19	184	9	102	3
C2	-	-	479	38	341	16	209	5
C3	-	-	742	56	517	25	297	7
C4	-	-	1000	71	658	32	403	9

Table A73: Cumulative water and solids recovery error over a 4 minute float with iron ore, using a 20 cm column height.

Cumulative Error in Recoveries over a 4 minute float (g)

	10 min grind		5 min grind		2 min grind		0 min grind	
	Water	Solids	Water	Solids	Water	Solids	Water	Solids
C1	-	-	14.2	2.1	10.3	0.2	2.8	0.1
C2	-	-	14.9	2.4	26.1	0.5	2.8	0.1
C3	-	-	22.9	2.5	34.5	0.9	27.3	0.4
C4	-	-	32.5	3.8	49.9	1.9	27.9	0.4

iii. 25 cm Column

Table A74: Cumulative water and solids recovery over a 4 minute float with iron ore, using a 25 cm column height.

Cumulative Recoveries over a 4 minute float (g)

	10 min grind		5 min grind		2 min grind		0 min grind	
	Water	Solids	Water	Solids	Water	Solids	Water	Solids
C1	-	-	249	21	175	7	78	2
C2	-	-	494	39	329	13	160	3
C3	-	-	733	58	482	20	249	5
C4	-	-	948	76	586	25	305	6

Table A75: Cumulative water and solids recovery error over a 4 minute float with iron ore, using a 25 cm column height.

Cumulative Error in Recoveries over a 4 minute float (g)

	10 min grind		5 min grind		2 min grind		0 min grind	
	Water	Solids	Water	Solids	Water	Solids	Water	Solids
C1	-	-	61.2	0.5	19.8	0.3	27.3	0.6
C2	-	-	72.9	0.9	69.1	1.5	52.3	0.6
C3	-	-	81.8	2.0	121.5	2.9	77.1	0.6
C4	-	-	104.3	3.2	146.5	3.5	97.9	0.9

e. Hybrid cell top of froth bubble sizes

i. UG2 ore tests

Table A76: Top of froth bubble sizes for test work done using UG2 ore.

	Top of froth average bubble size (mm)		
	25 cm Column	15 cm Column	10 cm Column
30 min grind	1.11	1.38	1.30
25 min grind	1.38	1.52	1.35
20 min grind	1.50	1.51	1.36
15 min grind	1.89	1.63	1.55
10 min grind	1.91	1.73	1.57

iv. Iron ore tests

Table A77: Top of froth bubble sizes for test work done using iron ore.

	Top of froth average bubble size (mm)		
	25 cm Column	20 cm Column	10 cm Column
0 min grind	1.77	1.64	1.65
2 min grind	1.53	1.43	1.38
5 min grind	1.22	1.21	1.19
10 min grind	-	-	0.98

a. Hybrid cell side of froth bubble sizes

i. UG2 ore tests

Table A78: Side of froth bubble size using a 25 cm column for test work done using UG2 ore.

	Side of froth average bubble size for the 25 cm column (mm)		
	Bottom (40mm Froth height)	Middle (120 mm Froth height	Top (180 mm Froth height)
30 min grind	0.47	0.56	0.64
25 min grind	0.58	0.63	0.82
20 min grind	0.63	0.71	0.90
15 min grind	0.61	0.85	0.99
10 min grind	0.76	0.95	1.19

ii. Iron ore tests

Table A79: Side of froth bubble size using a 25 cm column for test work done using iron ore.

	Side of froth average bubble size for the 25 cm column (mm)		
	Bottom (40mm Froth height)	**Middle (120 mm Froth height**	**Top (180 mm Froth Height)**
0 min grind	0.55	0.86	1.04
2 min grind	0.57	0.64	0.82
5 min grind	0.51	0.60	0.64
10 min grind	-	-	-

Chapter 9. Ethics Form

EBE Faculty: Assessment of Ethics in Research Projects (Rev2)

Any person planning to undertake research in the Faculty of Engineering and the Built Environment at the University of Cape Town is required to complete this form before collecting or analysing data. When completed it should be submitted to the supervisor (where applicable) and from there to the Head of Department. If any of the questions below have been answered YES, and the applicant is NOT a fourth year student, the Head should forward this form for approval by the Faculty EIR committee: submit to Ms Zulpha Geyer (Zulpha.Geyer@uct.ac.za; Chem Eng Building, Ph 021 650 4791).
NB: A copy of this signed form must be included with the thesis/dissertation/report when it is submitted for examination

This form must only be completed once the most recent revision EBE EiR Handbook has been read.

Name of Principal Researcher/Student: **Chidzanira Tadiwanashe** Department:CMR – **EBE Chemical Engineering**

Preferred email address of the applicant: **chdtad001@myuct.ac.za**

If a Student: Degree: **MSc Chemical Engineering** Supervisor: **Mrs Jenny Wiese**

If a Research Contract indicate source of funding/sponsorship: **AMIRA P9, CMR**

Research Project Title: **Investigation into the effect of particle size on froth stability.**

Overview of ethics issues in your research project:

Question 1: Is there a possibility that your research could cause harm to a third party (i.e. a person not involved in your project)?	YES	NO X
Question 2: Is your research making use of human subjects as sources of data? If your answer is YES, please complete Addendum 2.	YES	NO X
Question 3: Does your research involve the participation of or provision of services to communities? If your answer is YES, please complete Addendum 3.	YES	NO X
Question 4: If your research is sponsored, is there any potential for conflicts of interest? If your answer is YES, please complete Addendum 4.	YES	NO X

If you have answered YES to any of the above questions, please append a copy of your research proposal, as well as any interview schedules or questionnaires (Addendum 1) and please complete further addenda as appropriate. Ensure that you refer to the EiR Handbook to assist you in completing the documentation requirements for this form.

I hereby undertake to carry out my research in such a way that

- there is no apparent legal objection to the nature or the method of research; and
- the research will not compromise staff or students or the other responsibilities of the University;
- the stated objective will be achieved, and the findings will have a high degree of validity;
- limitations and alternative interpretations will be considered;
- the findings could be subject to peer review and publicly available; and
- I will comply with the conventions of copyright and avoid any practice that would constitute plagiarism.

Signed by:

	Full name and signature	Date
Principal Researcher/Student:	Tadiwanashe Chidzanira Signed	09/02/2016
This application is approved by:		
Supervisor (if applicable):	Jenny Wiese Signed	09/02/2016
HOD (or delegated nominee): *Final authority for all assessments with NO to all questions and for all undergraduate research.*	ERIC VAN STEEN	9/2/16
Chair : Faculty EIR Committee For applicants other than undergraduate students who have answered YES to any of the above questions.		